UNITED STATES DEPARTMENT OF THE INTERIOR

GEOLOGICAL SURVEY

Temperature, thermal conductivity, and heat flow near Yucca Mountain, Nevada: Some tectonic and hydrologic implications

by

J. H. Sass[1], A. H. Lachenbruch[2], W. W. Dudley, Jr.[3],
S. S. Priest[1], and R. J. Munroe[2]

Open File Report 87-649

Prepared in cooperation with the
Nevada Operations Office
U.S. Department of Energy
(Interagency Agreement DE-AI08-78ET44802)

[1]U.S. Geological Survey, Flagstaff, AZ 86001
[2]U.S. Geological Survey, Menlo Park, CA 94025
[3]U.S. Geological Survey, Denver, CO 80225

1988

CONTENTS

List of Tables

List of Illustrations

Abstract

Repeated temperature logs were obtained in 18 geologic and hydrologic test wells near Yucca Mountain, Nevada. Single logs were also obtained (using a specially designed sonde with fast response in air) in the air column of 17 wells drilled to monitor water level below and around Yucca Mountain. The temperature data suggest that the thermal regimes of both the saturated and unsaturated zones are strongly influenced by a complex hydrologic regime in the saturated tuffs and underlying Paleozoic carbonate rocks. Temperature gradients in the unsaturated zone (UZ) appear primarily conductive, but they range from about 15°C km^{-1} to nearly 60°C km^{-1}. However, one profile indicates rapid penetration to a depth of 150 m beneath a major channel by water from run-off following a local heavy rain. From the water table (which ranges in depth from about 300 m to over 700 m) to depths of 1 km or more, the temperature gradient in the saturated zone (SZ) typically is very irregular with evidence for locally controlled water movement in the Tertiary volcanic rocks, laterally and both up and down vertically. Vertical seepage velocities inferred from one-dimensional hydrologic models range from a few millimeters to 100 millimeters or more per year. Below depths of 1 km, temperature profiles are linear, suggesting conductive heat flow, but as in the case of the UZ, the gradients are quite variable, suggesting that the heat flux here is being controlled by fluid flow in the Paleozoic carbonate aquifer that underlies Yucca Mountain.

Measurements of thermal conductivity were performed (at room temperature) on 204 carefully preserved specimens of core, mostly from the volcanic rocks. Fifty-seven conductivities from the UZ are bimodally distributed (the modes of 1.0 and 2.1 $Wm^{-1} K^{-1}$ represent nonwelded and welded tuffs, respectively) with a mean of 1.66 ± 0.06 $Wm^{-1} K^{-1}$.

Conductivities of 134 specimens of tuffs from the SZ are normally distributed with a mean of 1.72 ± 0.03 $Wm^{-1} K^{-1}$. Variations in conductivity are due primarily to variations in porosity, which is negatively correlated with degree of welding. By contrast, 13 conductivities from the Paleozoic carbonate aquifer average nearly 5.0 $Wm^{-1} K^{-1}$. Conductivities from the SZ correlate well ($R = 0.78$) with compressional wave velocity.

Thermal conductivities were combined with individual thermal gradients for both the UZ and SZ to provide estimates of heat flow. Heat flows from the SZ are variable both laterally and vertically, particularly in the upper 1 km, and apparently are affected both by flow in the annulus between casing and borehole wall and in the adjacent formation. The average conductive heat flow from the SZ at Yucca Mountain, calculated from nine wells, was 40 ± 9 mW m^{-2} using least-squares gradients for the entire SZ intervals, including hydrologically disturbed segments, and 49 ± 8 mW m^{-2} using short, linear segments of the thermal profiles. The anomaly with respect to the regional heat flow ($\sim$85 mW m^{-2}) is attributed principally to lateral flow with a downward component beneath the depth of exploration, probably in the Paleozoic carbonate aquifer; however, the downward flow required to recharge the carbonate aquifer need not occur at Yucca Mountain and, in fact, is not evident there from the limited hydrologic data currently available.

Heat flows in the UZ also vary but in a systematic fashion, both geographically and as a function of UZ thickness. Considering the limitations on data abundance for the SZ and on data quality, the average heat flow from the UZ ($\sim$41 mW m^{-2}) may be interpreted to be about the same as that from the SZ or perhaps as much as 20% lower. If heat is being removed nonconductively from the UZ, vaporization and advective removal of infiltrating water by air circulating in fractures combined with an as yet

undetermined amount of hydrologic recharge can explain the conductive heat-flow deficiency.

An unambiguous interpretation of the heat-flow field near Yucca Mountain in terms of its hydrologic implications requires data of higher quality. For the UZ, this means reconfiguring the WT series of holes so that temperatures can be measured in water-filled pipes. For the SZ, access pipes must be grouted in to total depth to ensure that all hydrologic disturbances observed are in the formation, and not merely in the annulus between casing and borehole wall.

INTRODUCTION

Among the factors to be evaluated in assessing the suitability of the Yucca Mountain area as a candidate repository for high-level nuclear waste, are the regional tectonic setting and the regional and local hydrologic regimes. Seismic and volcanic hazards are the most directly recognized tectonic factors, and these have been the subject of intense investigations (see Carr and Rogers, 1983; Crowe and others, 1983). Regional heat-flow studies are, however, an important adjunct to the more focused investigations. Regional thermal regimes can help to put contemporary seismic/volcanic activity into an historical perspective (as regards regional tectonics) and local thermal anomalies may help pinpoint magma bodies that have no contemporary surface expression.

Thermal and hydrologic regimes are closely related. In fact, both on local and regional scales, the deep thermal regime can be effectively masked or substantially altered by relatively slow movement of ground water (see Lachenbruch and Sass, 1977; Mase and others, 1982). This, in turn, makes thermal measurements sensitive indicators of fluid movement, and in some instances, allows quantitative estimates of flow velocities.

The Geothermal Studies Project, U.S. Geological Survey, has been actively engaged in thermal studies in and around the Nevada Test Site since the late 1950's (see Lachenbruch, 1958; Lachenbruch and others, 1987). The initial thrust of these studies was to provide high-quality data to define the regional heat-flow field. Hydrologic disturbances were noted in many wells, however, and data from the NTS were instrumental in defining the Eureka Low, a large thermal anomaly, most probably of hydrologic origin, within the Basin and Range province (Sass and others, 1971). Our regional studies

provided a context for a focused study of the Yucca Mountain area (Figures 1 and 2). Preliminary results (Sass and others, 1980; Sass and Lachenbruch, 1982) confirmed that the thermal regime was indeed distorted by the effects of water movement, and provided data complementary to conventional hydrologic studies (Robison, 1984; Czarnecki and Waddell, 1984; Montazer and Wilson, 1984; Waddell and others, 1984).

The present report updates our preliminary results and incorporates detailed suites of temperature logs in all available wells and of thermal conductivity measurements on carefully preserved core. Gradients from linear portions of temperature profiles were combined with the appropriate thermal conductivity data to obtain values of heat flow. These values, in turn, were used to define the local conductive thermal regime and place it in the context of regional heat flow, with some comments on the implications for local water flow.

Techniques and procedures used are described by Sass and others (1971, 1984) and are the subject of Quality Assurance procedures NWM USGS-GPP-02, RO and -GPP-05, R1 (USGS Quality Assurance Manual, 1986). Work was performed in cooperation with the U.S. Department of Energy, Interagency Agreement DE-AI08-78ET44802. We are indebted to Frederick Grubb and Thomas H. Moses, Jr., for assistance in obtaining the temperature data. Eugene P. Smith performed the thermal conductivity measurements. We thank Ken Fox, Parviz Montazer, and D. T. Snow for their helpful comments.

SYMBOLS AND UNITS (SI)

°C	=	Degrees celsius
m	=	Meter (or 10^{-3} as a prefix)
K	=	Degrees Kelvin (or symbol for thermal conductivity in context)
W	=	Watts
SE	=	Standard error
SD	=	Standard deviation
v	=	Seepage velocity × 10^{-13} m sec or mm/y
V_p	=	Compressional wave velocity km s^{-1}
a	=	"Air"; used as a subscript
w	=	"Water"; used as a subscript
s	=	Seconds
N	=	Number of samples in population
q	=	Heat flow, mWm^{-2}
K	=	Thermal conductivity Wm^{-1} K^{-1}
Γ	=	Temperature gradient, °C km^{-1}

TEMPERATURES

Temperature profiles for all geologic and hydrologic test wells (Table 1) are plotted in Appendix 1. An additional set of temperature logs made in air in test well UZ-1 and the WT series holes (Table 2) is presented as Appendix 2. A brief discussion of the peculiarities of individual wells or groups of wells is also presented in Appendix 1. In this section, we shall look at some topographic, thermal, and hydrologic cross sections (Figure 3) within the study area in an attempt to identify and assess lateral variations in temperature.

The profiles are presented in two parts (Figures 4 through 8). An upper diagram displays all temperature profiles along the line in question plotted with common origin. The reader interested in more details of the temperature log or the thermal recovery history post-drilling of a given well is urged to look up the appropriate figure in Appendix 1. In the lower diagram (Figures 4 through 8), the wells are projected onto a topographic cross section on which is also plotted (as a dotted line) the static water level, or piezometric surface. The depth to a given temperature is indicated at 5°C intervals and every other temperature is joined by a dashed line across the section to show interpolated isothermal surfaces.

The longest cross section is that connecting J-13 in Fortymile Wash to G2, the northernmost geologic corehole (Figures 3 and 4). This section is also presented in two segments (Figures 5 and 6) to allow more detailed consideration of individual wells. The most noteworthy features of this profile are the large lateral hydraulic gradient between G2 and G1 (Figures 4 and 6) and the apparent thermal high (Figures 4 and 5) in the vicinity of UE25p1. This well was drilled into a local basement high to examine the

TABLE 1. Location, elevation and static water level (SWL) for geologic and hydrologic test wells near Yucca Mountain, Nevada

Well	Latitude	Longitude	Elevation (m)	Depth to SWL (m)
USW G-1	36° 51.8'	116° 27.5'	1326	572
USW G-2	36° 53.3'	116° 26.4'	1554	526
USW G-3	36° 50.1'	116° 28.1'	1480	751
USW G-4	36° 51.3'	116° 26.8'	1270	541
USW H-1	36° 52.0'	116° 27.2'	1302	572
USW H-3	36° 49.7'	116° 28.0'	1483	751
USW H-4	36° 50.5'	116° 26.9'	1249	519
USW H-5	36° 51.2'	116° 27.9'	1478	704
USW H-6	36° 50.8'	116° 28.7'	1302	526
UE25a4	36° 51.6'	116° 26.8'	1277	---
UE25a5	36° 51.4'	116° 26.8'	1234	---
UE25a6	36° 51.2'	116° 26.8'	1231	---
UE25a7	36° 51.3'	116° 26.6'	1219	---
UE25b1H	36° 51.1'	116° 26.4'	1200	469
UE25p1	36° 49.5'	116° 25.3'	1114	384
VH-1	36° 47.5'	116° 32.6'	954	56
VH-2	36° 48.4'	116° 34.6'	974	163
J-13	36° 48.5'	116° 23.7'	1011	282

TABLE 2. Location, elevation and static water level (SWL) for test well UZ-1 and the WT series

Well	Latitude	Longitude	Elevation (m)	Depth to SWL (m)
UZ-1	36° 52.1'	116° 27.7'	1349	---
WT-1	36° 49.3'	116° 27.0'	1202	471
WT-2	36° 50.4'	116° 27.3'	1301	571
WT-3	36° 47.9'	116° 25.0'	1030	300
WT-4	36° 51.7'	116° 26.1'	1167	439
WT-5	36° 50.6'	116° 24.8'	1088	---
WT-6	36° 53.7'	116° 26.75'	1313	284
WT-7	36° 49.5'	116° 28.9'	1197	421
WT-10	36° 48.4'	116° 29.2'	1123	348
WT-11	36° 46.8'	116° 28.1'	1094	364
WT-12	36° 46.9'	116° 26.3'	1075	345
WT-13	36° 49.7'	116° 23.9'	1032	303
WT-14	36° 50.6'	116° 24.6'	1076	346
WT-15	36° 51.3'	116° 23.7'	1083	354
WT-16	36° 52.7'	116° 25.7'	1210	473
WT-17	36° 48.5'	116° 26.5'	1124	395
WT-18	36° 52.25'	116° 26.75'	1336	---

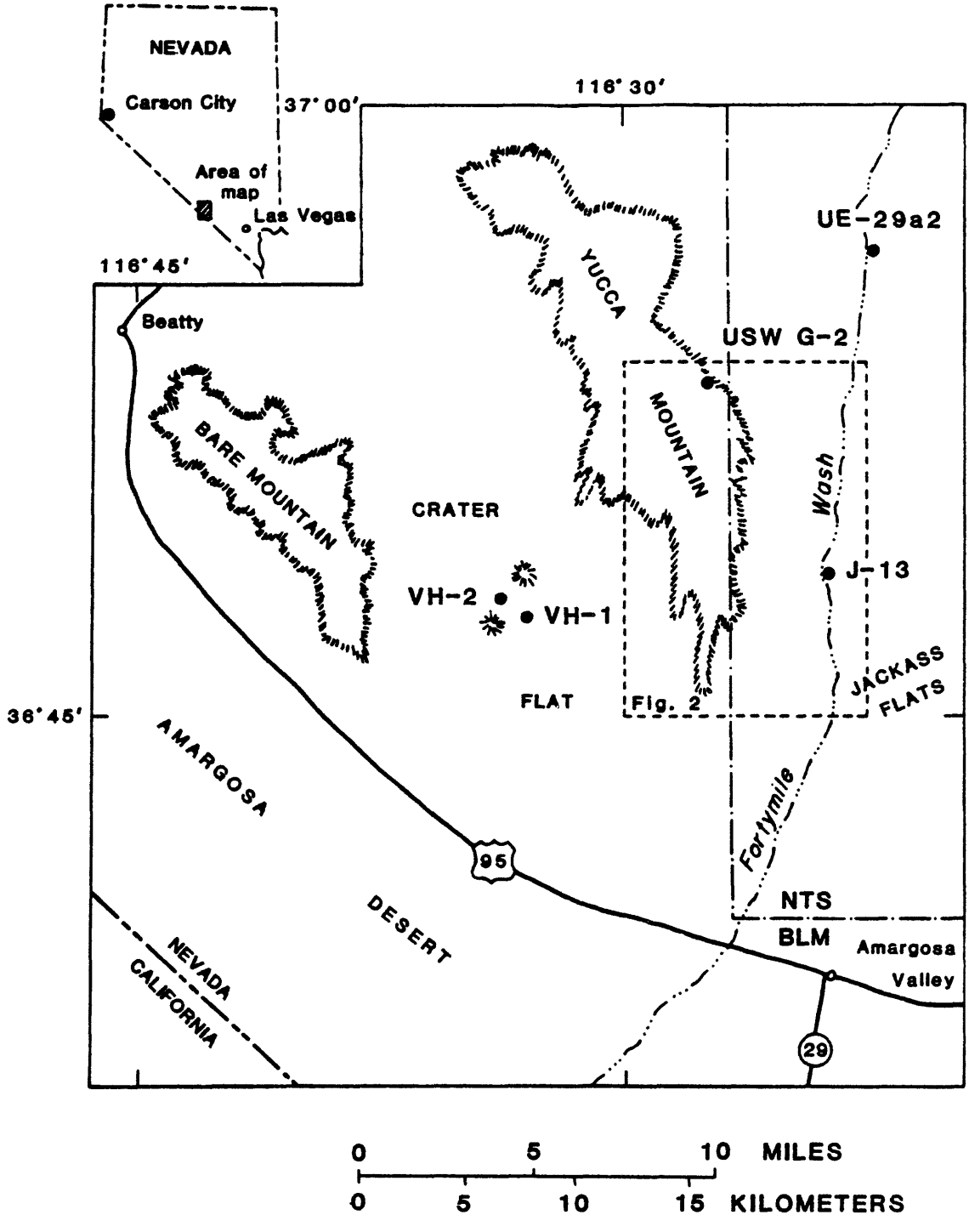

Figure 1. Map of Yucca Mountain and vicinity with selected test well locations.

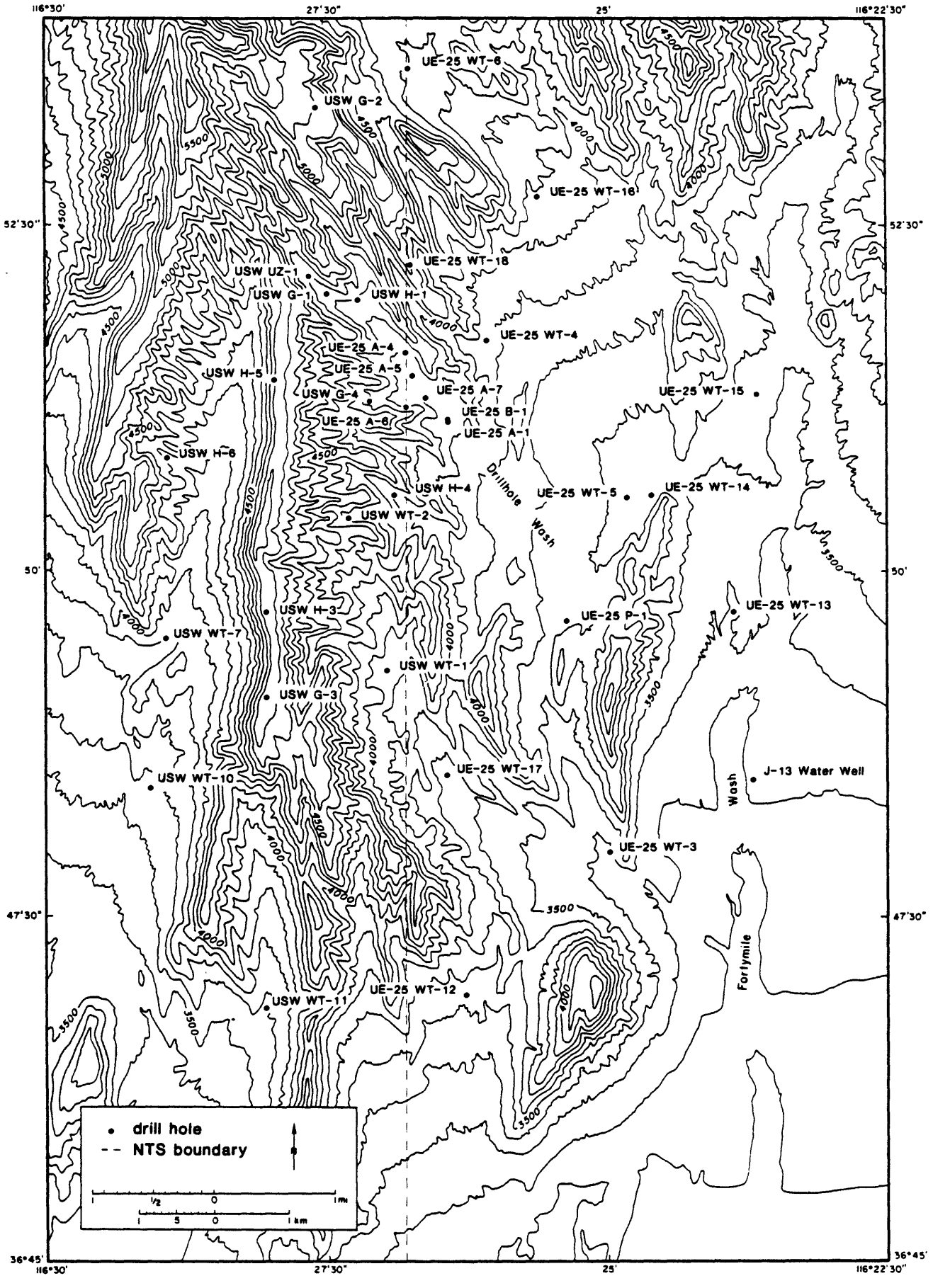

Figure 2. Map showing locations of wells studied (see index, Figure 1). Contour interval, 100 ft.

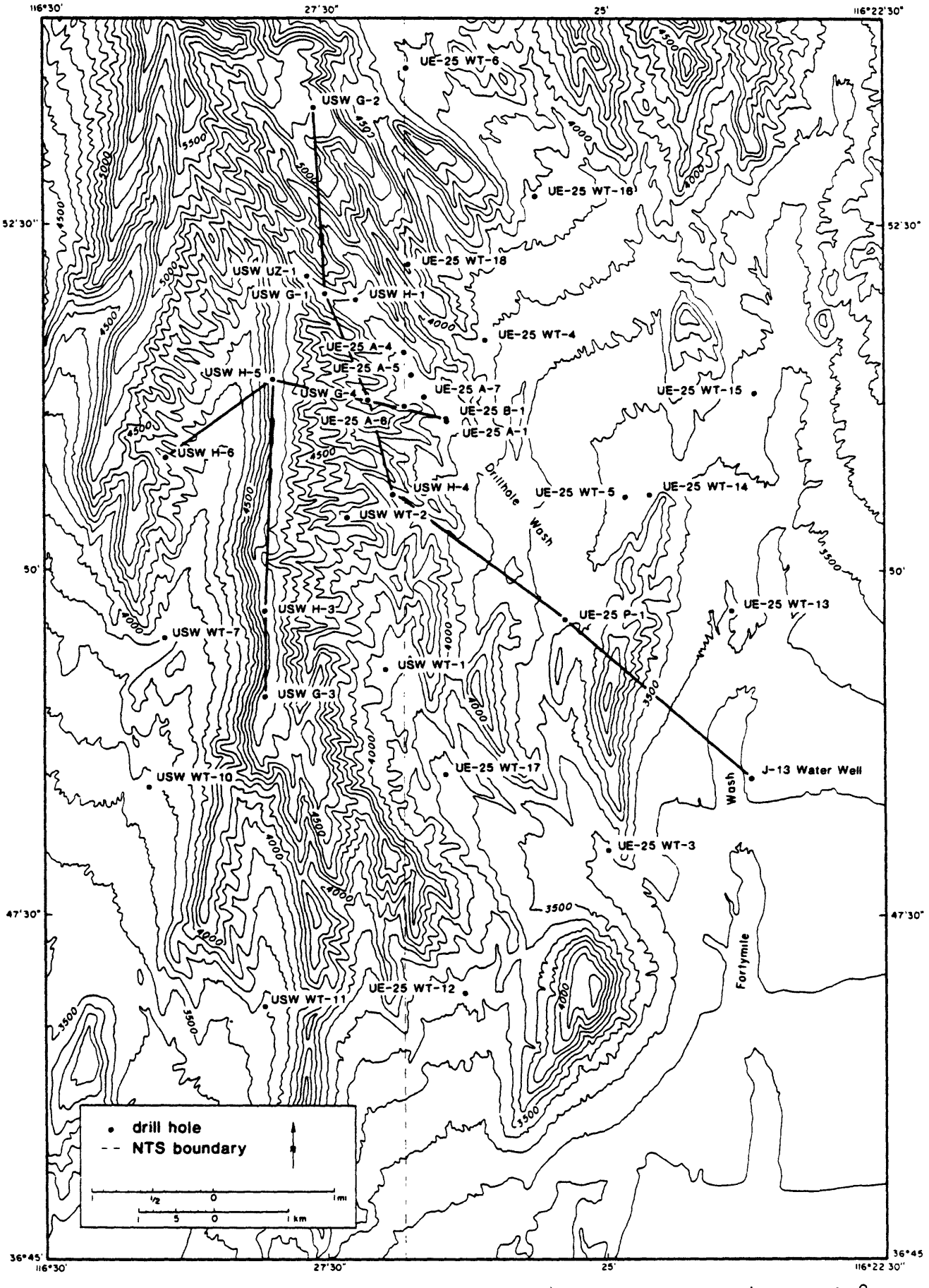

Figure 3. Test wells near Yucca Mountain. Profiles of Figures 4 through 8 are identified by solid lines.

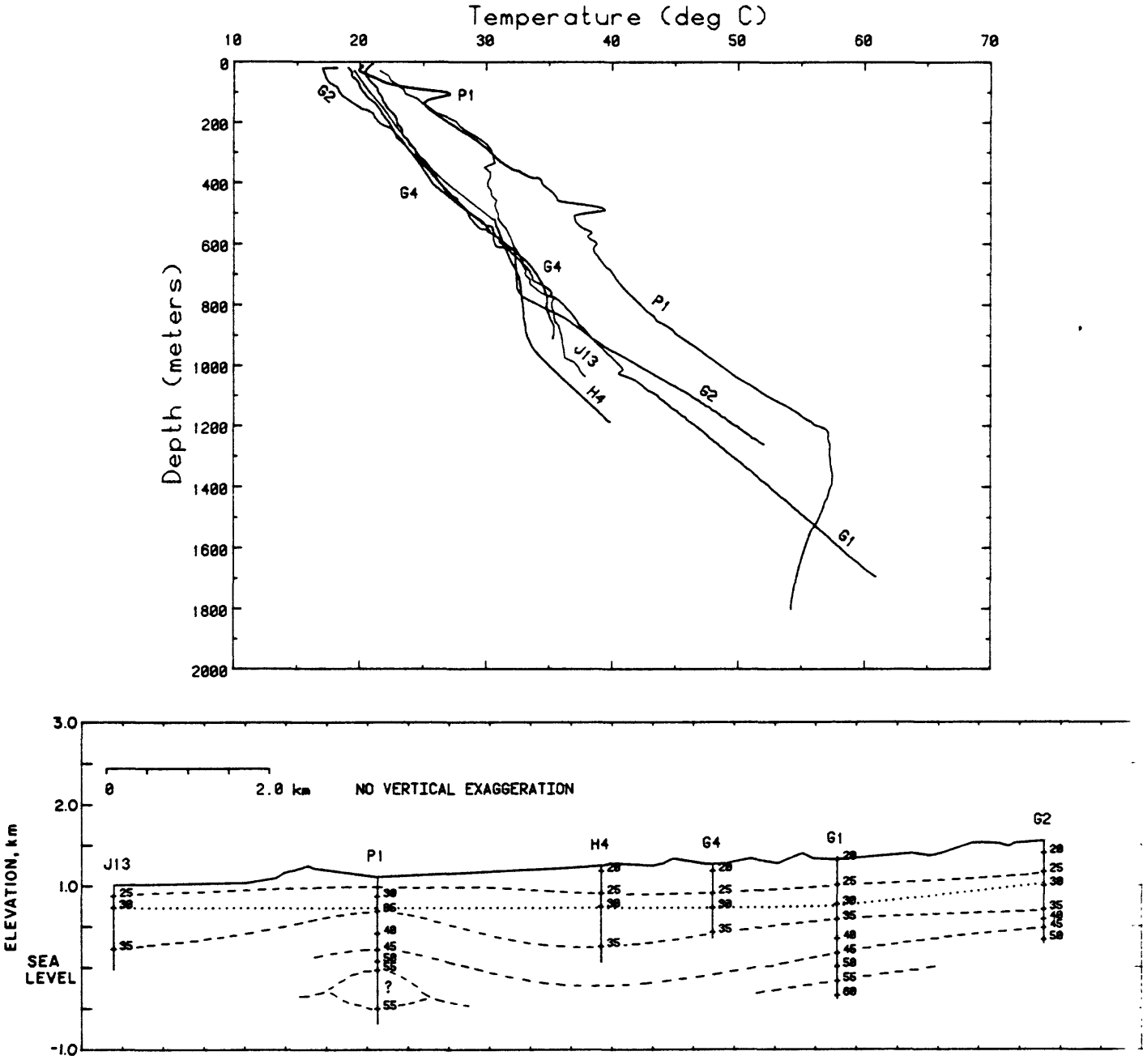

Figure 4. Thermal profile J13-G2 (Figure 3). Temperature profiles are plotted above with common origin. Dashed lines, isotherms; dotted line, static water level.

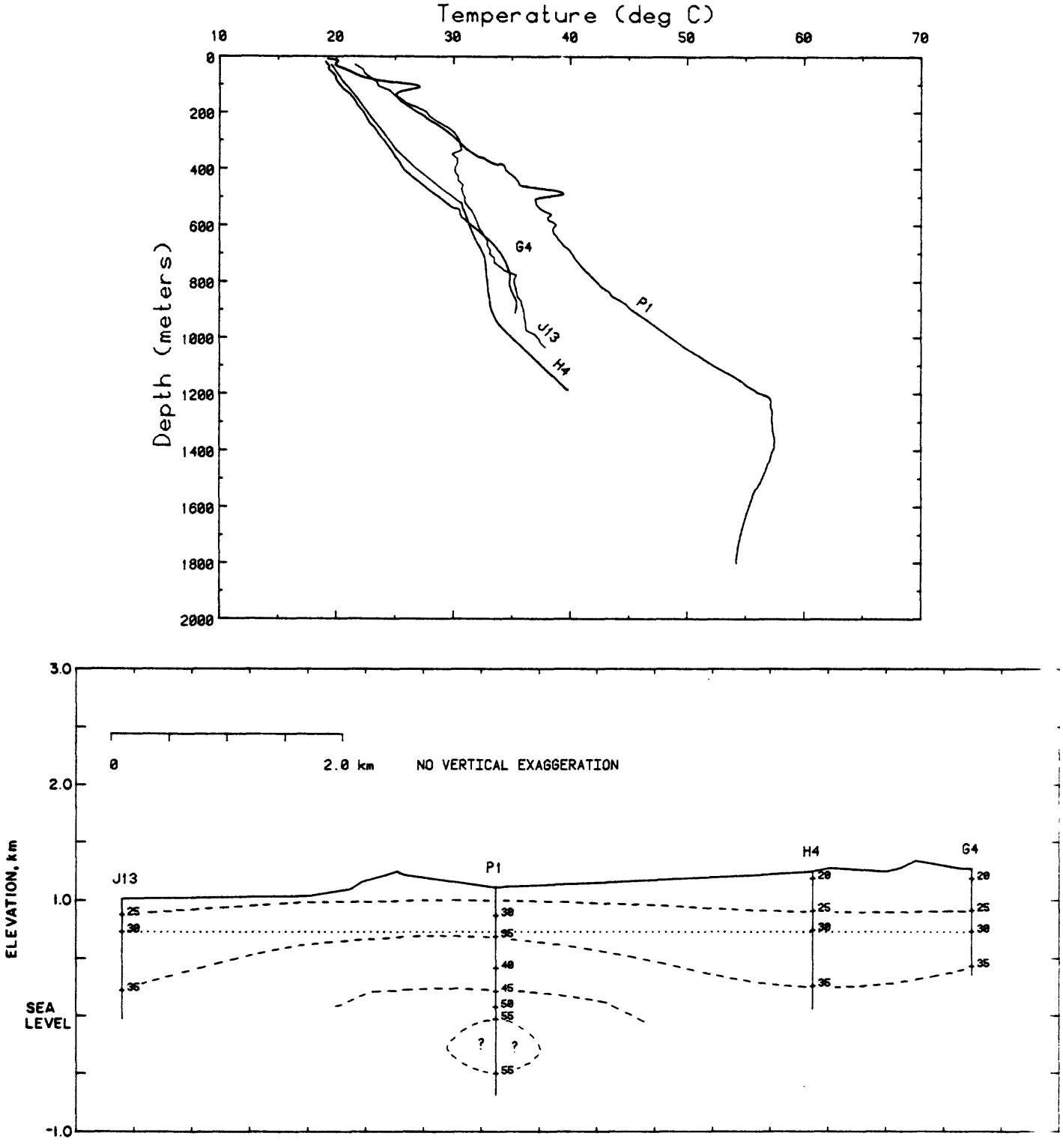

Figure 5. Thermal profile, J13-G4 (Figure 3). Temperature profiles are plotted above with common origin. Dashed lines, isotherms; dotted line, static water level.

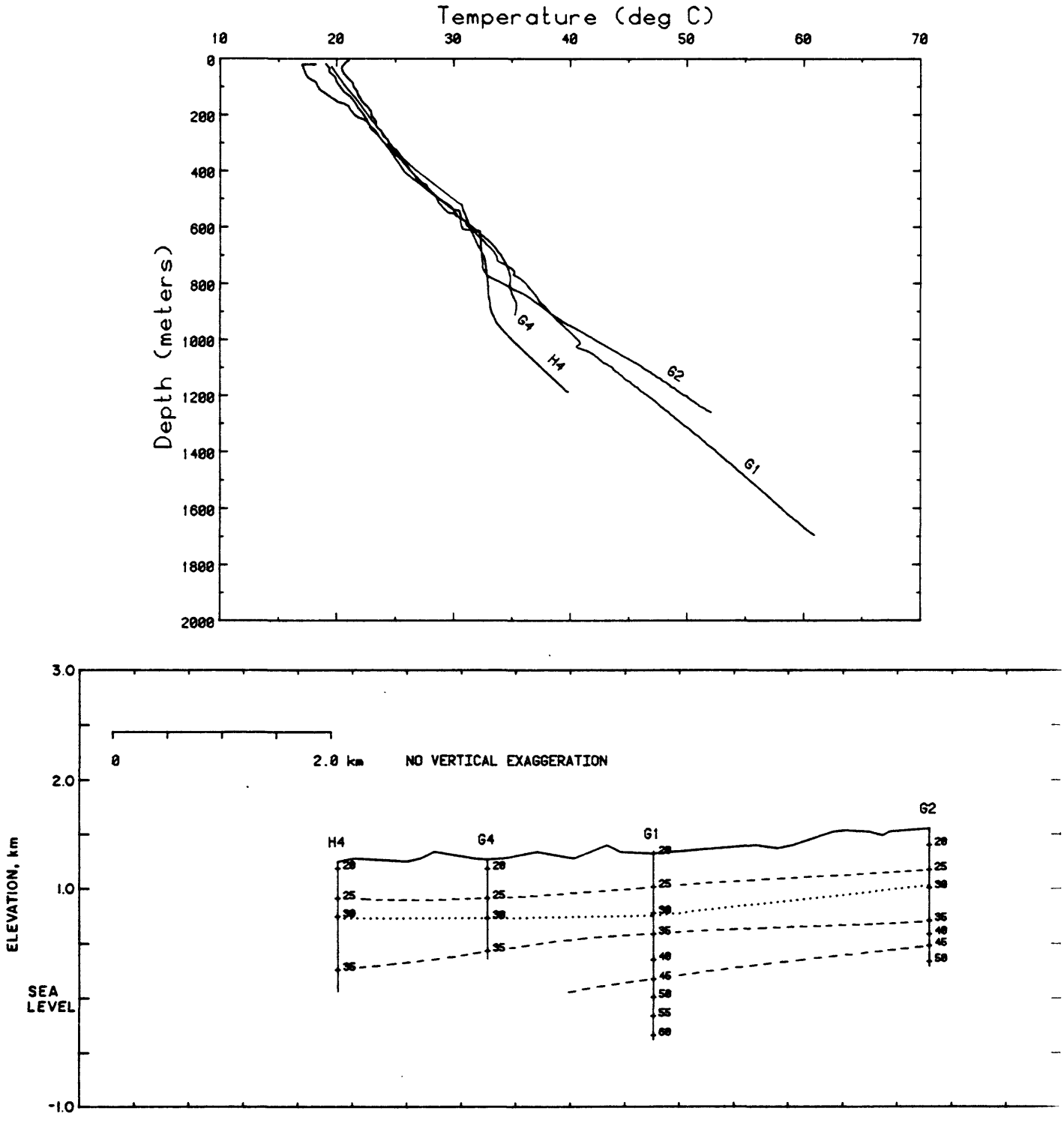

Figure 6. Thermal profile, H4-G2 (Figure 3). Temperature profiles are plotted above with common origin. Dashed lines, isotherms; dotted line, static water level.

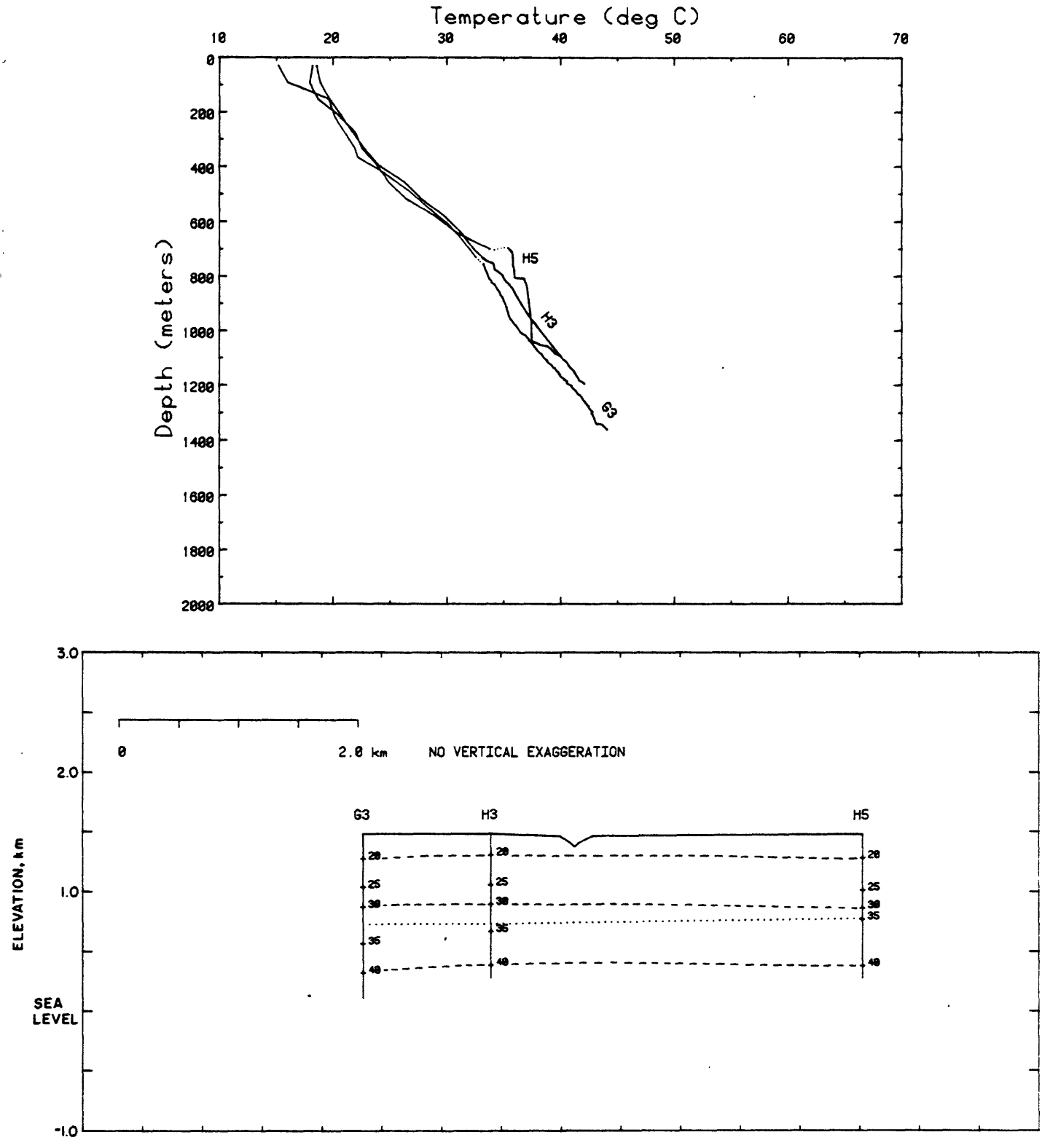

Figure 7. Thermal profile, G3-H5 (Figure 3). Temperature profiles are plotted above with common origin. Dashed lines, isotherms; dotted line, static water level.

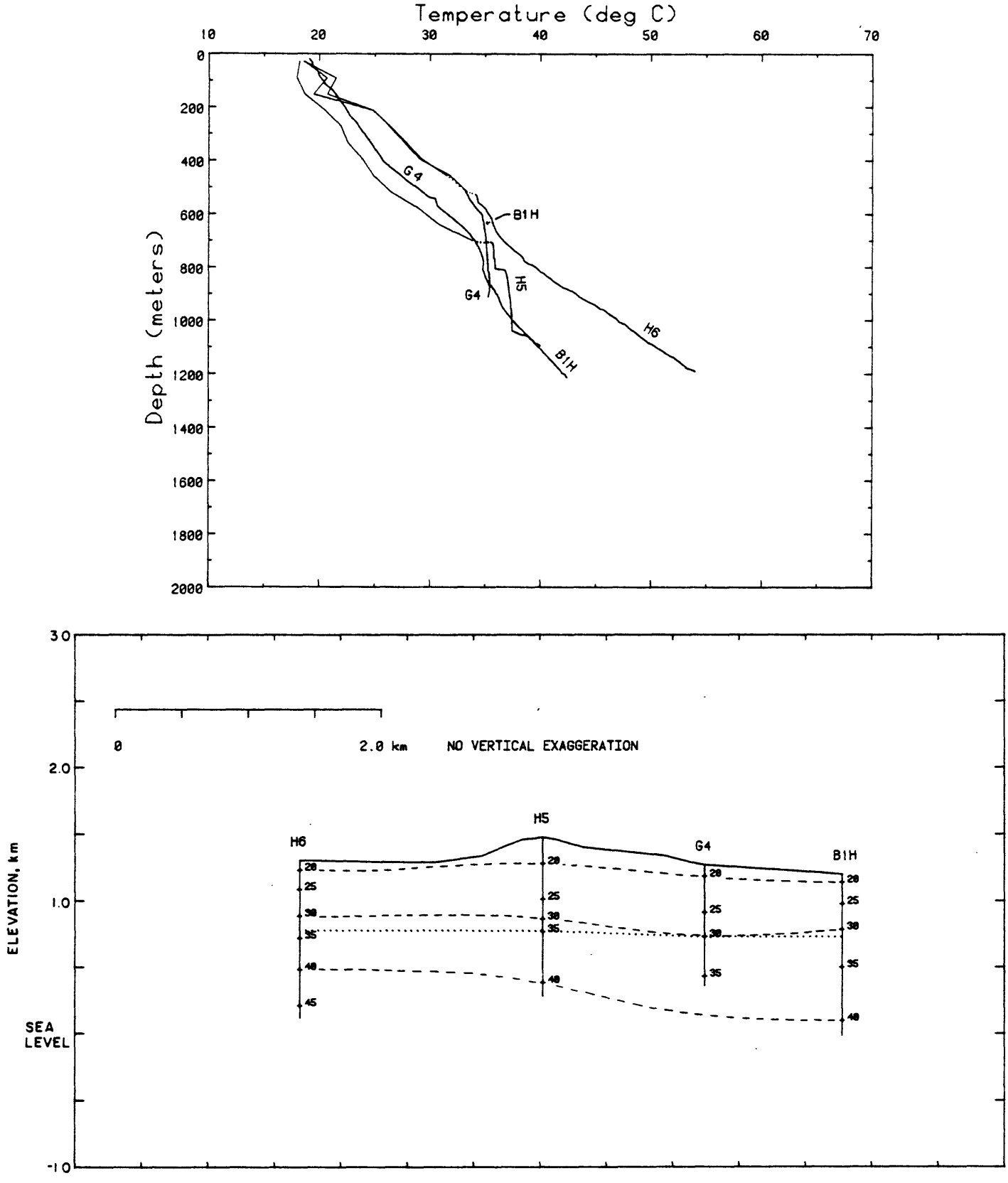

Figure 8. Thermal profile, H6-B1H (Figure 3). Temperature profiles are plotted above with common origin. Dashed lines, isotherms; dotted line, static water level.

geologic, hydrologic, and geophysical properties of the pre-Tertiary rocks, which were identified as Silurian dolomites (Carr and others, 1986) that comprise part of the "lower carbonate aquifer" defined by Winograd and Thordarson (1975). Below the contact between volcanic rocks and that aquifer at a depth of about 1200 m (Figure 4 and 1-19) the temperature profile becomes nearly isothermal, then reverses indicating a complex pattern of lateral throughflow of higher temperature water (cf. profile and cross section, Figures 4 and 5).

We examined the temperature profile from Ue25p1 in the light of hydraulic head and temperature data of Craig and Robison (1984) and of some additional geologic data (Carr and others, 1986). The analysis suggests that the apparent anomaly at this site could be explained in terms of the breaching (by the drill) of a hydraulic barrier in the lower part of the tuffs above the Paleozoic carbonate sequence, causing a relatively long-lived transient thermal response to annular uphole flow previous to our only temperature log in the saturated zone. This suggestion is testable in part by additional thermal profiling but can be resolved completely only by completing a well in the Paleozoic carbonate rocks and grouting in a water-filled access pipe. As this procedure is beyond the scope and timing of the present report, we are retaining a literal interpretation of our observations (Figures 4, 5, and 1-19) with the caveat that further observations may change the interpretation significantly. The important indications of both thermal and hydrologic observations at the Ue25p1 site are that locally, there is a strong potential for a net vertical upflow from the Paleozoic carbonate aquifer. Whether this is actually occurring requires additional observation.

The north-south cross section along the ridge (G3 - H5, Figures 3 and 7) features widely separated isotherms (low temperature gradients) and local

vertical flow below the water table, particularly for USW H5 (see temperature profile, Figure 7). The cross section otherwise is undistinguished with all relevant surfaces nearly parallel to the topography along strike. The section across the ridge (H6 - B1H, Figures 3 and 8) provides some evidence for lateral water flow away from the ridge in an easterly direction. Local upflow with vertical seepage velocity (v) of about 0.1 meter per year is suggested in USW G4 (Figure 9) and both upward and downward components of flow are evident in the profile from UE25B1H (Figure 8 and 1-6). For a detailed review and documentation of the one-dimensional vertical seepage calculation, the reader is referred to Sass and others (1980).

Measurements in air in the WT-series and UZ-1. As the focus of engineering studies shifted from the saturated to the unsaturated zone (UZ), it seemed important to obtain as many thermal data as possible above the water table in support of hydrologic investigations. We routinely logged above the water table in the G- and H-series test wells, the preferred configuration being an access pipe plugged at the bottom and filled with water to allow good thermal contact for the temperature probe and thus a continuous temperature log. In UZ-1, the principal activity was detailed monitoring of the unsaturated zone in its natural state. Thus the risk of introducing water into the system via a leaky coupling was considered too high for our preferred completion. The WT-series was completed with a single, open piezometer to monitor water levels. These wells were thus also unsuitable for water-filled pipes, and we were forced to settle for single point measurements at 100 or 200 foot (30.5 - 61 m) intervals. The measurement technique and method of data reduction are described in detail in Appendix 2 which also contains individual temperature profiles. Thermal gradients in the UZ (Figure 10) vary laterally from about 20°C/km to nearly 60°C/km. In the

absence of corresponding lateral variations in thermal resistivity, this suggests a lateral variation in heat flow which we discuss further in a later section.

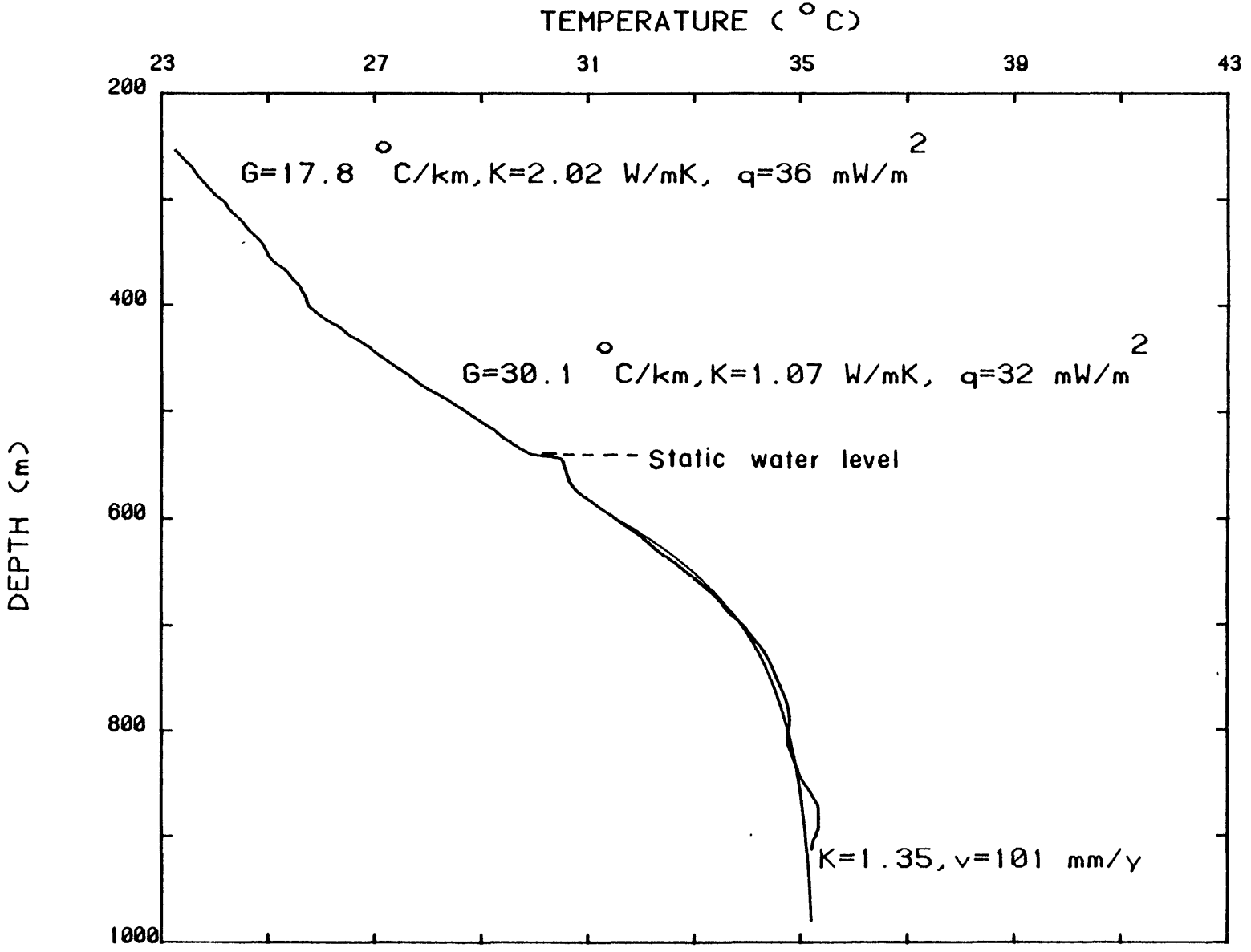

Figure 9. Temperature profile, heat-flow calculations (G is gradient, K is thermal conductivity, q is heat flow) above the water table and a one-dimensional model calculation (smooth curve, see Lachenbruch and Sass, 1977; Sass and others, 1980) for well USW G-4.

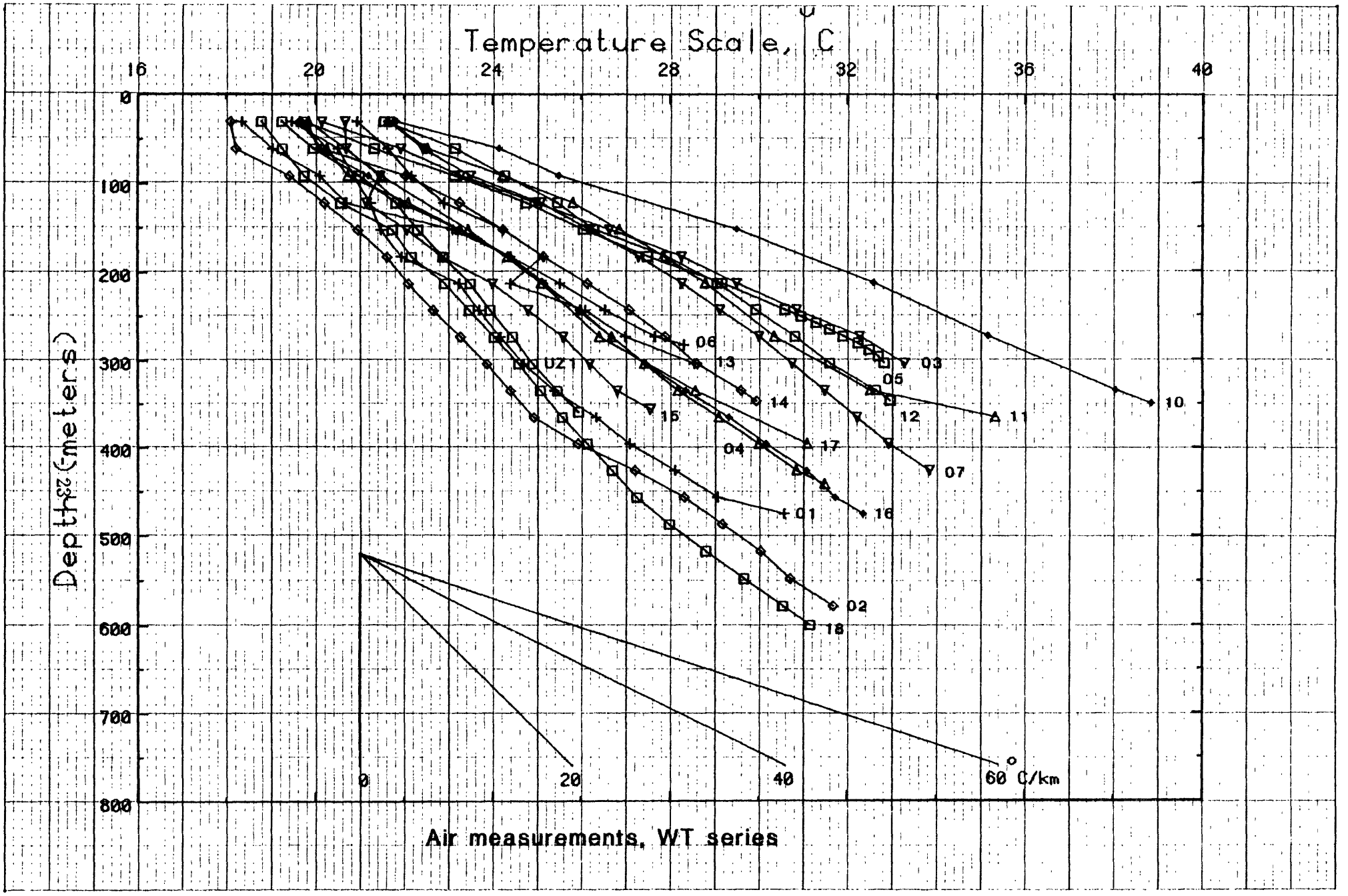

Figure 10. Temperature profiles from WT series wells (see Appendix 2 for individual profiles).

From a consideration of individual temperature profiles in Appendices 1 and 2, we may infer that heat transfer above the water table (i.e., in the unsaturated zone) is primarily by conduction. Most temperature profiles in the UZ are linear or consist of linear segments, the significant exception being "conductor" well UE25a7 in drillhole wash (Figures 1-1 and 1-5), which is discussed in detail in Appendix 1. Ue25a7 apparently responded almost instantaneously to a depth of 150 m to a flash flood following a locally heavy rain. The primary conduit may have been the annulus between casing and borehole wall, but the persistence of the disturbance for at least a year indicates that significant lateral infiltration occurred near or in this well.

The apparent conductive nature of the temperature profiles in the UZ may be the result of the wide separation in data points (see discussion, Appendix 2). Measurements in water-filled access pipes might well reveal significant thermal structure in the UZ on the scale of tens of meters. Linear segments of UZ temperature profiles having different gradients are in rocks of correspondingly different thermal conductivity (see in particular, discussion of G-4 in "heat flow"). By contrast, although portions of many temperature profiles below the water table are linear (particularly below a depth of 1 km), heat transfer in the saturated zone seems to be disturbed by lateral and vertical fluid motion over much of the study area (see individual profiles, Appendix 1 and Figures 4 through 8).

THERMAL CONDUCTIVITY

A total of 204 determinations of thermal conductivity was performed on specimens of solid core from coreholes in the Yucca Mountain area. Individual values of thermal conductivity are tabulated in Appendix 3. The results are summarized in Table 3 by lithologic unit and according to whether the rocks were saturated or unsaturated. For the unsaturated zone, the range of values is greater than that for the saturated zone (Figure 11), but the means are not significantly different. Unsaturated conductivities have a bimodal distribution with peaks at about 1 and 2 $Wm^{-1} K^{-1}$, reflecting different degrees of welding. By contrast, the conductivities from the saturated zone have a near-normal distribution, and the deviations from the mean are probably the result of variations in porosity and mineralogy. To the extent that degree of welding and porosity are negatively correlated, and that welded tuffs tend to incorporate minerals of relatively high thermal conductivity, welded saturated tuffs tend also to be more conductive than non-welded. Because of the subjective nature of "degree of welding," however, we choose not to attempt a numerical correlation.

Correlation of thermal conductivity with compressional wave velocity from well logs. A number of workers have attempted correlations between thermal conductivity and various well-log parameters. For monomineralic aggregates or those not containing variable amounts of exotic constituents with extreme values of conductivity, such well-log parameters as neutron porosity (ϕ) and compressional wave velocity V_p can be used with some success as predictors of thermal conductivity.

Goss and Combs (1975) used such relations to predict thermal conductivities for the Imperial Valley in California. We had V_p-log information at depths corresponding to 130 of our conductivity determinations

TABLE 3. Average thermal conductivities for various tuff units of Yucca Mountain and for Paleozoic rocks from UE-25p1

Designation	Unit	Thermal conductivity $Wm^{-1} K^{-1}$							
		N	unsat	S.D.	S.E.	N	sat	S.D.	S.E.
Tpb	Paintbrush Tuff, bedded tuffs	2	0.78	0.13	0.13				
Tpc	Paintbrush Tuff, Tiva Canyon Mem.	5	1.86	0.35	0.15				
Tpp	Paintbrush Tuff, Pah Canyon Mem.	3	1.12	0.36	0.21				
Tpt	Paintbrush Tuff, Topopah Spr. Mem.	31	1.87	0.36	0.07	1	1.16		
Tht	Tuff beds, Calico Hills	7	1.08	0.16	0.06	11	1.22	0.11	0.03
Tcp	Crater Flat Tuff, Prow Pass Mem.	5	1.47	0.62	0.28	12	1.42	0.21	0.06
Tcb	Crater Flat Tuff, Bullfrog Mem.	4	1.94	0.07	0.03	20	1.63	0.26	0.06
Tct	Crater Flat Tuff, Tram Mem.					34	1.72	0.26	0.04
Tfb	Flow breccia					4	1.68	0.26	0.13
Tlr	Lithic Ridge Tuff					27	1.84	0.18	0.03
Tllr	Rhyolitic lava - flow breccia					3	2.25	0.18	0.11
Tllq	Qtz-latitic lava - flow breccia					5	2.07	0.24	0.11
Tlld	Latitic lava - flow breccia					3	2.32	0.24	0.14
Tta	Older ash flows - bedded tuffs. Units A, B, and C.					6	2.01	0.15	0.06
Ttb						1	2.12		
Ttc						7	1.87	0.09	0.03
Slm	Lone Mtn. dolomite					12	4.90	0.25	0.07
Srm	Roberts Mtn. Fm.					1	5.47		
All		57	1.66	0.49	0.06	134*	1.72	0.32	0.03

*Excluding Paleozoic rocks from UE25-p1

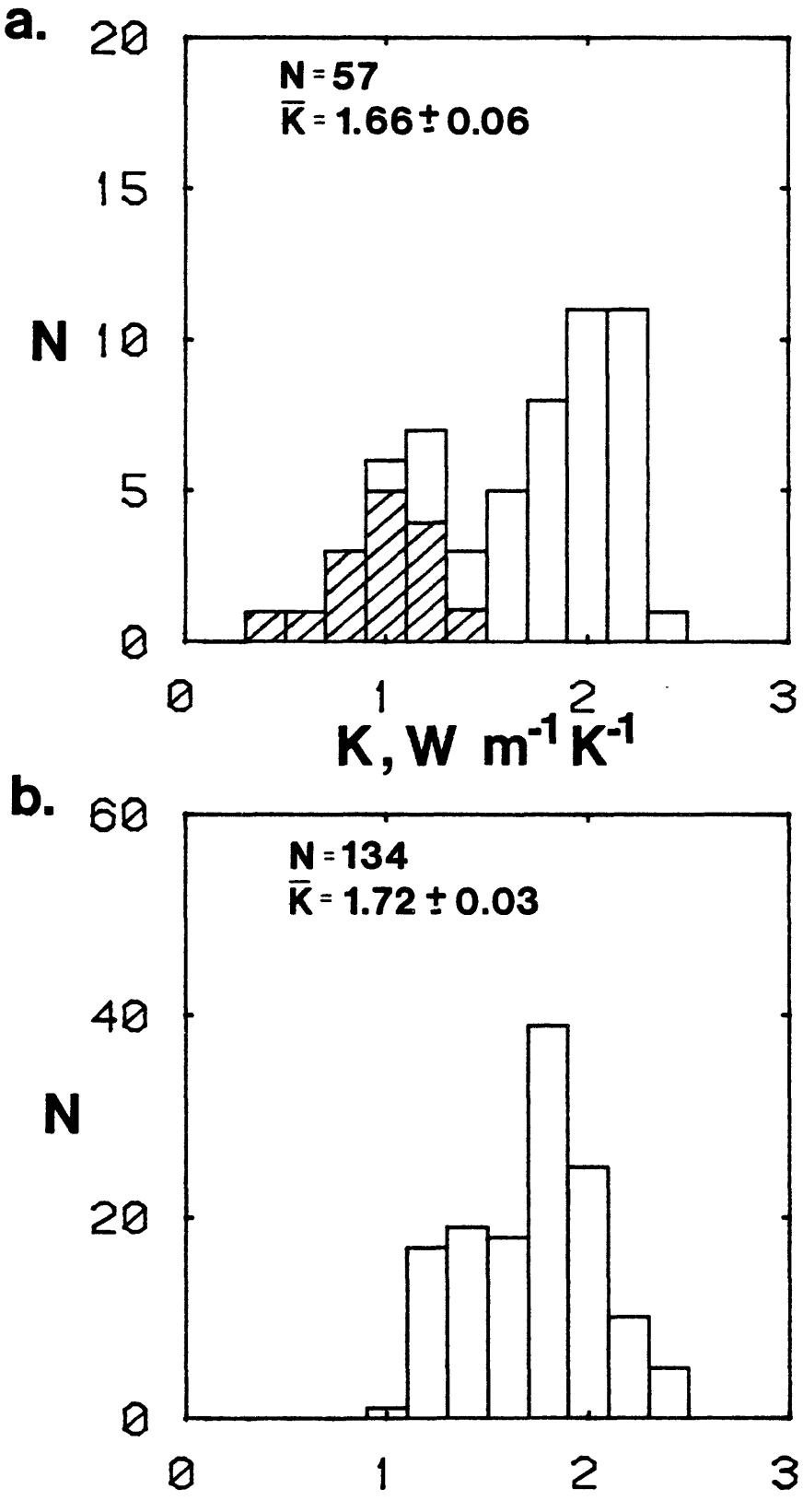

Figure 11. Histograms of thermal conductivity of tuffs from Yucca Mountain, Nevada: (a) unsaturated zone; cross-hatched non-welded, unshaded, welded; (b) saturated zone.

from the G-series wells (Muller and Kibler, 1984; Spengler and Chornack, 1984; D. C. Muller, written commun., 1983, 1984). Coefficients for linear regression of K on V_p are listed for each of the G series wells and for the combined sample in Table 4. The regression line for the combined sample, together with the data plot is shown in Figure 12. There is considerable scatter, but a definite correlation exists. We estimate, based on the RMS residual of 0.2 $Wm^{-1} K^{-1}$ for the general relation (Figure 12) that we can predict thermal conductivity from compressional wave velocity to within ±10 percent to 15 percent.

TABLE 4. Linear regression of thermal conductivity (K, $Wm^{-1} K^{-1}$) on compressional wave velocity (V_p, km s^{-1}) for G series wells, Yucca Mountain, Nevada

Well	N	Coefficient of correlation	Intercept (SE)	Slope (SE)
USW G-1	52	0.65	0.086 (0.08)	0.438 (0.072)
USW G-2	40	0.87	-0.382 (0.04)	0.564 (0.053)
USW G-3	24	0.50	0.406 (0.22)	0.337 (0.125)
USW G-4	14	0.69	0.022 (0.19)	0.430 (0.130)
All wells	130	0.78	-0.197 (0.02)	0.509 (0.036)

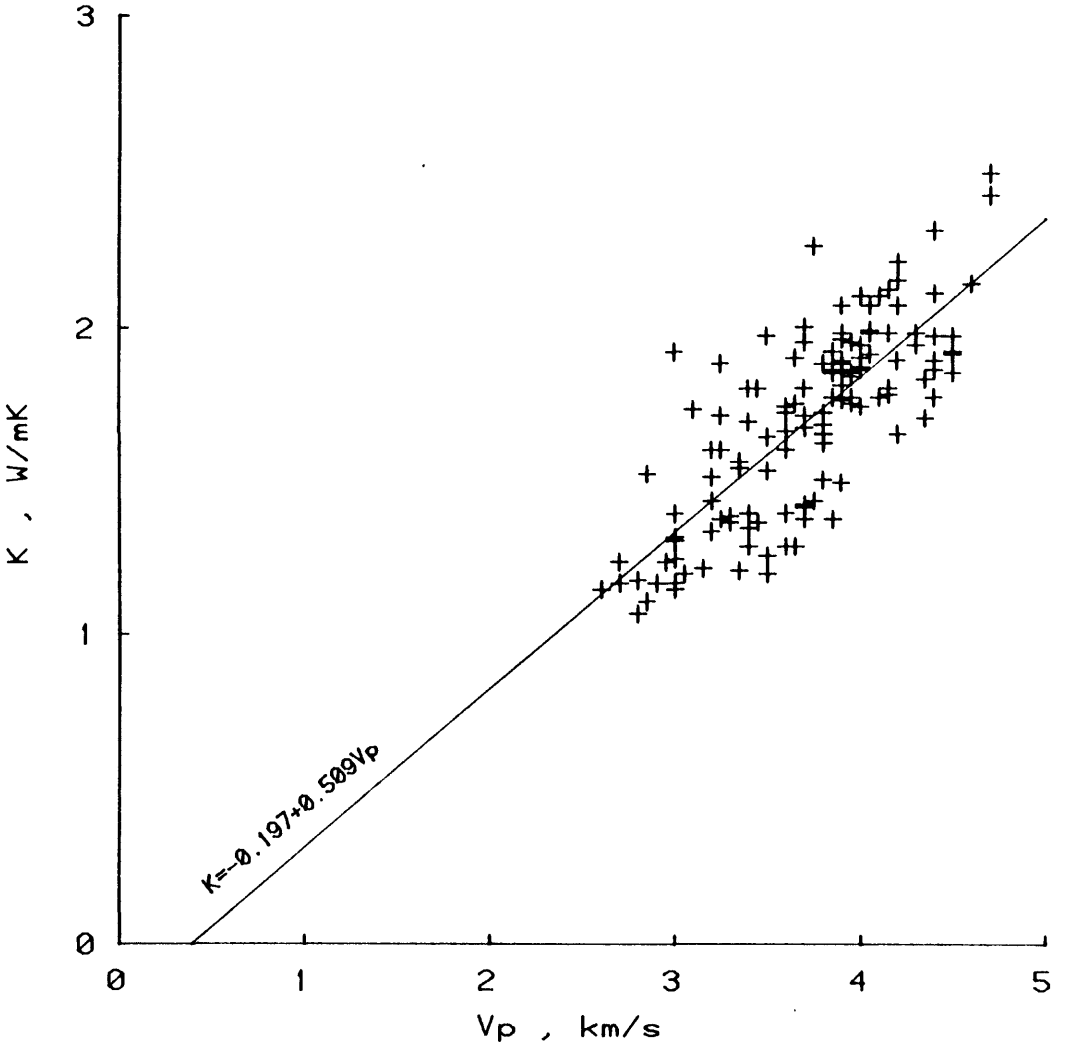

Figure 12. Thermal conductivity (K) as a function of compressional wave velocity (V_p) for tuffs from core holes at Yucca Mountain.

HEAT FLOW

The study area is near the southern boundary of a regional heat-flow anomaly, the Eureka Low (Figure 13). Hydrologic studies of the region (e.g., Winograd and Thordarson, 1975) indicate a complex interbasin flow in Paleozoic carbonate aquifers. This flow has a downward component with seepage velocity on the order of a few centimeters per year to depths as great as 3 km. Flow in the regional aquifer beneath Yucca Mountain discharges by evapotranspiration and perhaps at springs south and southwest of Yucca Mountain (Figure 1). Average heat flow in the Eureka Low is about half that for the adjacent region. Lachenbruch and Sass (1977) calculated that, if the average depth to the interbasin conduit were about 1.4 km, this could be accomplished by downward percolation with seepage velocity of 1 cm/yr. This is consistent with the observations of Winograd and Thordarson (1975) and with a more recent hydrologic study of the Yucca Mountain region by Waddell and others (1984). It is also consistent with a preliminary one-dimensional interpretation of the variation of heat flow with depth in well USWG-1 (Sass and Lachenbruch, 1982). Heat-flow data that were available from near Yucca Mountain in 1981 and earlier (Sass and others, 1980; Sass and Lachenbruch, 1982) were interpreted as a local excursion of the 63 mWm^{-2} contour (1.5 heat-flow units), which defines the boundary of the Eureka Low (Figures 13 and 14). The interpretation of Figure 14, from Sass and Lachenbruch (1982), shows this excursion and includes the Yucca Mountain area within the Eureka Low. It could as easily have been contoured as an isolated thermal sink with then-existing heat-flow data. For either interpretation, the tectonic implications of the heat-flow data are largely inconclusive, inasmuch as the true regional heat flow is obscured by hydrologic processes. The regional data outside the Eureka Low suggest a

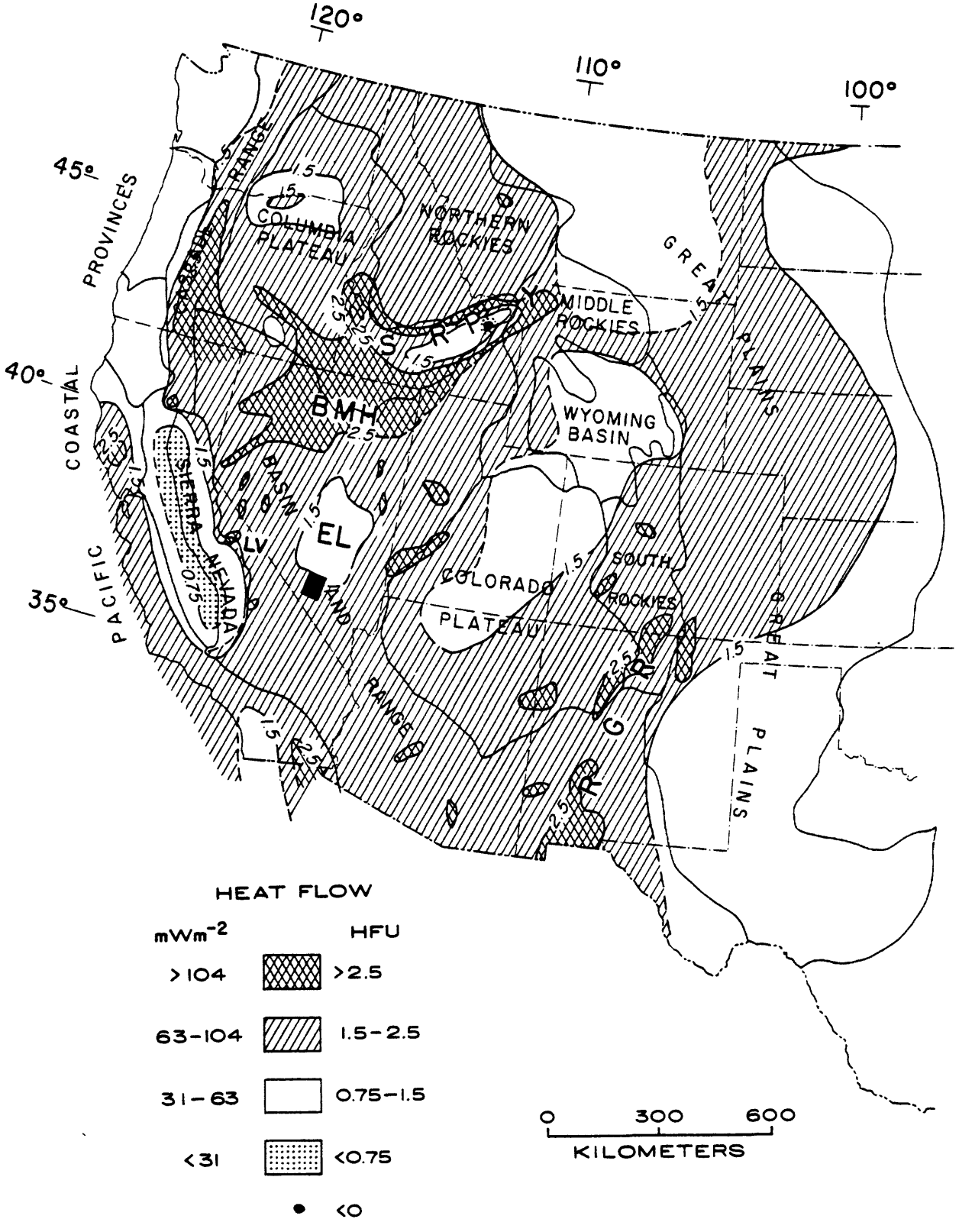

Figure 13. Distribution of heat flow in the western United States (after Sass and others, 1981). Abbreviations: SRP, Snake River Plain; BMH, Battle Mountain High; EL, Eureka Low; RGR, Rio Grande Rift zone; Y, Yellowstone; LV, Long Valley. Black box at the south end of EL is location of Figure 14.

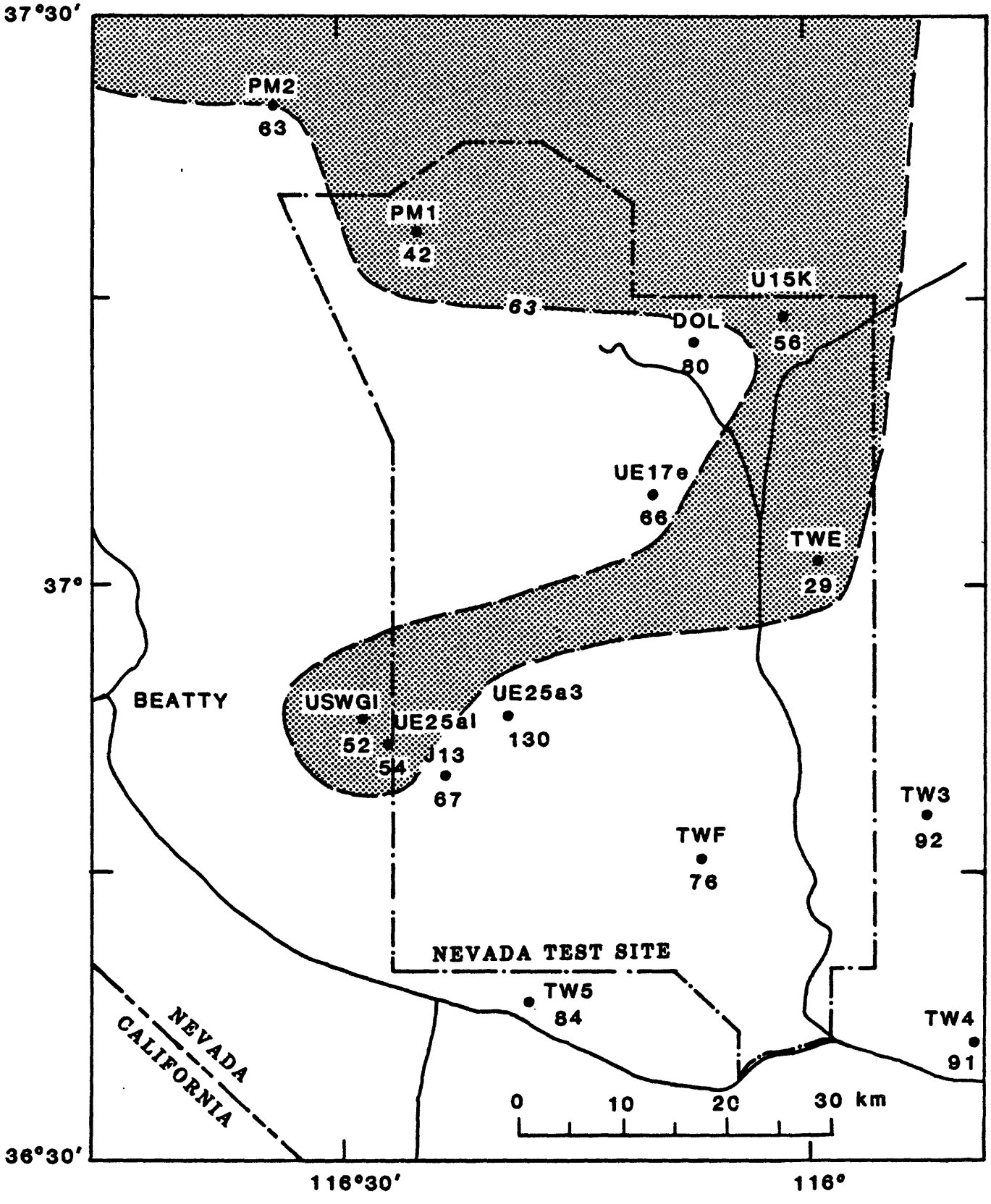

Figure 14. Configuration of 63 mW m^{-2} contour (1.5 heat-flow units) in the vicinity of the Nevada Test Site (from Sass and Lachenbruch, 1982). Stippled area has heat flow less than 63 mW m^{-2}.

regional heat flux (65-90 mWm^{-2}) typical of the average for the Basin and Range. However, higher heat flows cannot be ruled out entirely. In fact, Swanberg and Morgan (1978) include the entire Nevada Test Site in a southerly extension of the Battle Mountain High (Figure 13) based on the application of an empirical relation between heat flow and silica geotemperatures. However, the abundance of highly soluble volcanic glass in the rhyolitic rocks of southern Nevada casts serious doubt on the validity of uncompensated silica geotemperatures in this area.

Three methods were applied to the current data from the geologic and hydrologic test wells in order to estimate conductive heat flow (q) for both saturated and unsaturated zones (Table 5). The preferred method is to combine the least-squares thermal gradient, Γ, for a linear interval of a given temperature profile with the harmonic mean thermal conductivity, $\langle K \rangle$, from the same interval according to

$$q = \langle K \rangle \cdot \Gamma \qquad (1)$$

Because all thermal conductivity specimens came from the G series of coreholes, this method could be used only in these wells. In the second method, the weighted formation average was substituted for the harmonic mean. Third, where velocity logs were available, the relation between K and V_p (Table 4, Figure 12) was used to estimate the appropriate K. We evaluated the formation average method by comparing values calculated by equation (1) with those calculated using the weighted formation average. Agreement between the two methods was excellent (within about 15%, Table 5), lending credence to our estimates of thermal conductivity in other wells.

Estimates of heat flow from the unsaturated zone were also made in UZ1 and the WT series of wells (Table 6). These values, together with the UZ

heat flow from Table 5, are plotted and contoured in Figure 15; they have a systematic geographic distribution. The southernmost group of wells have heat flows approaching regional values (Figure 15). The lowest heat flows are within a kilometer or two of USWG-4 which is near the location of the planned exploratory shaft and within the area of the proposed repository. We also note that the heat flow in the UZ correlates negatively with the thickness of the UZ (Figure 16). Within the area of Figure 15, this thickness is generally greatest in the proposed repository area. The heat flow from the UZ at G4 is probably the best documented of all. It is based on a large number of measured thermal conductivities and on a thermal profile obtained in water-filled tubing. Between 150 and 400 m (Figure 1-12, Figure 9, Table 5), the gradient is 17.8±0.04 (SE) °C/km and 13 samples of the densely welded Topopah Spring member of the Paintbrush Tuff yield a well constrained average thermal conductivity of 2.02±0.06 W m^{-1} K^{-1}. The heat flow from equation 1 is 36±1 mWm^{-2}. Just below 400 m, there is an abrupt increase in gradient to 30.1±0.06°C/km and a corresponding decrease in conductivity (from eight samples of the unwelded tuffaceous beds of Calico Hills) to 1.07±0.04 resulting in a heat flow of 32±1 mWm^{-2}. Considering the numerous sources of possible error, the agreement between these two independent heat-flow determinations is excellent, supporting our conclusion that heat flow in the UZ is primarily by conduction. Also of interest is the inference (from the curvature of the temperature profile) that the upward component of seepage velocity in the saturated zone at this site is about 100 mm per year.

For the nine wells providing both SZ and UZ heat-flow estimates, the mean values determined from Table 5 are very similar, 40 mW m^{-2} for the SZ and 41 mW m^{-2} for the UZ. However, estimates for the SZ are strongly

TABLE 5. Heat-flow estimates from test wells near Yucca Mountain, Nevada

Well	Depth range (m)	Method*	Heat flow mWm^{-2}	
			q_{uns}	q_{sat}
USW G-1	100-527	2	41	
	1067-1697	1		53
USW G-2	200-526	1	42	
		2	45	
		Avg	44	
	610-1250	1		52
		2		54
		Avg		53
USW G-3/GU-3	100-751	1	39	
		2	44	
		Avg	42	
	750-1360	1		27
		2		29
		Avg		28
USW G-4	150-402	1	36	
		2	32	
		Avg	34	
	410-541	1	32	
		2	37	
			34	
USW H-1	80-454	2	34	
	1000-1830	2		54
		3		46
		Avg		50
USW H-3	150-750	2	40	
	750-1200	2		42
		3		52
		Avg		47
USW H-4	65-520	2	34	
	520-1220	2		24
		3		26
		Avg		25

TABLE 5. Heat-flow estimates from test wells near Yucca Mountain, Nevada (continued)

Well	Depth range (m)	Method*	Heat flow mWm^{-2}	
			q_{uns}	q_{sat}
USW H-5	165-700	2	41	
	720-1220	2		27
USW H-6	100-526	2	49	
	530-1210	2		51
UE25a4	100-150	2	29	
UE25a5	100-150	2	32	
UE25a6	75-150	2	47	
UE25a7	180-270	2	33	
UE25a1	150-469	2	48	
b1H	470-1220	2		23
UE25p1	80-380	2	62	
J-13	130-262	1	65	
		2	67	
		Avg	66	

*Method 1: Least-squares gradient × harmonic mean of measured conductivities over same interval.

Method 2: Least-squares gradient × conductivity calculated from formation means.

Method 3: Least-squares gradient × harmonic mean of conductivities inferred from K vs. V_p relation.

TABLE 6. Heat-flow estimates (±SE) from the unsaturated zone in UZ-1 and WT series wells based on average formation conductivities

Well	Depth range (m)	Member	K* $Wm^{-1} K^{-1}$	Γ °C km^{-1}	q mWm^{-2}
UZ-1	30-90	Tpp	1.12	28.5	32
	122-350	Tpt	1.87	17.1	32
				Mean	32
WT-1	30-144	Tpc	1.86	15.7	29
	144-422	Tpt	1.87	23.2	43
	422-475	Tht	1.08	41.5	45
				Mean	39±5
WT-2	82-397	Tpt	1.87	19.7	37
	397-488	Tht	1.08	35.7	39
	488-628	Tcp	1.47	25.3	37
				Mean	38±1
WT-3	30-112	Tpt	1.87	51.5	96
	112-154	Tht	1.08	55.3	60
	154-257	Tcp	1.47	42.8	63
	257-305	Tcb	1.94	39.7	77
				Mean	74±8
WT-4	30-86	Tpc	1.86	17.2	32
	86-132	Tpp	1.12	41.7	47
	132-352	Tpt	1.87	26.4	49
	352-442	Tht	1.08	30.4	33
				Mean	40±5
WT-5	30-180	Tpb	0.78	51.1	40
	180-305	Tpc	1.86	44.4	82
				Mean	61±21
WT-6	52-117	Tpt	1.87	26.6	50
	117-290	Tht	1.08	43.2	47
				Mean	48±2
WT-7	30-120	Tpc	1.86	37.1	69
	120-427	Tpt	1.87	27.9	52
				Mean	60±8
WT-10	46-191	Tpb	0.78	58.6	46
	191-290	Tpc	1.86	42.2	78
	290-350	Tpt	1.87	48.0	90
				Mean	71±13
WT-11	30-96	Tpc	1.86	42.2	78
	96-366	Tpt	1.87	36.2	68
				Mean	73±5

TABLE 6. Heat-flow estimates (±SE) from the unsaturated zone in UZ-1 and WT series wells based on average formation conductivities (continued)

Well	Depth range (m)	Member	K* $Wm^{-1} K^{-1}$	Γ $°C\ km^{-1}$	q mWm^{-2}
WT-12	30-110	Tpc	1.86	42.1	78
	110-350	Tpt	1.87	33.2	62
				Mean	70±8
WT-13	67-155	Tpc	1.86	21.6	40
	155-305	Tpt	1.87	31.4	59
				Mean	50±10
WT-14	33-350	Tpt	1.87	32.6	61
WT-15	128-350	Tpt	1.87	26.9	50
WT-16	175-325	Tpt	1.87	26.9	50
	325-472	Tht	1.08	28.0	30
				Mean	40±10
WT-17	30-75	Tpc	1.86	27.2	51
	75-300	Tpt	1.87	27.0	51
	300-371	Tht	1.08	38.4	42
				Mean	48±3
WT-18	30-110	Tpc	1.86	15.8	29
	110-214	Tpp	1.12	24.6	27
	214-493	Tpt	1.87	18.0	33
	493-610	Tht	1.08	28.3	31
				Mean	30±1

*Average conductivity for member, see Table 3.

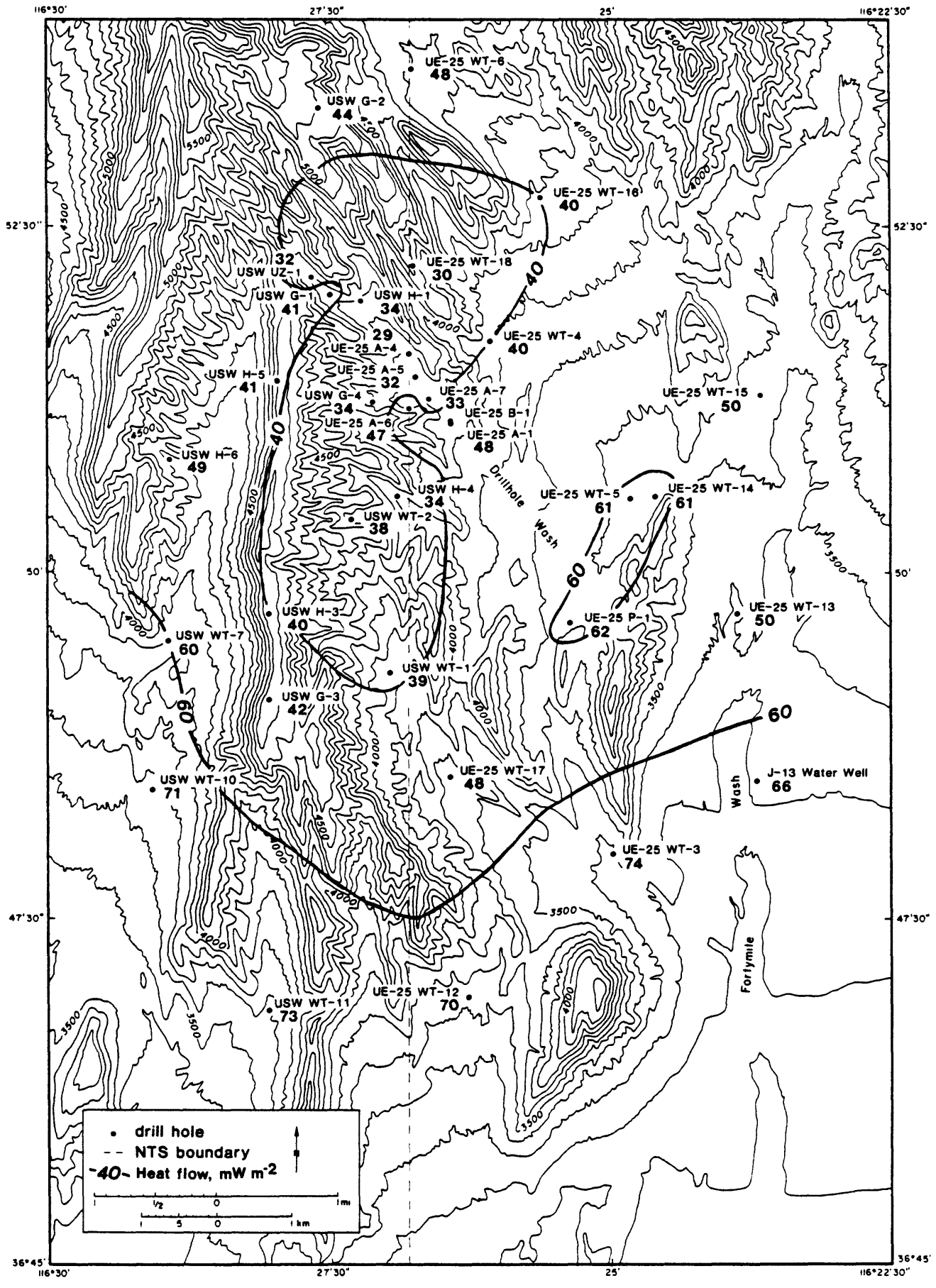

Figure 15. Conductive heat flow from the unsaturated zone in the vicinity of Yucca Mountain (see Index, Figure 1).

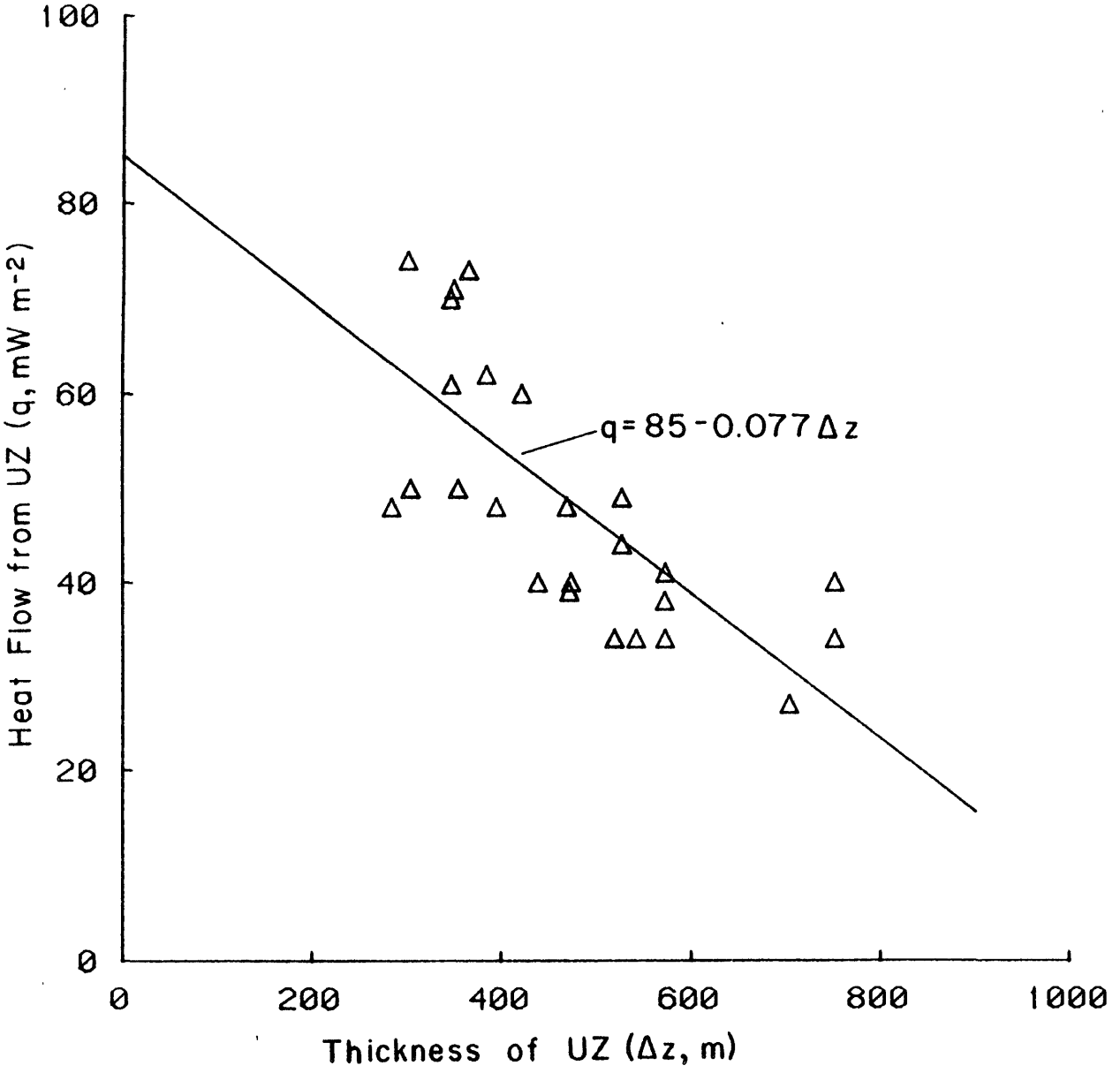

Figure 16. Heat flow from the unsaturated zone as a function of the thickness of the zone.

bimodal (Figure 17B), and those comprising the lower group (USW G-3, USW H-4, USW H-5, and UE25b1) have SZ heat flows that are substantially less than the UZ values (Figure 17C) for the same wells. The temperature profiles in these wells and in USW G-1 and USW H-6) are non-linear, indicating upward or downward flow of water in the well bore or the surrounding formations (see profiles in Appendix 1). The least-squares temperature gradients used to calculate the heat flows on Table 5 were determined for all or most of the SZ parts of the wells. Because flow in either direction generally increases the efficiency of heat transfer, thereby suppressing gradients in the affected interval, the calculated estimates are probably minimum values. We are more confident of the estimates for USW G-1, USW H1, and USW H-3, which were based on gradients defined by long, apparently conductive segments.

An alternative approach to defining gradients on hydraulically disturbed temperature profiles is to force measurements on short linear segments in the deepest parts of the wells, where the probability of significant in-hole flow is least. This procedure involves the risk of including sections of distributed inflow or outflow, as well as the risk of forcing use of the data beyond their limit of reliability. However, hydrologic testing in the Yucca Mountain area indicates that hydraulic conductivity is provided mainly by thin, discrete intervals, which are probably fracture-controlled (Waddell and others, 1984). Under these conditions, the assumption that linear segments of at least several tens of meters represent zones of primarily conductive heat flow may be justified. The depths and thermal gradients of these segments for the wells in question are discussed in Appendix 1.

We calculated alternative heat-flow estimates, using average thermal conductivities (Tables 3-2 and 3-3) for the appropriate depths in USW G-2

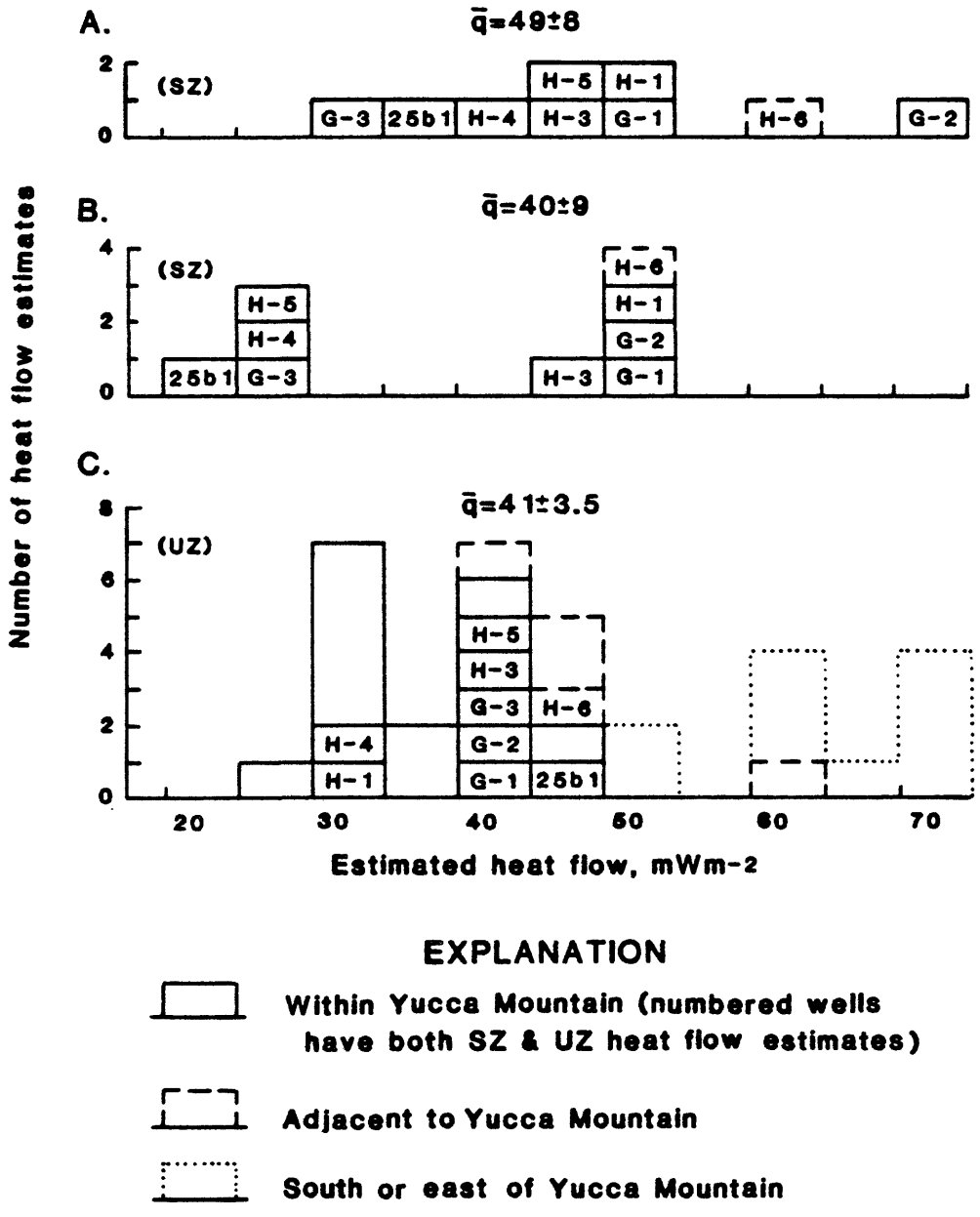

Figure 17. Comparison of heat-flow estimates for the unsaturated zone (C) with those for the saturated zone using the least-squares gradients (B) and gradients of linear segments (A). $\bar{q}$ is average for numbered wells $\pm$95% confidence limits.

and USW G-3 and the weighted formation averages for the other four holes. The revised distribution is shown in Figure 17A, as compared with Figure 17B. Heat flows for the SZ in USW G-3 and UE25b1 are still less than those for the UZ, although the differences are reduced. It is questionable that the gradient (21°C/km) in the interval used for USW G-3 represents the actual, undisturbed conductive gradient, as the interval (1000-1280 m) is considerably above the 1533-m total depth of penetration. In UE25b1, however, the interval used, 1000-1220 m extends to the total drilled depth. The mean for the nine holes is increased to 49±8 mW m^{-2} (Figure 17A), however, within the limits of 95% confidence, neither SZ mean is significantly different from that for the UZ (Figure 17).

The geographic influence on UZ heat flow is clearly evident in Figure 17C, which includes all of the UZ estimates. Wells that are within the smoothed boundary of Yucca Mountain (Figure 15) have the lowest heat flows. Those that are closely adjacent have intermediate values, and those farther east and south have the highest.

With reference to the regional heat flow (about 85 mW m^{-2}) outside of the Eureka Low, the deficiency at the repository site is 35-45 mW m^{-2} for the SZ and 45-50 mW m^{-2} for the UZ. We can conclude that 80%, and perhaps all, of the anomaly is attributable to the SZ. The removal of significant amounts of heat from the SZ requires intense lateral flow of relatively cool water in regional aquifers. In active recharge areas, infiltration further reduces surface heat flow according to the one-dimensional relationship (Lachenbruch and Sass, 1977, equation 8),

$$\Delta q[mW/m^{-2}] \cong 0.14\ V_w\ [mm/yr] \times G\ [°C/km] \times \Delta z\ [km], \qquad (2)$$

where Δq is the reduction of surface heat flow, V_w is the downward infiltration rate, G is the thermal gradient, and Δz is the depth of infiltration

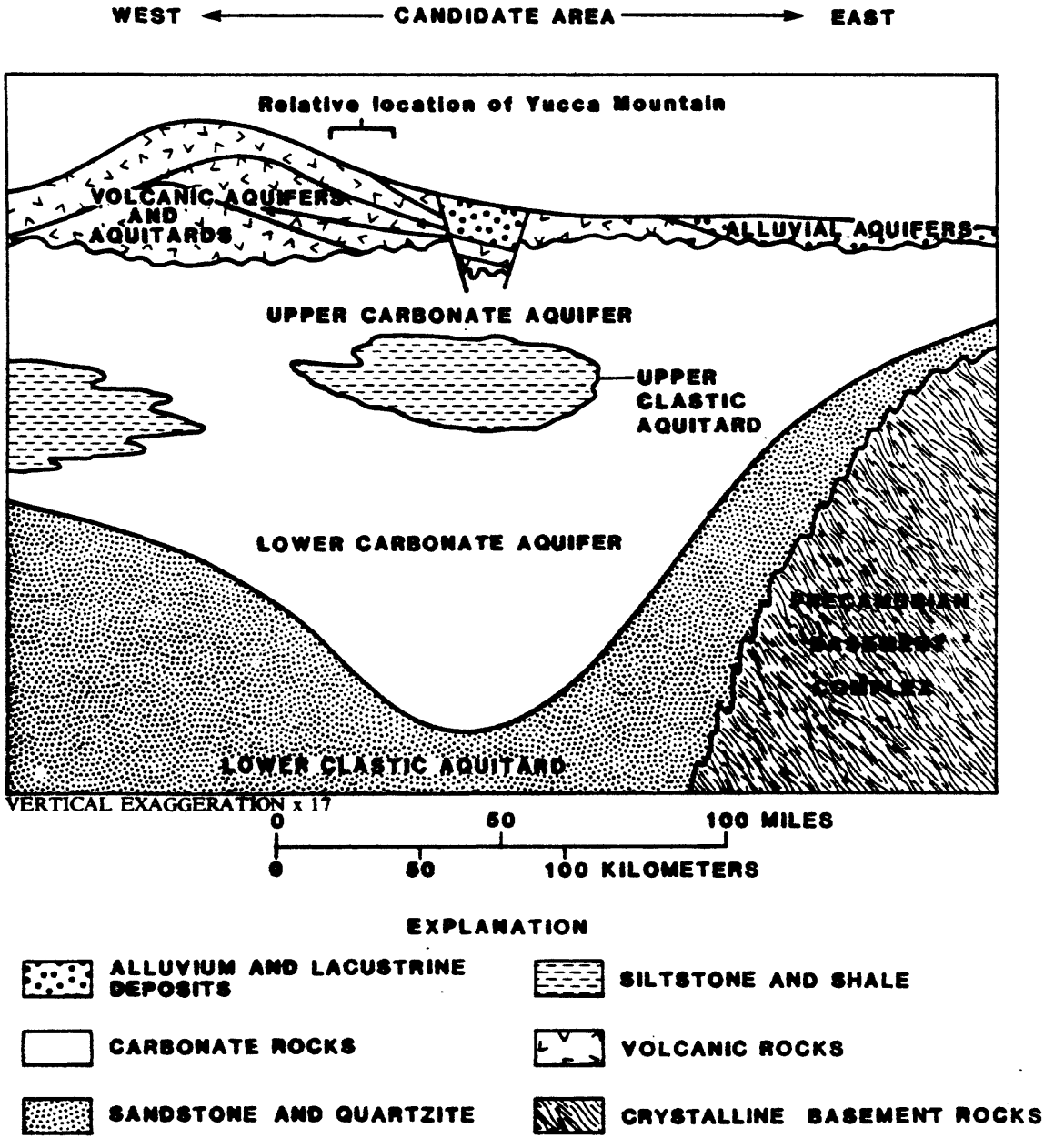

Figure 18. Stratigraphic relationships among hydrostratigraphic units near Yucca Mountain (reproduced with permission from Figure 2 of Waddell and others, 1984).

to the regional aquifer. In the previously defined Eureka Low (Figure 13), downward percolation may persist to depths of 4 km or so, and recharge rates of 2 to 3 mm/yr on a regional scale would produce the observed reductions. It is tempting to call upon the same process in explaining the heat-flow anomaly at Yucca Mountain because of its proximity to the Eureka Low, the great depth of the water table, and the probable occurrence of the regional carbonate aquifer at depths of 2-4 km (Figure 18). Downward infiltration of a few mm/yr would account for the anomaly. However, a necessary constraint is that the thermal and hydrologic data that are available must at least be consistent with the dominance of downward components of flow over upward components. Short segments of some of the Yucca Mountain SZ temperature profiles indicate downward flow, but upward flow is indicated by others, most notably and persistently in USW G-4 (Figure 9). Furthermore, Robison (1984) reports significant hydraulic potentials for upward flow at USW H-1, USW H-3 and UE25p1. Hence, the existing limited data do not support pervasive downward flow throughout the vicinity of Yucca Mountain as the principal cause of the average SZ heat-flow deficiency. For the area of Figure 15, pervasive lateral flow in the Paleozoic carbonates with a net downward component of velocity is the most likely principal cause of the anomaly.

Neither the hydrologic nor the thermal data rule out locally heavy recharge within the study area as a significant factor. Heavy infiltration along permeable, high angle fractures at high elevations would produce the observed potential for upward flow in less permeable systems or systems with impermeable caps at lower elevation. This type of gravitationally driven convection is common in many regions of the Basin and Range (see e.g., Mase and others, 1982).

The possible additional reduction of heat flow (5-10 mW m^{-2}) in the UZ, if confirmed, could be attributed to the coupled action of three processes. The first, downward infiltration, can be limited by equation 2, using 14°C as the typical produce of $G \times \Delta z$ (Figure 10). This small UZ anomaly could be accounted for by 2-5 mm/yr of infiltration, about an order of magnitude greater than that postulated from hydrologic considerations (Montazer and Wilson, 1984). D. T. Snow and Parviz Montazer (written communications, July and April 1987) have suggested the additional processes of vaporization and of advective transport of heat in upward movement of air (presumably containing water vapor). The latent heat of liquid water is about 580 cal/cm^3. Therefore, the vaporization of only 0.1 mm/yr would consume about 5.8 cal/cm^2/yr, which is about 8 mW m^{-2} or approximately the UZ heat-flow deficiency. Vaporization requires the circulation of air through the mountain. As currently postulated (Parviz Montazer, written communication, April 1987), cool, dry air enters the outcrop of the Topopah Spring member (fractured welded tuff) low on the west side of the mountain and discharges near its crest. By analogy with equation 2 and again using 14°C as the temperature differential, we can estimate an upper limit of the air discharge, V_a, from

$$v_a = \frac{\rho_w C_w}{\rho_a C_a} V_w \quad , \qquad (3)$$

where ρ and C denote the densities and heat capacities of water and air, respectively. The required upward discharge of air is about 3,000 times that of water, or about 15 m/yr to produce the small 10 mW m^{-2} anomaly if indeed it exists.

Though the thermal profiles in the UZ possibly lack resolution owing to the wide separation in data points, they appear primarily conductive throughout the UZ thickness. This might result from vertically uniform

action of the heat-removing processes discussed above; alternatively, it could be attributed to shallow SZ lateral flow, above depths used to calculate SZ heat flows. The credibility of this alternative is supported by borehole flow surveys while pumping (Benson and others, 1983), which show that most of the water production occurred within a few hundred meters beneath the water table.

The large lateral variability of heat flow over distances of one or two kilometers suggests a relatively shallow, hydrologic source for the observed anomaly, primarily convection in the saturated tuffs and underlying carbonate rocks. Confirmation of this hypothesis or the identification of an alternative will require additional thermal and hydrologic data of higher quality than are currently available.

In summary, the thermal regime of the Yucca Mountain area, based on the data available, seems similar to that of the Eureka Low, a regional heat-flow anomaly of hydrologic origin defined by Sass and others (1971). The large, systematic lateral variations of heat flow in both saturated and unsaturated zones, coupled with thermal and hydrologic indications of vertical head gradients, indicate a complex local hydrologic regime superimposed on the regional interbasin flow in the Paleozoic carbonate rocks.

The quality of the presently available data set does not allow an unambiguous interpretation of heat-flow data from either the UZ or the SZ. Some of the apparent hydrologic activity in the upper part of the SZ could be limited to the annulus between casing and the borehole wall, where water will respond readily to small head differences owing to the high transmissivity of the annulus. The ambiguity can be resolved only by completing some of the presently planned wells with access pipes grouted into place. It will be necessary to have water-filled pipes (also preferably with annulus grouted) to

characterize adequately the thermal state of the UZ. We also encourage thermal measurements in conjunction with hydrologic testing, particularly to correct for water density as a routine part of water-level measurements for the purpose of detecting head variations with depth.

References

Benson, L. V., Robison, J. H., Blankennagel, R. K., and Ogard, A. E., 1983, Chemical composition of ground water and the locations of permeable zones in the Yucca Mountain area, Nevada: U.S. Geological Survey Open-File Report 83-854, 19 p.

Carr, M. D., Waddell, S. J., Vick, G. S., Stock, J. M., Monsen, S. A., Harris, A. G., Cork, B. W., and Byers, F. M., Jr., 1986, Geology of drill hole Ue25p#1: A test hole into pre-Tertiary rocks near Yucca Mountain, southern Nevada: U.S. Geological Survey Open-File Report 86-175, 87 p.

Carr, W. J., and Rogers, A. M., 1983, Tectonics, seismicity, and volcanism of the southern Great Basin, in U.S. Geological Survey Research in Radioactive Waste Disposal--Fiscal Year 1981: U.S. Geological Survey Water Resources Investigations Report 83-4105.

Craig, R. W., and Robison, J. H., 1984, Geohydrology of rocks penetrated by test well UE-25p#1, Yucca Mountain area, Nye County, Nevada: U.S. Geological Survey Water-Resources Investigations Report 84-4248, 57 p.

Crowe, B. M., Amos, R., Perry, F., Self, S., and Vaniman, D. T., 1983, Aspects of potential magmatic disruption of a high-level radioactive waste repository in southern Nevada: Journal of Geology, v. 91, p. 259-276.

Czarnecki, J. B., 1984, Simulated effects of increased recharge on the ground-water flow system of Yucca Mountain and vicinity, Nevada-California: U.S. Geological Survey Water-Resources Investigations Report 84-4344, 33 p.

Czarnecki, J. B., and Waddell, R. K., 1984, Finite-element simulation of ground-water flow in the vicinity of Yucca Mountain, Nevada-California: U.S. Geological Survey Water-Resources Investigations Report 84-4349, 38 p.

Goss, R., and Combs, J., 1975, Thermal conductivity measurement and prediction from geophysical well log parameters with borehole application, in United Nations Symposium on the Development and Use of Geothermal Resources, 2nd, San Francisco, CA, May 20-29, 1975, Proceedings, v. 2: Lawrence Berkeley Lab., Univ. of California, p. 1019-1027.

Lachenbruch, A. H., 1958, Thermal measurements in Oak Springs formation, in Properties of Oak Spring Formation in Area 12 at the Nevada Test Site, edited by W. H. Diment and others: U.S. Geological Survey Open-File Report (TEI 672, Chapter 11).

Lachenbruch, A. H., Marshall, B. V., and Roth, E. F., 1987, Thermal measurements in Oak Springs formation at the Nevada Test Site, southern Nevada: U.S. Geological Survey Open-File Report 87-610, 19 p.

Lachenbruch, A. H., and Sass, J. H., 1977, Heat flow in the United States and the thermal regime of the crust, in The Earth's Crust, edited by J. G. Heacock, Geophysical Monograph 20, p. 626-675: American Geophysical Union, Washington, D. C.

Mase, C. W., Sass, J. H., Lachenbruch, A. H., and Munroe, R. J., 1982, Preliminary heat-flow investigations of the California Cascades: U.S. Geological Survey Open-File Report 82-150, 240 p.

Montazer, P., and Wilson, W. E., 1984, Conceptual hydrologic model of flow in the unsaturated zone, Yucca Mountain, Nevada: U.S. Geological Survey Water-Resources Investigations Report 84-4345, 55 p.

Muller, D. C., and Kibler, J. E., 1984, Preliminary analysis of geophysical logs from drill hole UE-25p#1, Yucca Mountain, Nye County, Nevada: U.S. Geological Survey Open-File Report 84-649.

Robison, J. H., 1984, Ground-water level data and preliminary potentiometric-surface maps of Yucca Mountain and vicinity, Nye County, Nevada: U.S. Geological Survey Water-Resources Investigations Report 84-4197, 8 p.

Sass, J. H., Blackwell, D. D., Chapman, D. S., Costain, J. K., Decker, E. R., Lawver, L. A., and Swanberg, C. A., 1981, Heat flow from the crust of the United States, in Touloukian, Y. S., Judd, W. R., and Roy, R. F., editors, Physical Properties of Rocks and Minerals: McGraw-Hill, New York, p. 503-548, 1981.

Sass, J. H., Kennelly, J. P., Smith, E. P., and Wendt, W. E., 1984, Laboratory line-source methods for the measurement of thermal conductivity of rocks near room temperature: U.S. Geological Survey Open-File Report 84-91, 21 p.

Sass, J. H., and Lachenbruch, A. H., 1982, Preliminary interpretation of thermal data from the Nevada Test Site: U.S. Geological Survey Open-File Report 82-973, 30 p.

Sass, J. H., Lachenbruch, A. H., and Mase, C. W., 1980, Analysis of thermal data from drill holes UE25a-3 and UE25a-1, Calico Hills and Yucca Mountain, Nevada Test Site: U.S. Geological Survey Open-File Report 80-826, 25 p.

Sass, J. H. Lachenbruch, A. H., Munroe, R. J., Greene, G. W., and Moses, T. H., Jr., 1971, Heat flow in the western United States: Journal of Geophysical Research, v. 76, p. 6376-6413.

Spengler, R. W., and Chornack, M. P., 1984, Stratigraphic and structural characteristics of volcanic rocks in core hole USW G-4, Yucca Mountain, Nye County, Nevada, with a section on Geophysical logs by D. C. Muller and J. E. Kibler: U.S. Geological Survey Open-File Report 84-789, 77 p.

Spengler, R. W., and Rosenbaum, J. G., 1980, Preliminary interpretations of geologic results obtained from boreholes Ue25a4, -5, -6, and -7, Yucca Mountain, Nevada Test Site: U.S. Geological Survey Open-File Report 80-929, 39 p.

Swanberg, C. A., and Morgan, P., 1978, The linear relation between temperature based on the silica content of groundwater and regional heat flow: A new heat flow map of the United States: Pure and Applied Geophysics, v. 117, p. 227-241.

U.S. Geological Survey, 1986, Quality Assurance Program Plan for Nevada Nuclear Waste Storage Investigations NNWSI-USGS-QAPP-01, R3.

Waddell, R. K., Robison, J. H., and Blankennagel, R. K., 1984, Hydrology of Yucca Mountain and vicinity, Nevada-California--Investigative results through mid-1983: U.S. Geological Survey Water-Resources Investigations Report 84-4267.

Winograd, I. J., and Thordarson, W., 1975, Hydrogeologic and hydrochemical framework, South-Central Great Basin, Nevada-California, with special reference to the Nevada Test Site: U.S. Geological Survey Professional Paper 712-C, C1-C126.

APPENDIX 1. Temperature logs from geologic and hydrologic test wells, Yucca Mountain

A series of precise temperature logs was obtained from all available wells at the Yucca Mountain site. This appendix contains the latest temperature logs together with time series for wells that have been logged more than once.

NOTES ON PRESENTATION OF DATA

Temperature-depth profiles for all logs are displayed as a time-series. The leftmost profile is the earliest. Later profiles are identified by month and year and are stepped to the right by a sufficient amount relative to the first curve (shown after the date in °C) to separate data from successive logs. All measurements made in air in the unsaturated zone are indicated as discrete symbols joined by straight lines. Where appropriate, the static water level (SWL) is indicated by a horizontal line. It should be noted that this is the level measured by us at the time of the temperature log, and in some instances, it is different from that listed in other publications (e.g., Robison, 1984).

THE CONDUCTOR WELLS

This series of four shallow wells was originally drilled to investigate a geoelectric anomaly within the unsaturated zone in Drill Hole Wash. All but one (UE25a-6) were drilled within the main drainage of the wash (Figure 2). The wells were drilled with mud and water and considerable fluid loss occurred. Early logs showed some quite bizarre departures from the linear temperature profiles characteristic of steady-state one-dimensional heat flow, including temperature reversals (Figures 1-2, through 1-5). Most of the

reversals and high-frequency noise did decay conductively with time, indicating that they were drilling-related. There remain, however, irregularities and large contrasts in thermal gradient that cannot be explained by pure conduction, and must be associated with vertical and lateral movement of fluids (air, water vapor and liquid water) within the unsaturated zone in Drill Hole Wash.

UE25a4 and 5 were not available for logging after December 1981 so that we show only the time series ending then (Figures 1-2 and 1-3). The most prominent steady-state anomalies are the large changes in gradient in the 75-100 m depth range.

UE25a6 which is sited above the main surface drainage of Drill Hole Wash and is close to USWG4, the site of the exploratory shaft (Figure 2), does not show this gradient break and has an average gradient of about 25°C km^{-1} below 55 m (Figure 1-4). The time series for UE25a6 is a good example of the conductive decay of thermal transients resulting from the loss of drilling fluid. Temperatures in Ue25a7 (Figure 1-5) still indicate considerable disturbance. In fact, above 150 m , the latest two logs show a remarkable resemblance to the first log made in March 1981. By contrast, temperature disturbances below a vertical depth of 150 m appear to be decaying conductively. We know of no renewed circulation of fluids in this well after December 1981. We can speculate that the remarkable change in the temperature profile above 150 m was the result of lateral water movement in fractures in densely welded tuff of the Topopah Spring Member (Spengler and Rosenbaum, 1980) below the main drainage of Drill Hole Wash, arising from a major storm that occurred a week or so before the March 1983 log was obtained.

UE25b1H. This well is also collared near the main surface drainage of Drill Hole Wash (Figure 2) and some degree of disturbance to the temperature field is evident in the unsaturated zone. Between 610 and 869 m (Figure 1-6), the profile is nearly isothermal and suggests lateral flow with both upward (concave downward) and downward (concave upward) components of water flow over different depth-intervals. Below a depth of 1 km, the profile is linear with a gradient of about 23°C km^{-1}, possibly indicating conductive heat flow. Temperature profiles from Ue25a1, which was drilled on the same pad are presented in Figure 1-7.

UE29a2. UE29a2 is shown on the index map (Figure 1). It is located some 10 km NW of USWG2 near the main surface drainage of Forty-Mile Wash. Static water level was just below 30 m below which temperatures increased very slightly ($\sim$10°C km^{-1}) to a depth of nearly 90 m (Figure 1-8) whereupon there was a reversal and erratic temperature variations to the total accessible depth of 168 m. It would appear that the thermal regime at this site is dominated by lateral water movement below Forty-Mile Wash with just over 0.5°C variation in temperature in the accessible portion of the hole.

The "G" Series, Yucca Mountain. These wells were drilled primarily to obtain geologic data, although considerable hydrologic and other information also was obtained from them. They generally were completely cored to allow for detailed studies of lithology, fracture density, and physical properties. We have made thermal conductivity measurements in all of them (see Appendix 3).

USW G-1. Hole G1 has been instrumented by Sandia Corporation and is unavailable for temperature measurements. For completeness sake, we include here the time series comprising complete logs in September 1980 and April 1981 (Figure 1-9). Temperature gradients (which unfortunately had not reached equilibrium by the time of our last log) increase systematically to

1 km or so whereupon they become essentially constant at about 30°C km^{-1} yielding a mean heat flux of about 53 mWm^{-2} below 1 km (see Table 2, Sass and Lachenbruch, 1982). Our preliminary interpretation involved downward vertical water movement with seepage velocity of ~1 cm/y to depths of 2 to 2.5 km, an interpretation that ignores the essentially constant heat flow below 1.1 km in this well but accounts for its anomalously low value.

USW G-2: Temperatures to about 600 m are similar to those in G1 and other deep wells in the area. There is then a step rise in temperatures (Figure 1-10) followed by about 150 m that is nearly isothermal whereupon a quasi-conductive gradient is established to total depth of 1250 m. The least-squares gradient between 800 and 1250 m is about 41±0.1°C km^{-1} which, when combined with the average thermal conductivity of 1.74±0.04 Wm^{-1} K^{-1}, yields a typical Basin and Range heat flux of 71 mWm^{-2} in contrast with the heat flow of 44 mWm^{-2} from the unsaturated zone. Taken literally, this would support our one-dimensional interpretation of high (~20 mm/yr) rates of downward percolation of groundwater or lower rates combined with vaporization in the unsaturated zone. The high gradient may, however, reflect the anomalously low temperature boundary at 760 m brought on by water moving vertically downward from 600 to 750 m or laterally with a downward component of velocity. An alternative gradient can be obtained by joining the top edge of the "stairstep" at ~600 m to the bottom-hole temperature. This gradient (31°C km^{-1}) yields a heat flow of 54 mWm^{-2}.

USW G-3. This is the most southerly of three wells drilled on the steep ridge immediately to the west of Drill Hole Wash. The water table here is exceptionally deep (Figure 1-11). Below the water table, the temperature profile shows evidence for upward and downward water movement over different intervals. The linear part of the profile between about 1000 and

1280 m has a thermal gradient of about 21°C km^{-1}. For a mean conductivity in the saturated zone of 1.58 ± 0.05 Wm^{-1} K^{-1} (25 samples), we estimate a heat flux of 33 mWm^{-2}.

USW G-4. G4 is the most recently completed well and is the proposed site of the exploratory shaft. The temperature gradient (Figure 1-12) increases from about 18°C km^{-1} between 150 and 400 m to about 30°C km^{-1} between 400 and 536 m (approximate water table). The profile below the water table is nonconductive and is consistent with an upward component of water movement from near the bottom of the well, exiting near the water table.

The "H" series, Yucca Mountain. By contrast with the previous series with which it is interspersed (Figure 2), these wells were drilled primarily for hydrologic studies. As such, they have larger diameters, typically contain a number of piezometer tubes, and have a very limited amount of core available for properties measurements. Between our November 1982 and March 1983 loggings, all of these sites (except H1) were reoccupied and packers were set near the bottom to aid in the estimation of head gradients.

USW H-1. This well is only about 0.5 km WSW of G1 (Figure 2), and it has a similar temperature profile with the exception of the lowermost 150 m. Below 1680 m, the gradient decreases systematically from ∿30 to less than 20 °C km^{-1} (Figure 1-13). A piezometer was grouted in to nearly total depth in September(?) of 1982. Post-grout profiles show very little change from pre-grout (Figure 1-13) indicating that water is probably moving upward in the formation in this interval.

USW H-3. The temperature gradient in USWH3 between 975 and 1190 m averages about 19°C km^{-1}, similar to that observed in the linear portion of USWG3. H3 is about 1.5 km north of G3 on the west ridge of Yucca Mountain

(Figure 2). The temperature profiles (Figure 1-14) illustrate once more the great depth to the water table and the abnormally low thermal gradients found on the ridge.

USW H-4. H4 is located on the flank of the west ridge on one of the eastward drainages (Figure 2). The thermal profile becomes linear and apparently conductive below 1 km (Figure 1-15) with a value of 25.5 °C km^{-1}.

USW H-5. This well is the northernmost of the three deep wells on the ridge. Characteristically, the water table is very deep and non-conductive processes predominate to a depth of over 1 km (Figure 1-16). Below this depth, there is a quasi-linear profile with gradient of 28.5 °C km^{-1}; the average gradient below the static water level is ~15°C km^{-1}.

USW H-6. H6 is located on the west and slightly south of H5 in a subsidiary drainage northwest of Crater Flat (Figure 2). Because of its lower elevation, the static water level is higher than for G3, H3, and H5 on the ridge (compare Figures 1-16 and 1-17). Below 880 m, the temperature profile is essentially conductive, with a gradient of 36°C km^{-1}.

J-13. Well J-13 (formerly Test Well 6) was drilled in Forty-Mile Wash and is used as a water supply well. Below the water table (Figure 1-18), the profile shows signs of hydrologic disturbance. The gradient in the unsaturated zone was used by Sass and others (1971) to calculate a heat flow of 67 mWm^{-2}.

UE25P1. Well UE25P1 was drilled to test a basement high of Paleozoic carbonate rocks. Below the water table (Figure 1-19) the thermal regime is complex and appears dominated by lateral water flow or possibly by vertical flow within the well.

USW VH-1 and VH-2. These two wells are located in Crater Flat (Figure 1) near two Holocene cinder cones. Equilibrium temperature profiles

for both wells (Figures 1-20 and 1-21) indicate a thermal regime dominated by lateral water movement having both upward and downward vertical components. Particularly puzzling is the fact that, even though they are similar in character, the profile in VH-1 is consistently warmer by about 5°C than that in VH-2 (Figure 1-22). This indicates strong lateral gradients between the two wells. In fact, the range of temperatures in VH-2 is very similar to that in USW-H6 which is 330 m higher in elevation (Figure 1-22). This, in turn, suggests that VH-2 is in a region of net downward water flow rather than VH-1 being anomalously hot.

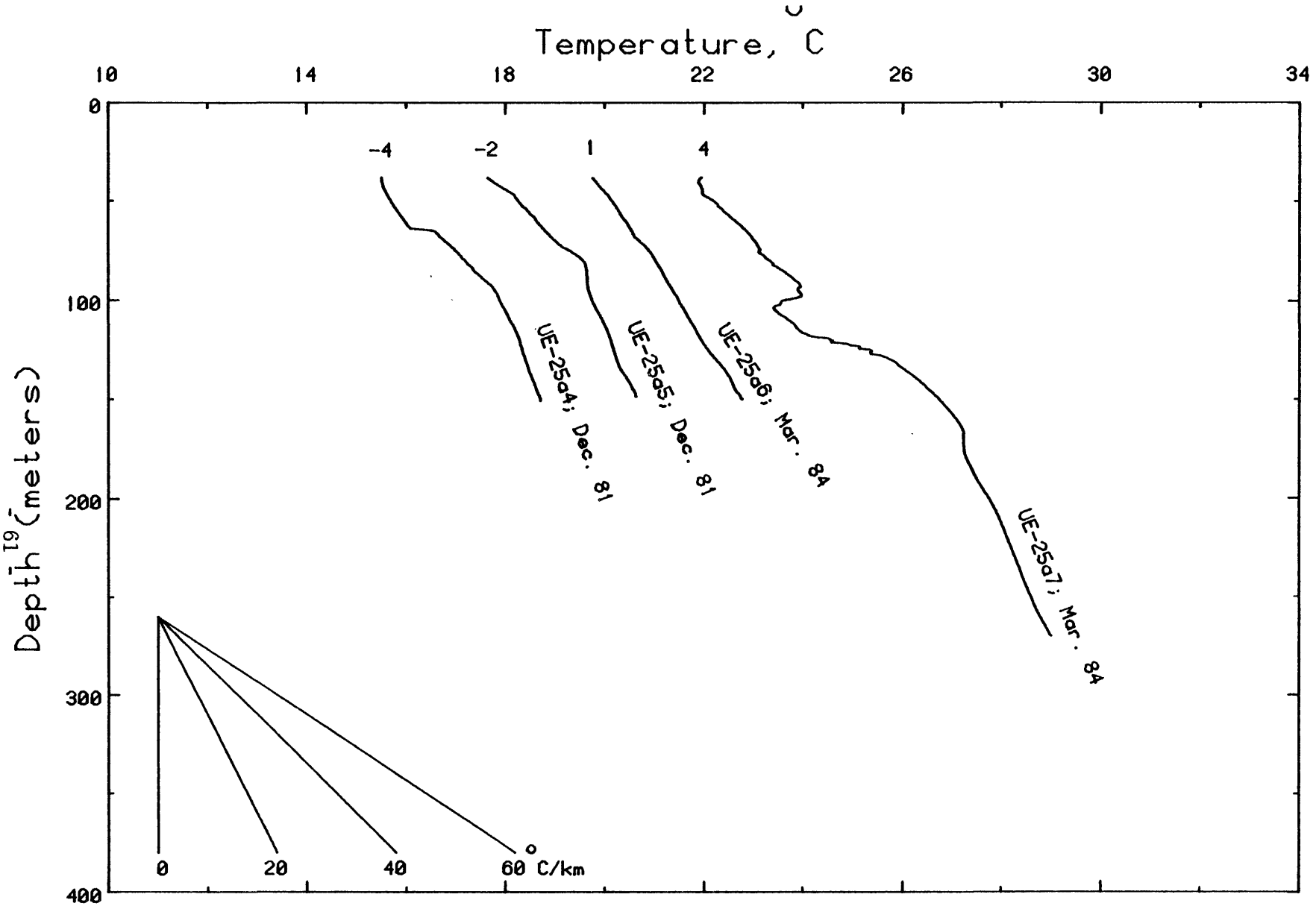

Figure 1-1. Most recent temperature logs from the "conductor" wells. Numbers near the top of each profile indicate the rightward shift of the profile relative to the temperature axis.

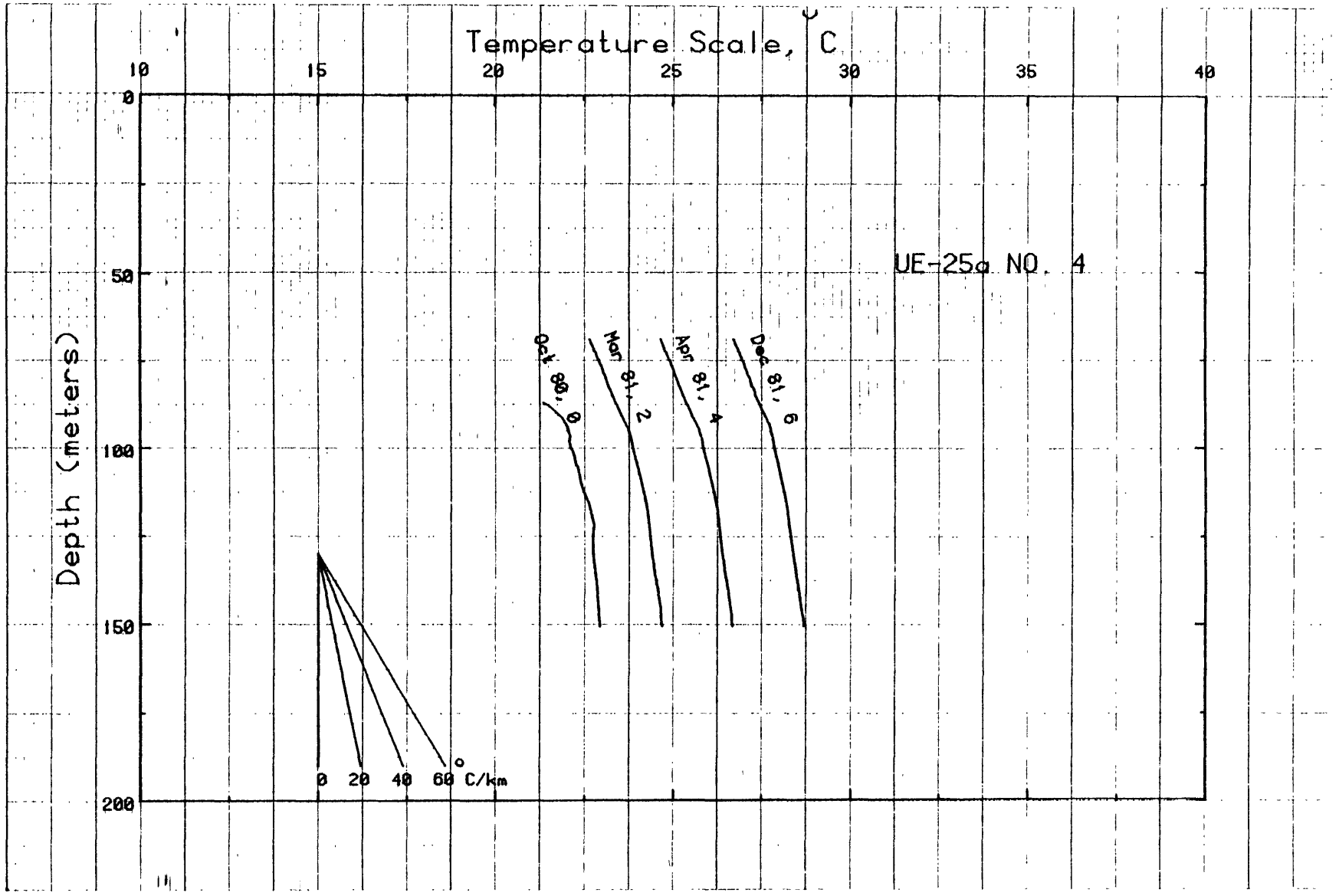

Figure 1-2. Temperature logs from Ue25a4. Numbers after date indicate rightward shift of profile relative to temperature axis.

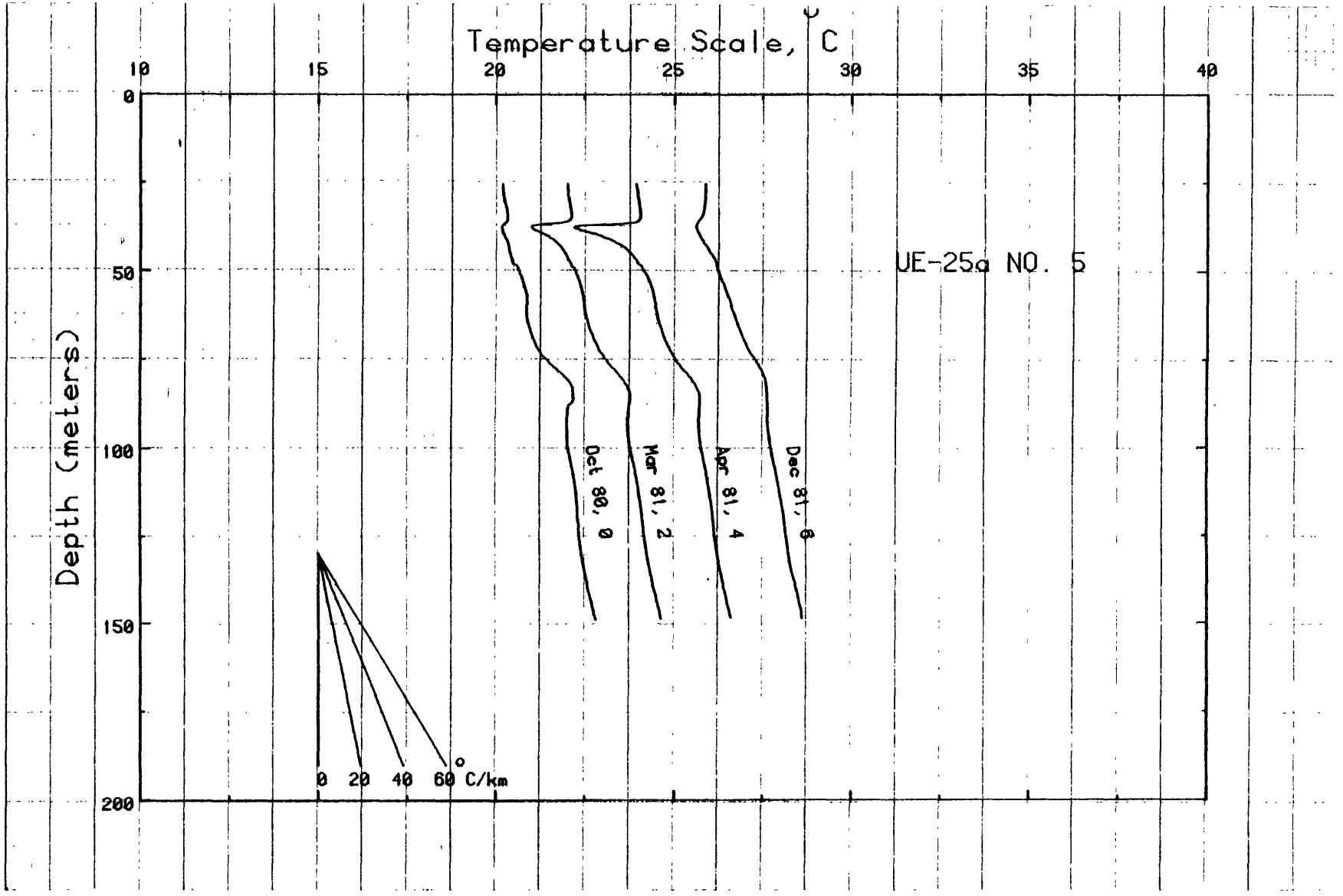

Figure 1-3. Temperature logs from Ue25a5. Numbers after date indicate rightward shift of profile relative to temperature axis.

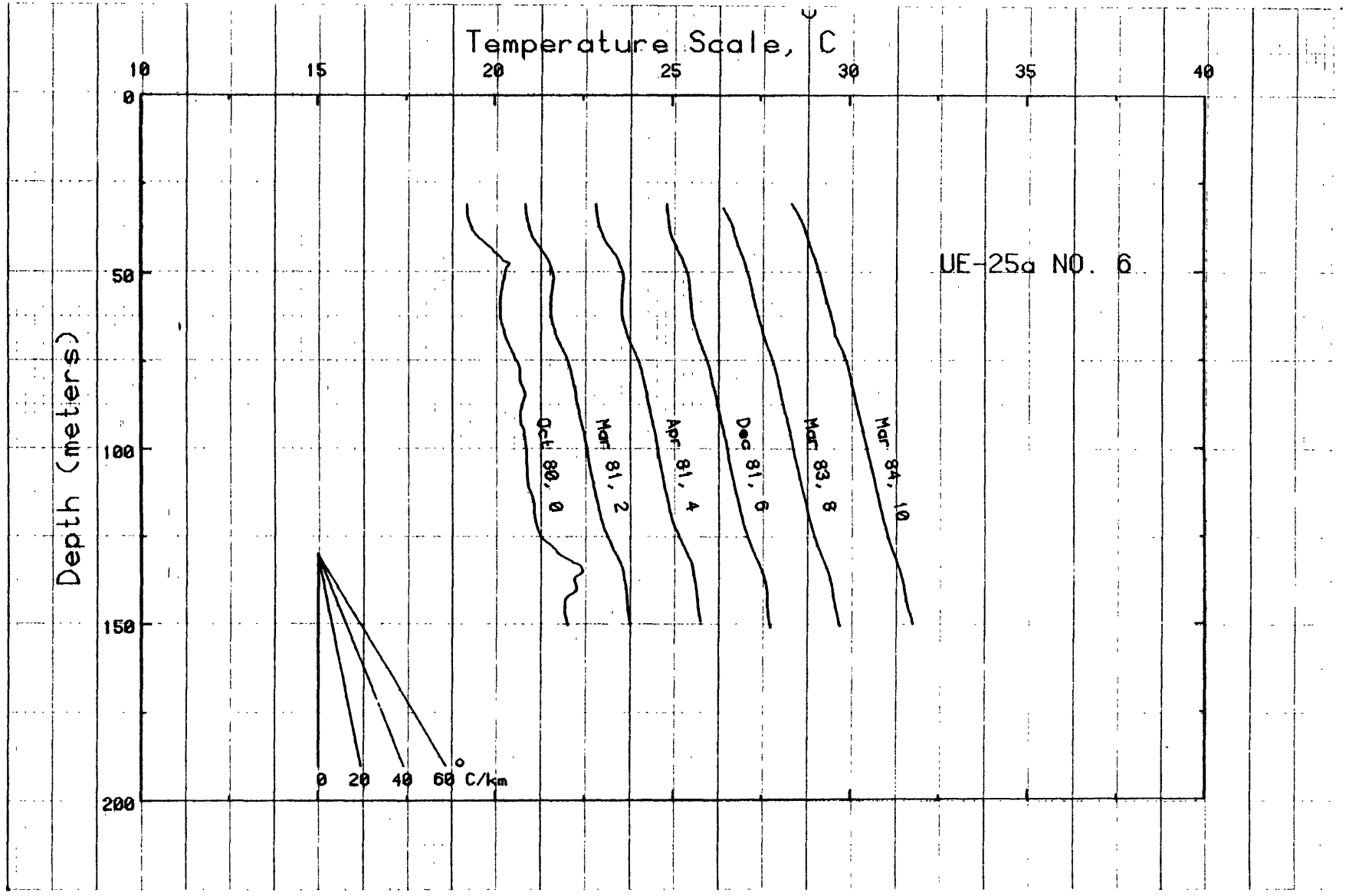

Figure 1-4. Temperature logs from Ue25a6. Numbers after date indicate rightward shift of profile relative to temperature axis.

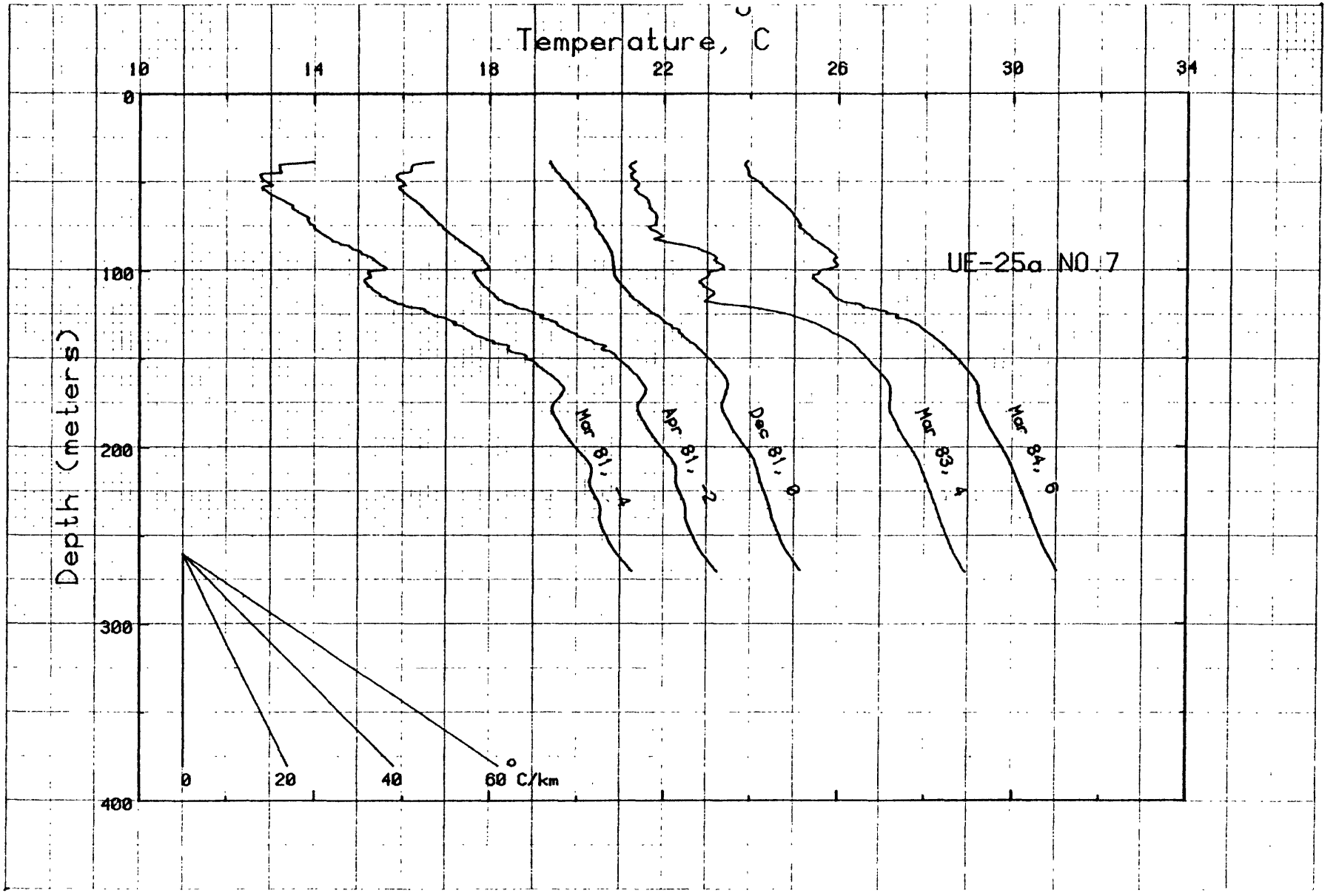

Figure 1-5. Temperature logs from Ue25a7. Numbers after date indicate rightward shift of profile relative to temperature axis.

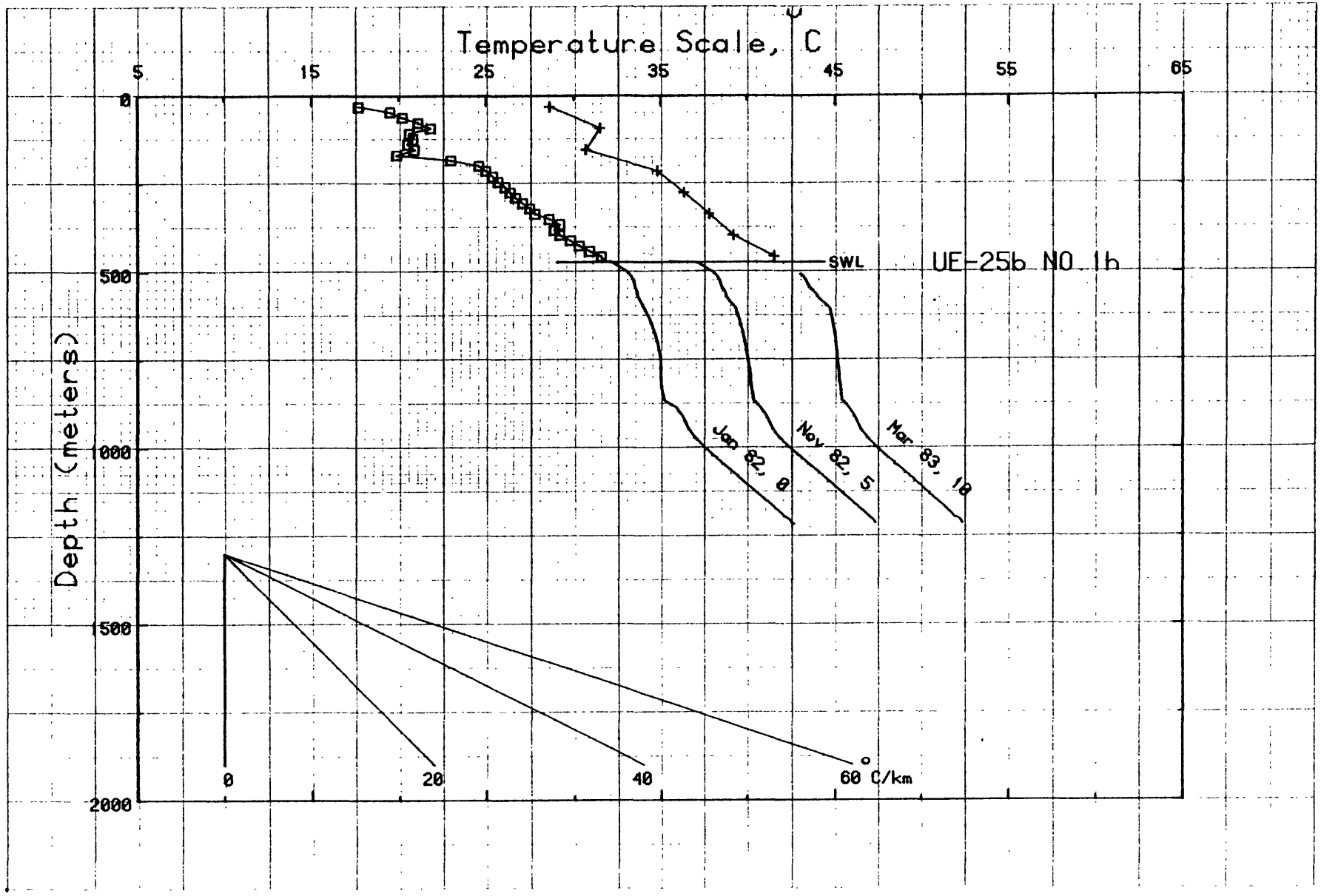

Figure 1-6. Temperature logs from Ue25blh. Numbers after date indicate rightward shift of profile relative to temperature axis. SWL is static water level.

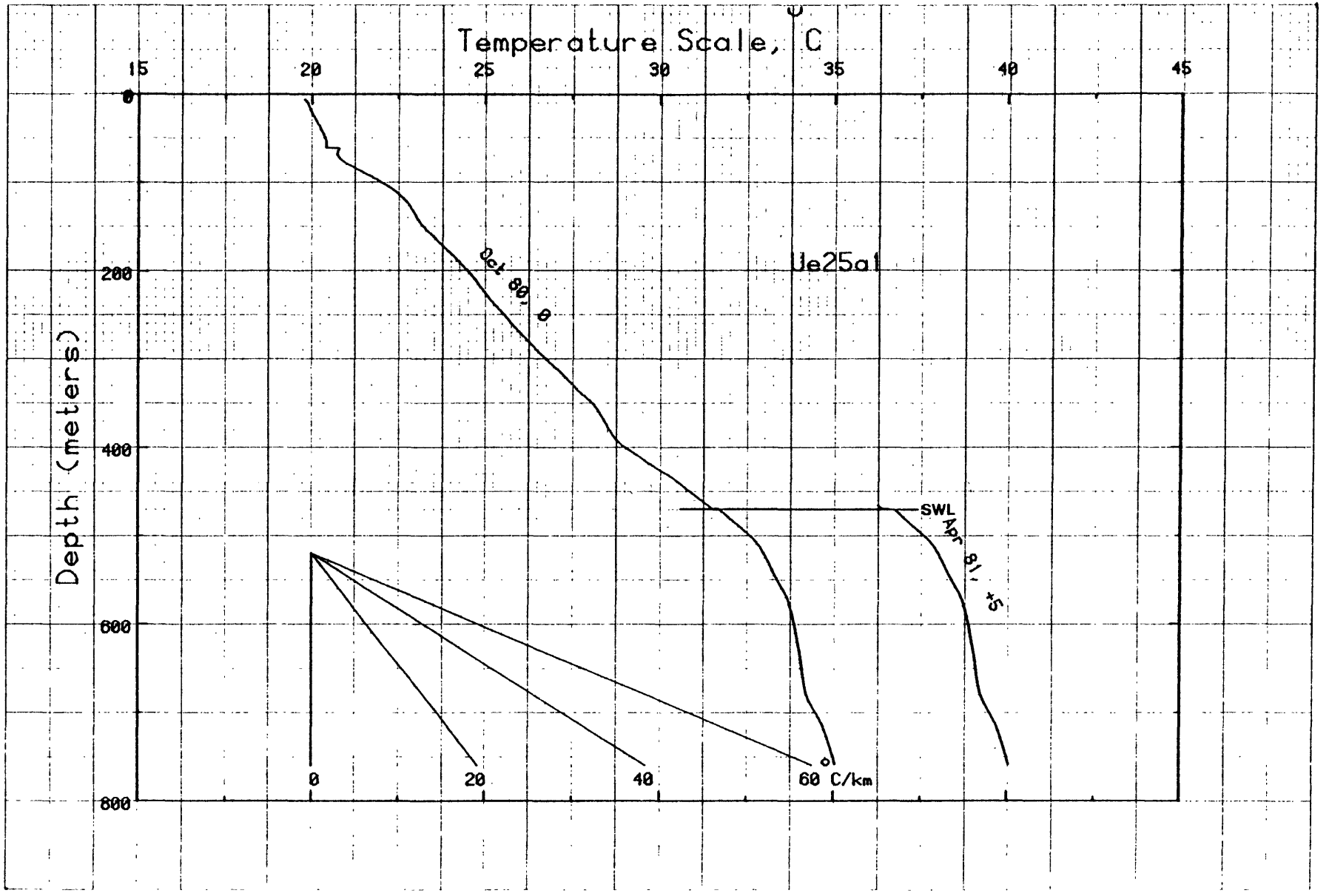

Figure 1-7. Temperature logs from Ue25a1. Numbers after date indicate rightward shift of profile relative to temperature axis. SWL is static water level.

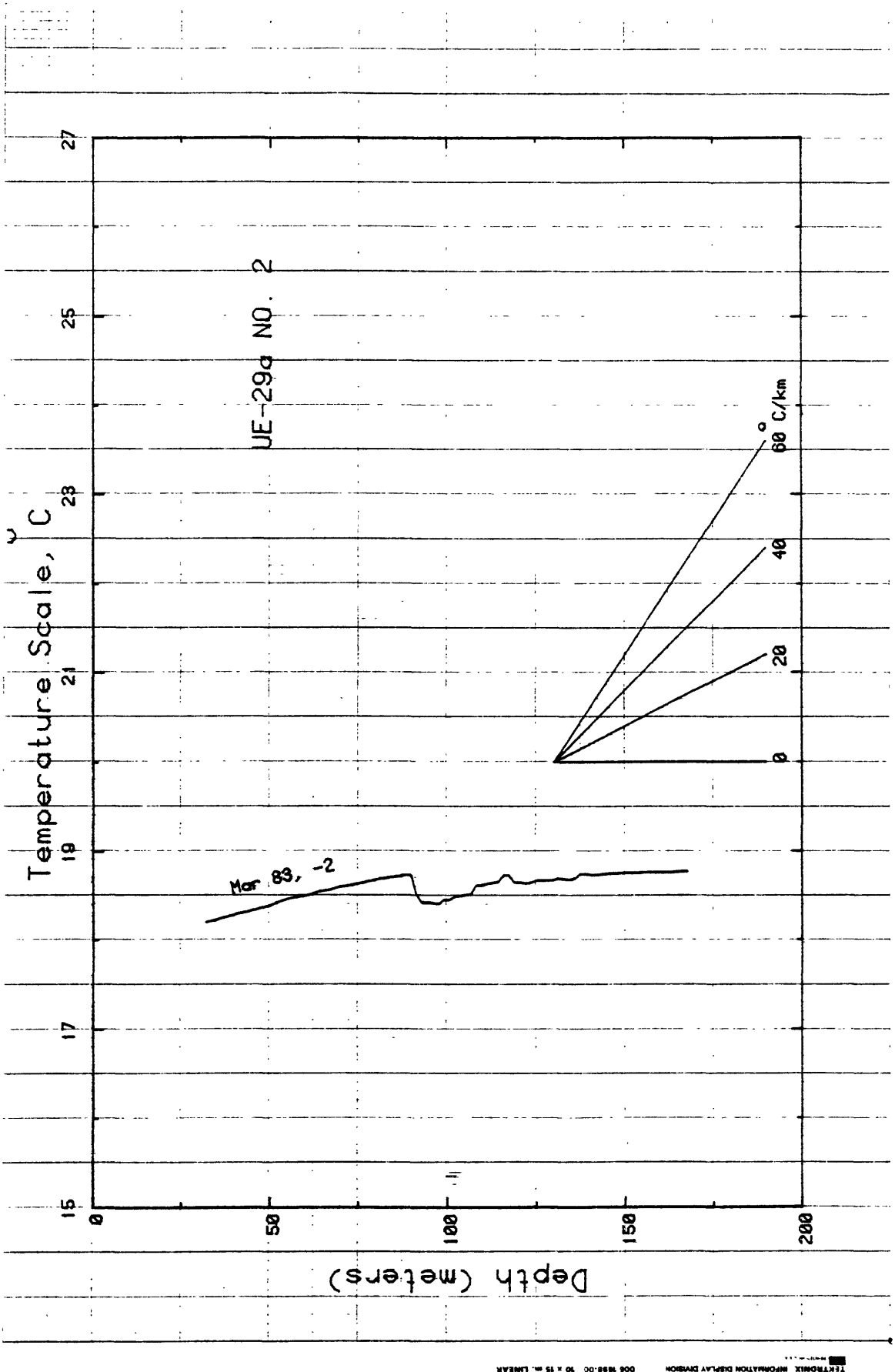

Figure 1-8. Temperature log for U-29a2.

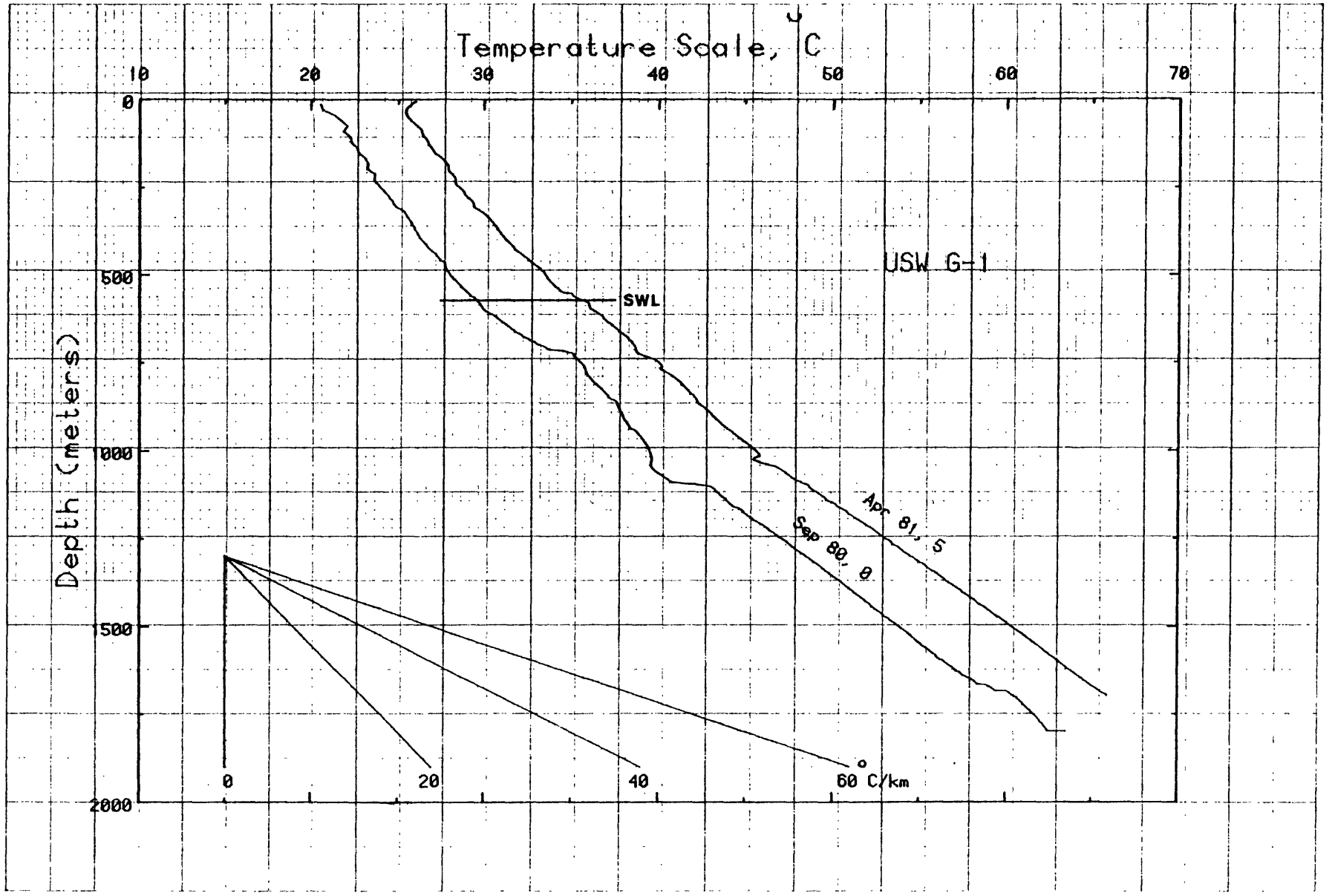

Figure 1-9. Temperature logs from USWG-1. Numbers after date denote the number of °C by which the profile is shifted to the right relative to the temperature axis. SWL is static water level.

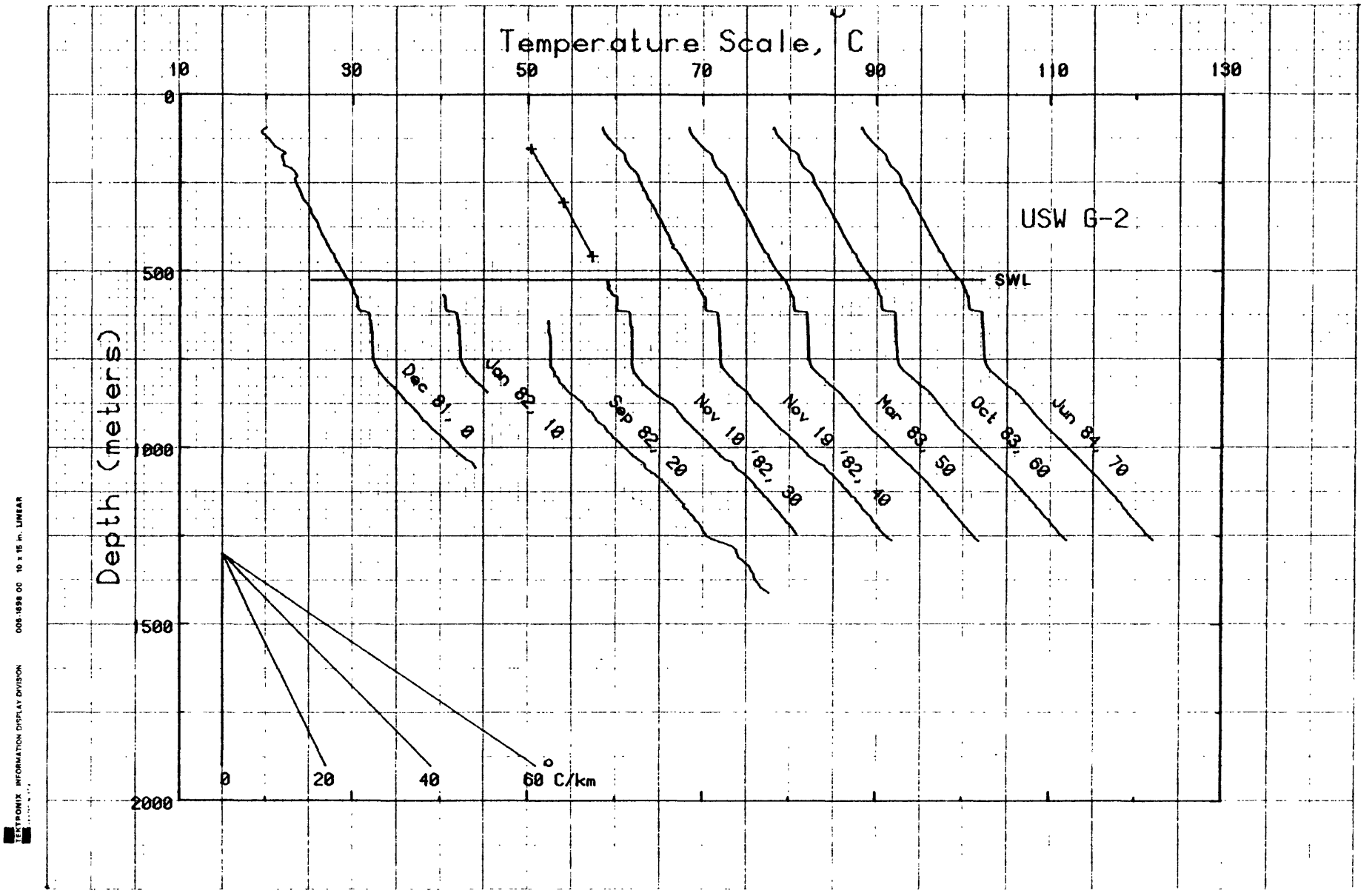

Figure 1-10. Temperature logs from USW G-2. Number after date denotes the amount of rightward shift relative to the temperature axis. SWL is static water level.

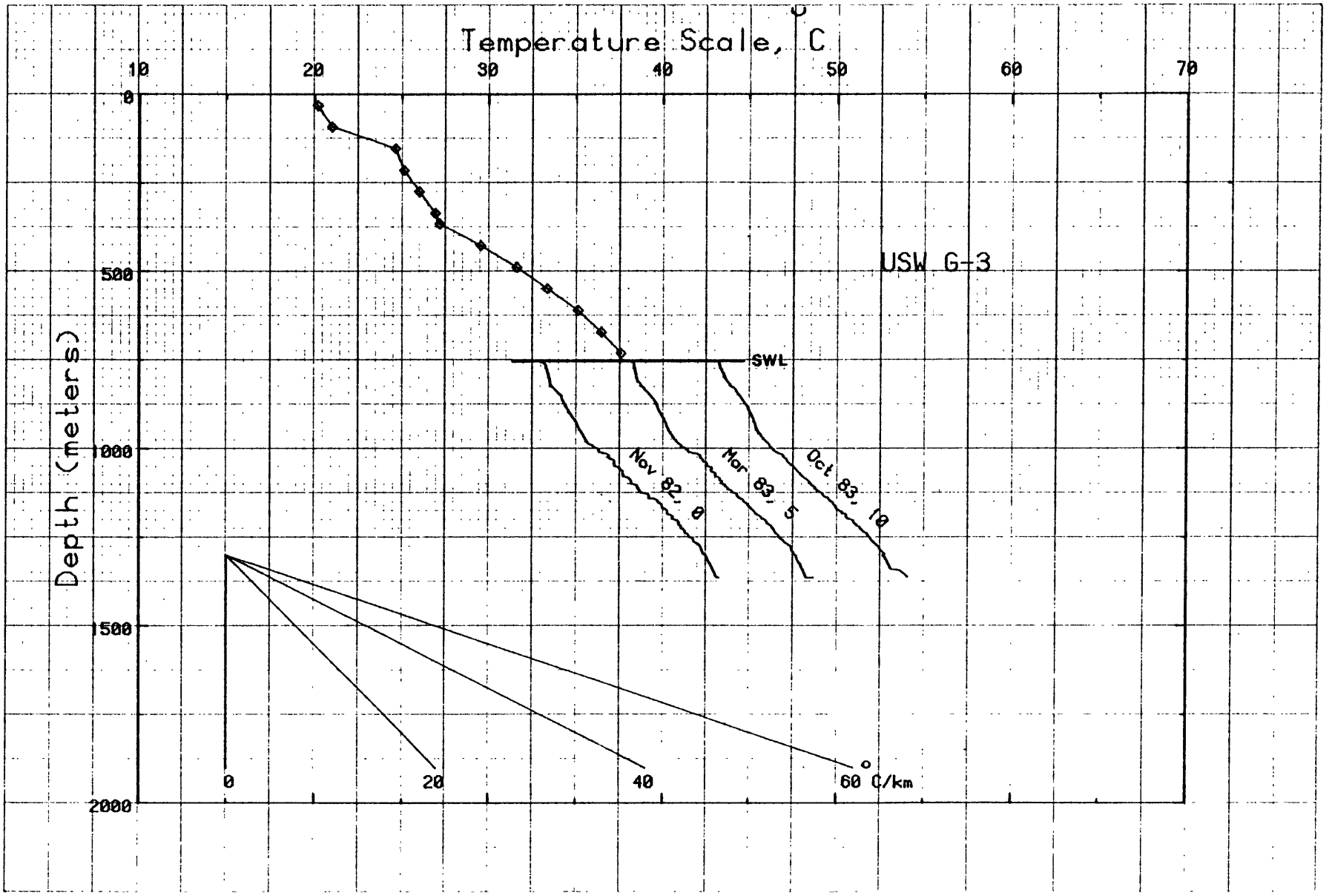

Figure 1-11. Temperature logs for USW G-3. Number after date denotes the amount by which profile is shifted to the right relative to the temperature axis. SWL is static water level.

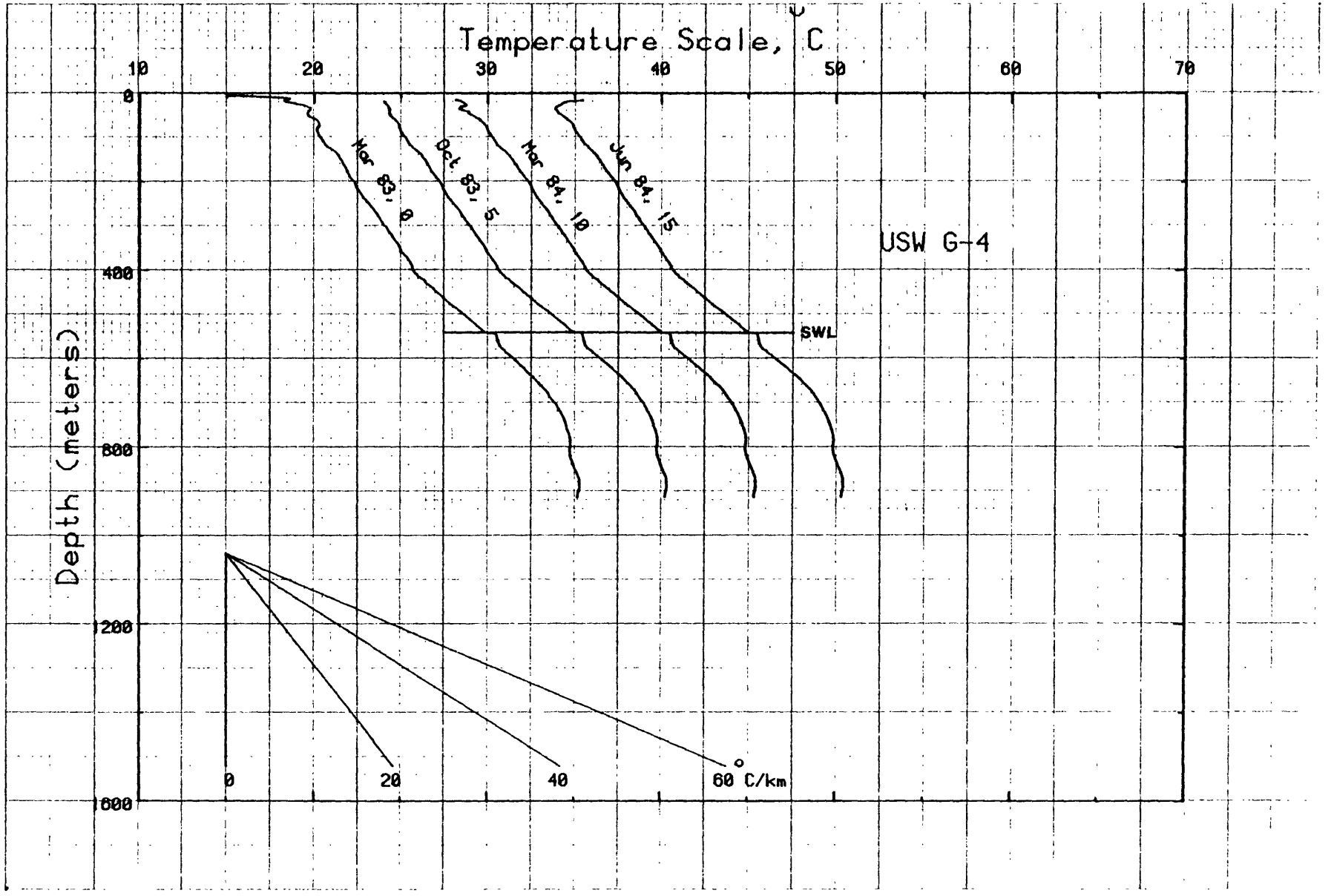

Figure 1-12. Temperature profiles from USW G-4. Number after date denotes the amount of rightward shift (in °C) relative to the temperature axis. SWL is static water level.

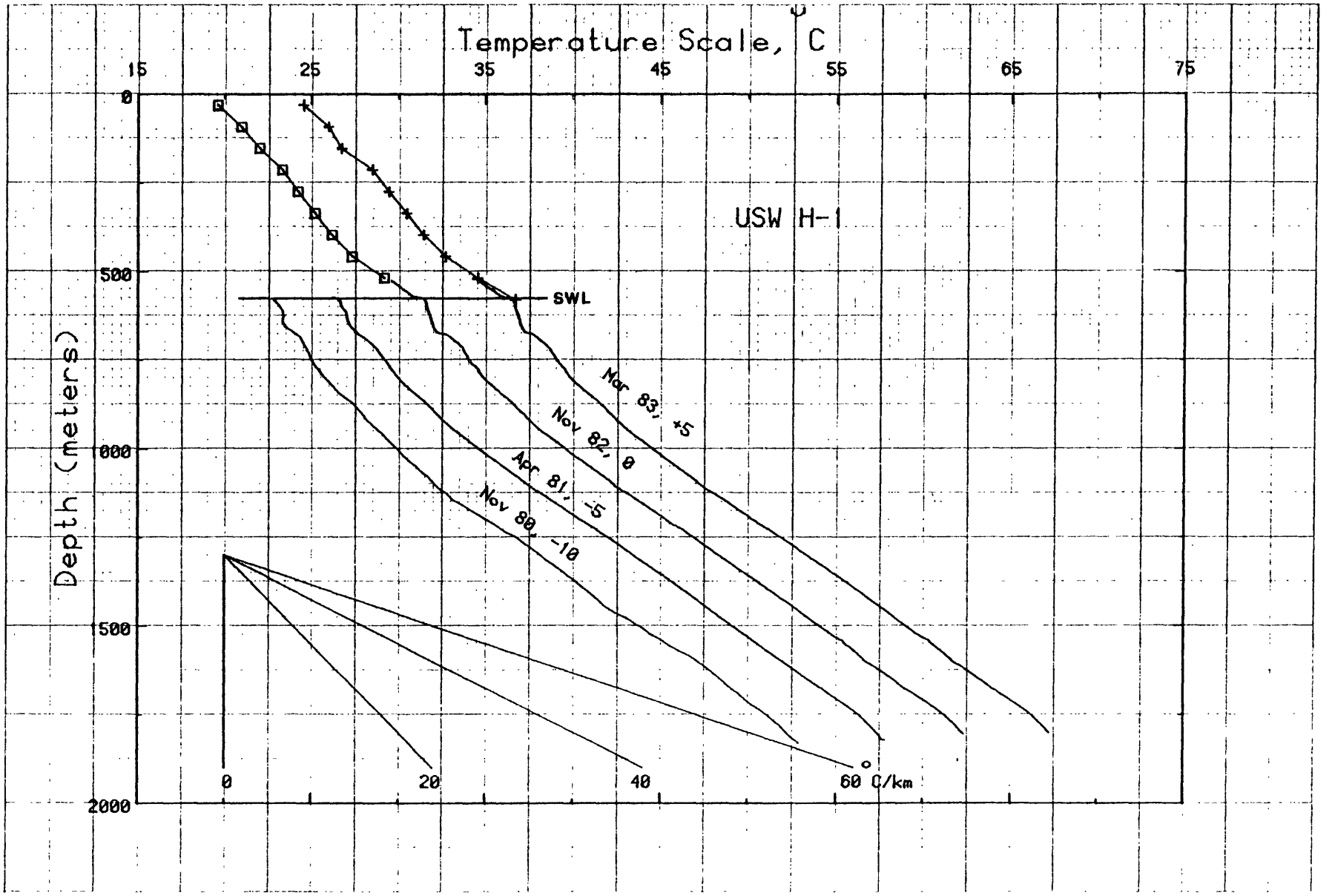

Figure 1-13. Temperature profiles from USW H-1. Number after date indicates the rightward (leftward if negative) shift of the profile relative to the temperature axis. SWL is static water level.

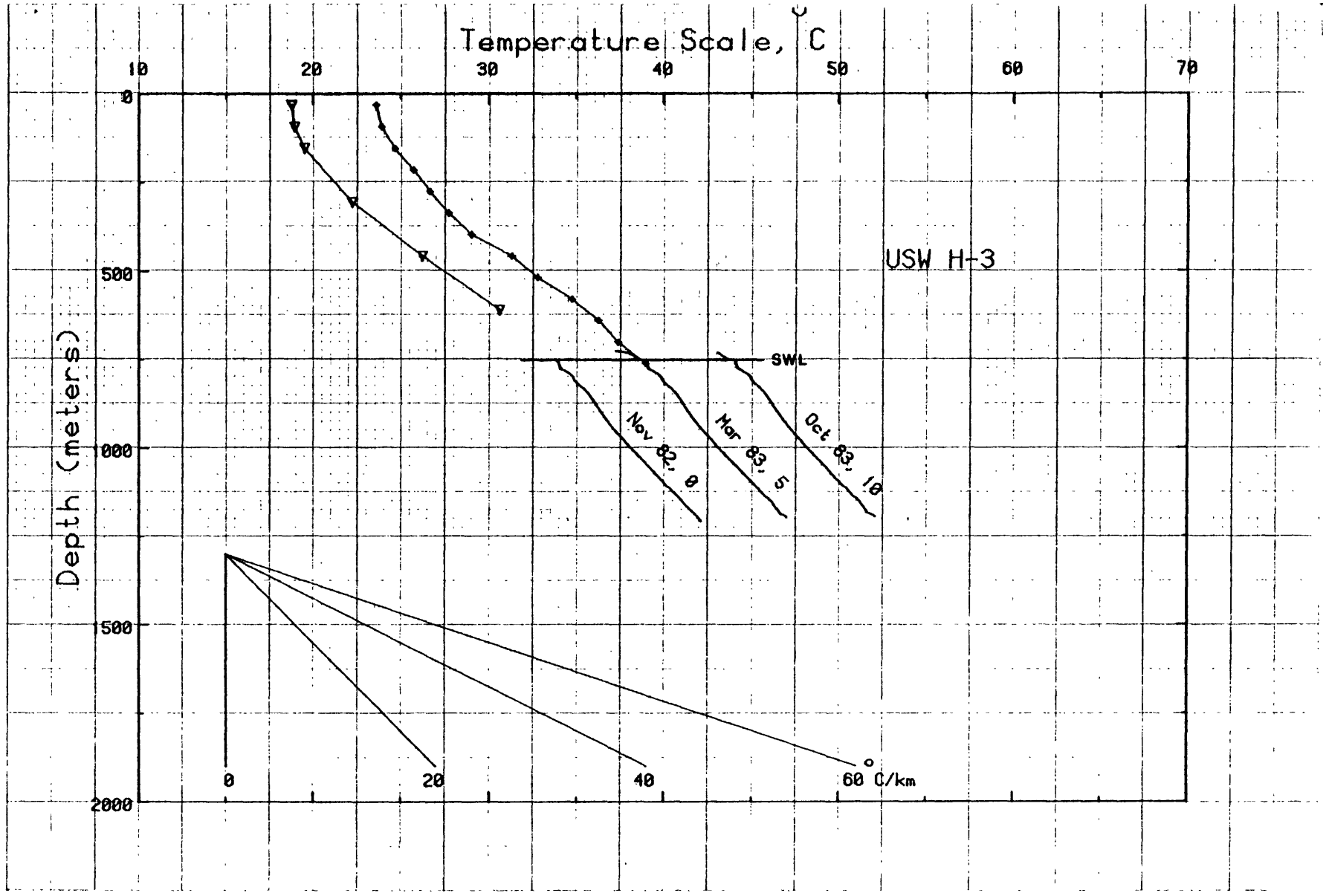

Figure 1-14. Temperature logs in USW H-3. Number after date denotes rightward shift of a profile relative to the temperature origin. SWL is static water level.

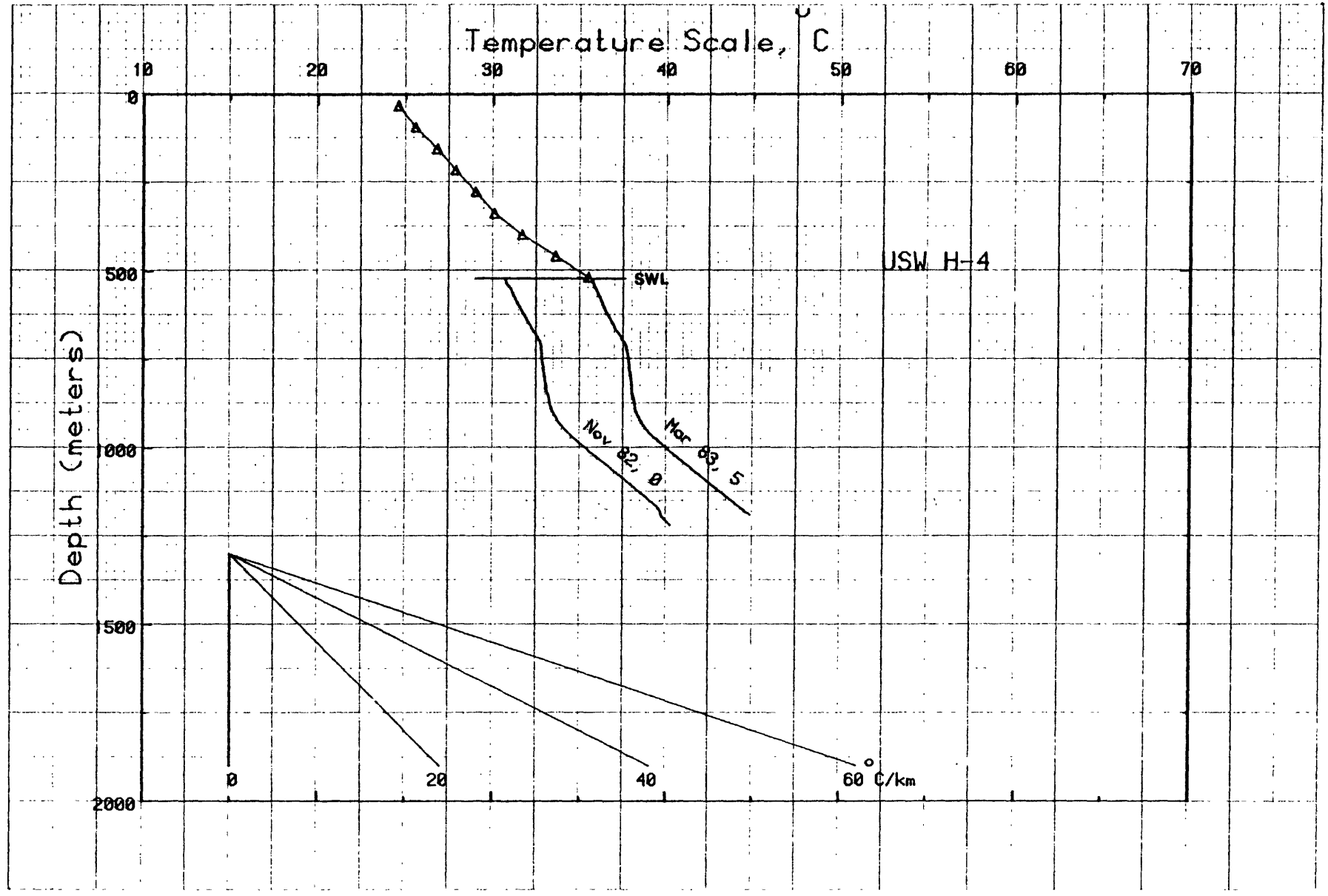

Figure 1-15. Temperature profiles for USW H-4. Number after date represents the rightward shift of the profile relative to the temperature origin. SWL is static water level.

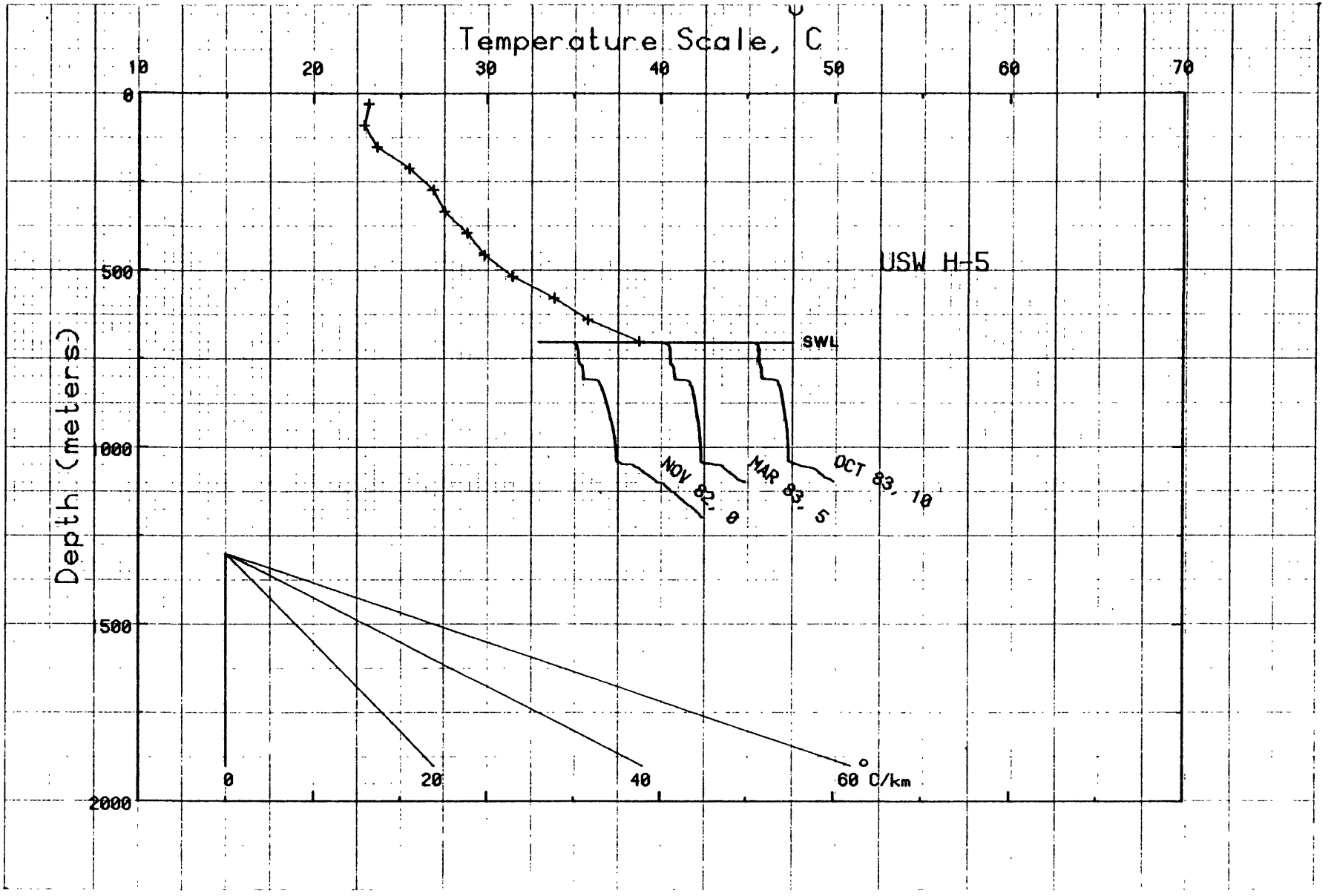

Figure 1-16. Temperature profiles from USW H-5. Number after date is the amount by which profile is shifted to the right. SWL is static water level.

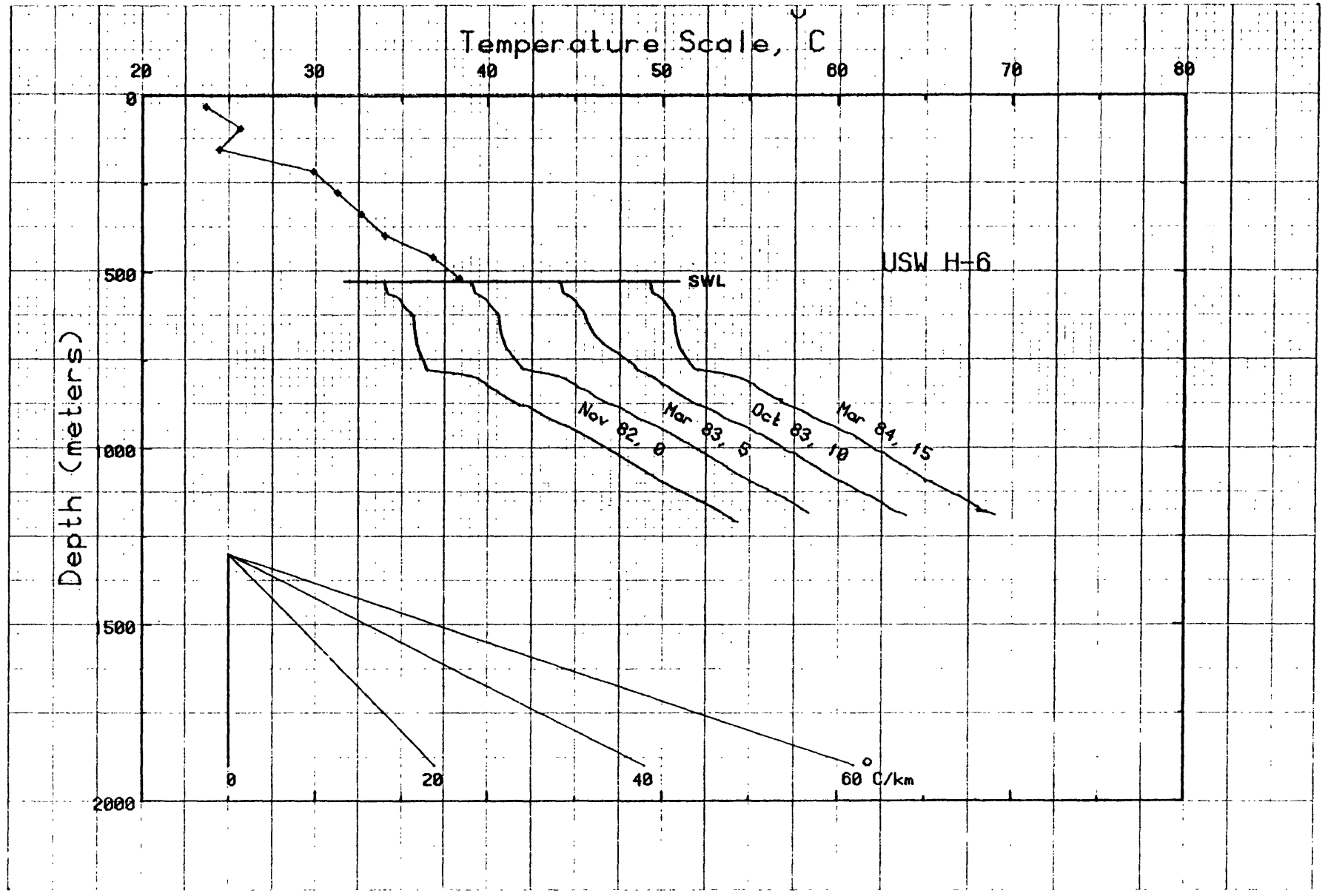

Figure 1-17. Temperature profiles for USW H-6. Number after date of log signifies rightward shift of the profile relative to the temperature origin. SWL is static water level.

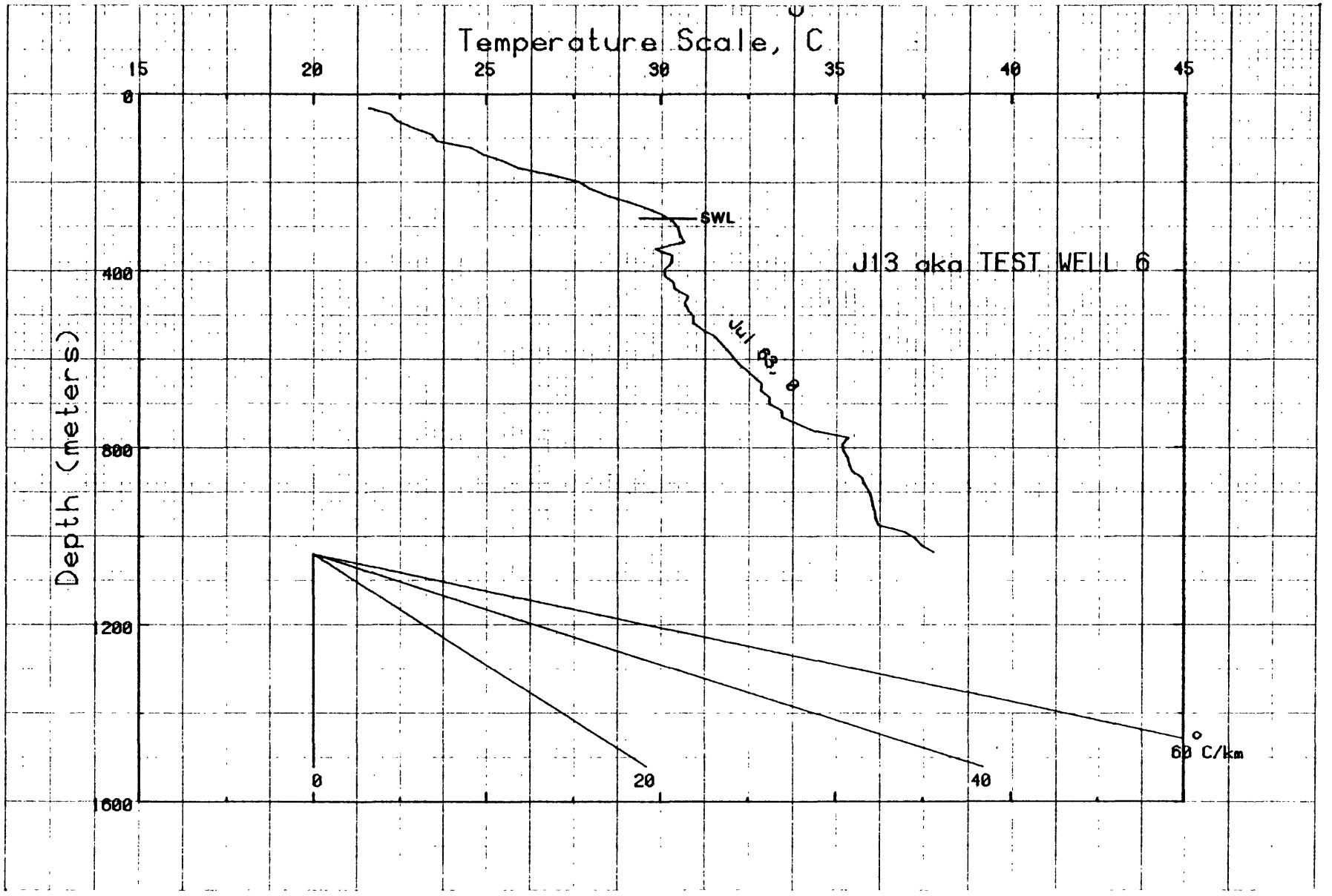

Figure 1-18. Temperature profile in well J-13. SWL is static water level.

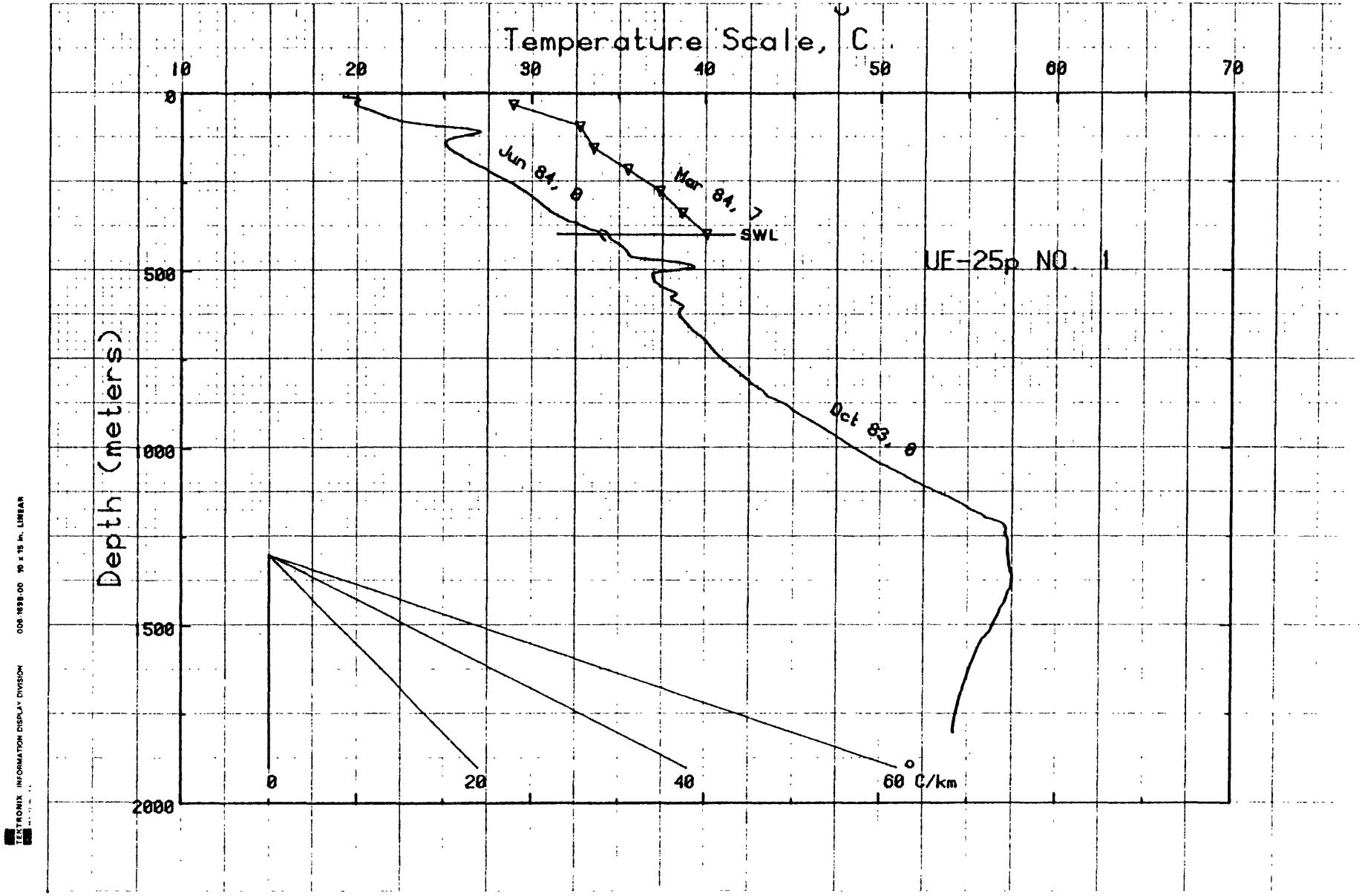

Figure 1-19. Temperature profiles in Ue25p. Rightward shift in profile is indicated by the number after the date. SWL is static water level.

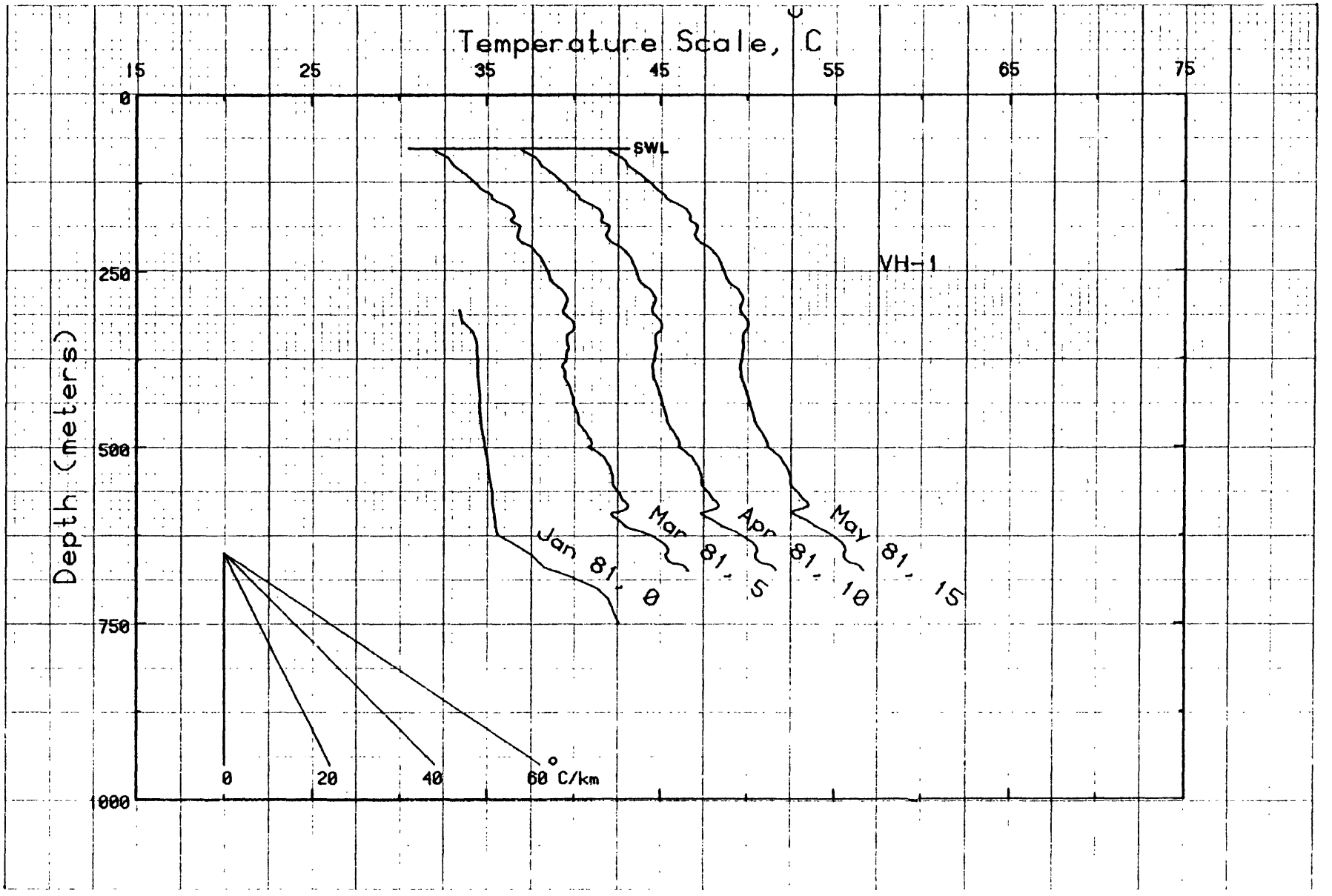

Figure 1-20. Temperature profiles from USW VH-1. Number after date signifies amount of rightward shift relative to temperature origin. SWL is static water level.

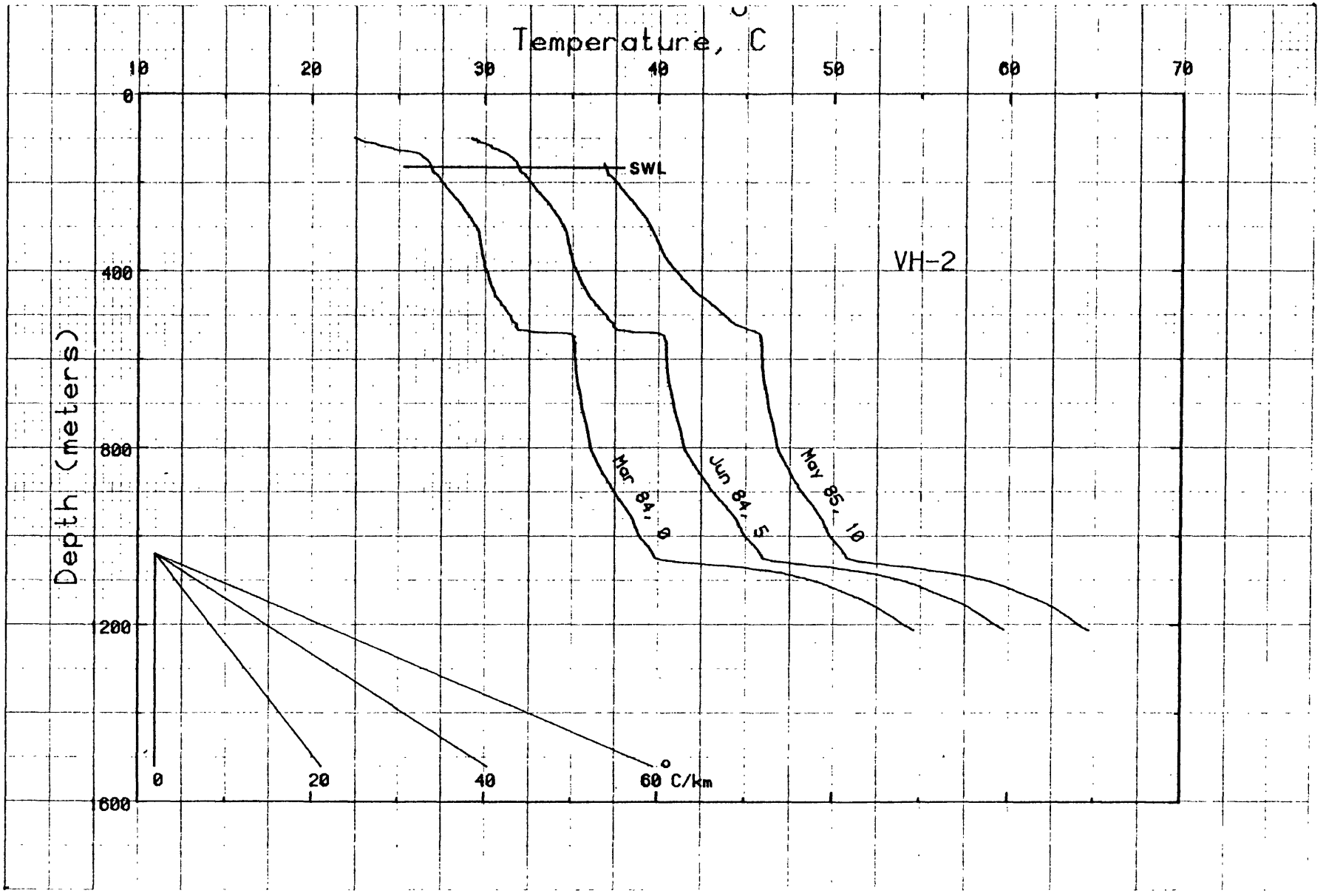

Figure 1-21. Temperature profiles for USW VH-2. Number after date denotes amount of rightward shift relative to temperature origin. SWL is static water level.

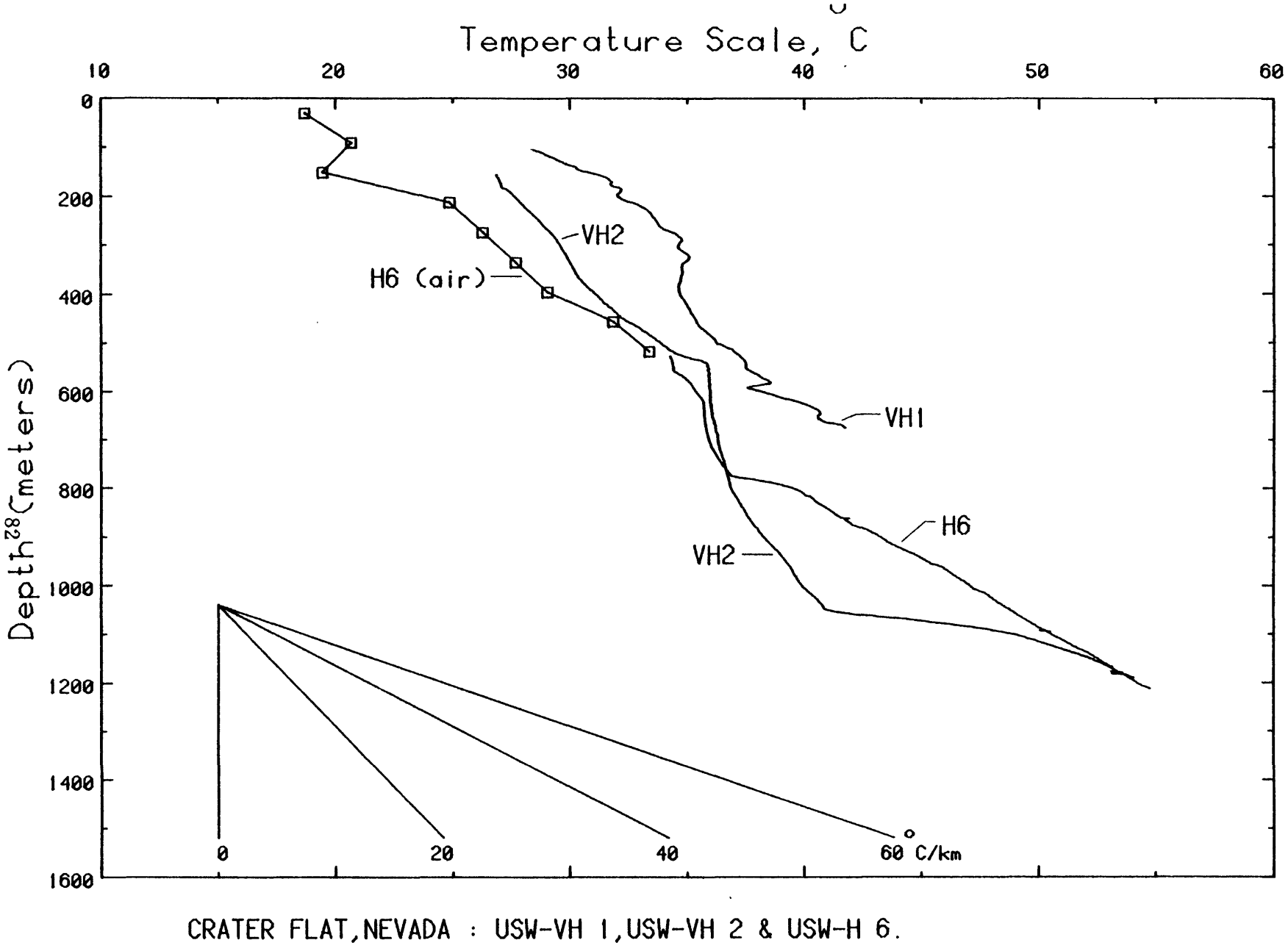

Figure 1-22. Temperature and gradient profiles from USW H-6, VH-1, and VH-2.

APPENDIX 2. Temperature measurements in air in the unsaturated zone

In many wells, we had available an access pipe plugged at the bottom and filled with water. For these (e.g., USW G-2 and USW G-4, figures 1-10 and 1-12), we were able to obtain logs through the unsaturated zone using our standard logging techniques (procedure GPP-02, RO, Sass and others 1971). For various reasons, however, it was not always possible to have such an access pipe and measurements had to be obtained at discrete points in air. Using our standard probe (Fenwall K212E, Sass and others, 1971), such measurements are very time consuming - the time constant of the probe in air is on the order of one hour as compared with a few seconds in water.

Faced with a formidable number of wells from which to obtain such temperature measurements, we elected to design and construct a special thermistor probe having a very small thermal mass. The probe (Figure 2-1) equilibrates with a column of still air to within 1% of a step temperature change in a period of four minutes.

By far the most serious problem in obtaining meaningful air-temperature measurements in a large (~0.5 m) diameter well results from convective motion induced by both the thermal instability of the air column (cooler, heavier air lying on top of warmer, lighter air) and by diurnal barometric changes. In the WT series wells, the usual casing configuration involved a large diameter (~400 mm) outer casing at the top of which was spot-welded a heavy flange (~20 mm thick) which in turn supported a string of smaller diameter tubing (~50-70 mm o.d.) with a well screen below the water table. It was common for the large casing to be "breathing" through gaps beneath the spot-welded flange, inhaling at certain times, and exhaling at others. When this was occurring, temperature fluctuations of varying periods were superimposed on the simple equilibration process with the result that temperatures were still

varying considerably after 20 minutes. As the magnitude of this problem became apparent, we were able to alleviate the disturbances somewhat by partially sealing the upper part of the large casing using materials that were available to us in the field (filament tape, weather stripping, etc.).

The measurement procedure consisted of lowering the probe in 100 to 200 foot (30.5 to 61 m) increments, then reading thermistor resistances at one-minute intervals until the resistance change in one minute was less than 1% of the accumulated change, or for 20 minutes, whichever was less. Data reduction consisted of converting resistances to temperatures, plotting temperature as a function of the reciprocal of time (t) and extrapolating linearly to $1/t = 0$ ($t=\infty$) for each depth. In this procedure, the time origin is difficult to fix precisely, as we are not dealing with an instantaneous step change in temperature. This is particularly true where the decay of a recent convective overturn is superimposed on the change imposed by moving the probe down in the geothermal gradient. A misplaced time origin is usually manifested as curvature in the later part of the temperature versus 1/t curve. When this was observed, we adjusted the time origin empirically (usually by no more than 1 or 2 minutes) so as to minimize the observed curvature.

When the air columns in both the outer casing and the observation tubing were truly stable (Figure 2-2), extrapolation of the θ versus 1/t curve resulted in an unambiguous intercept value for temperature (θ) accurate to within a few hundredths of a degree. On the other hand, there is a much larger degree of uncertainty ($\pm 0.1°C$ or more in the extrapolated temperature for a convecting air column, Figure 2-3), and disturbances with periods of tens to hundreds of minutes may cause undetectable errors of 1°C or more.

We are reasonably certain that the least squares temperature gradient between 100 feet (30.5 m) and the water table is representative of the average thermal gradient in the unsaturated zone. In the "well-behaved" wells, the 30.5 m or 61 m interval-gradients probably also are reliable. It is impossible, however, to apply objective criteria to the data set from the large-diameter wells to distinguish between reliable and unreliable data.

The data for all accessible WT series wells are presented in Figures 2-4 through 2-20. For each depth shown on each of these figures, a graph of the kind illustrated in Figures 2-2 and 2-3 was generated, a suitable interval selected, and an extrapolation to $1/t = 0$ (infinite time) was made. Thus the temperature symbol plotted at each depth represents our interpretation of the most likely equilibrium temperature.

The static water level, in each instance where it was encountered is indicated by the lowermost triangle in each of Figures 2-4 through 2-20. Below that, there is a short "tail" of a few meters to tens of meters continuous temperature depth profile below the water table. As we noted in the "G" and "H" series wells, immediately below the water table, these tails are generally not consistent with the more regular and conductive temperature profiles in the unsaturated zone.

In WT-13 (Figure 2-15) it was consistently difficult to obtain a consistent temperature versus 1/time profile (cf. Figures 2-2 and 2-3). We logged it on two different occasions (June 1 and June 4, 1984) but found it very difficult to get an internally consistent set of data except near the top and near the water table (Figure 2-15). This is a "worst-case" illustration of our contention that, even though the detailed structure of the thermal profiles from this series of wells may be suspect, the least-squares gradient over a ~300 m interval does have some status.

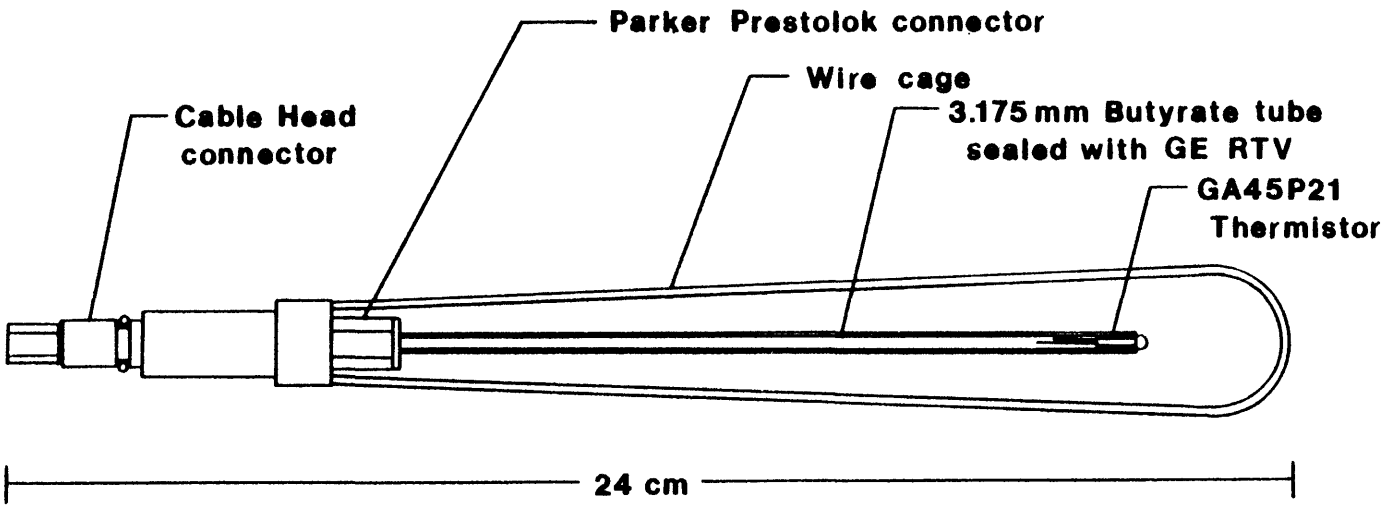

Figure 2-1. Temperature transducer having a low thermal mass for use in air.

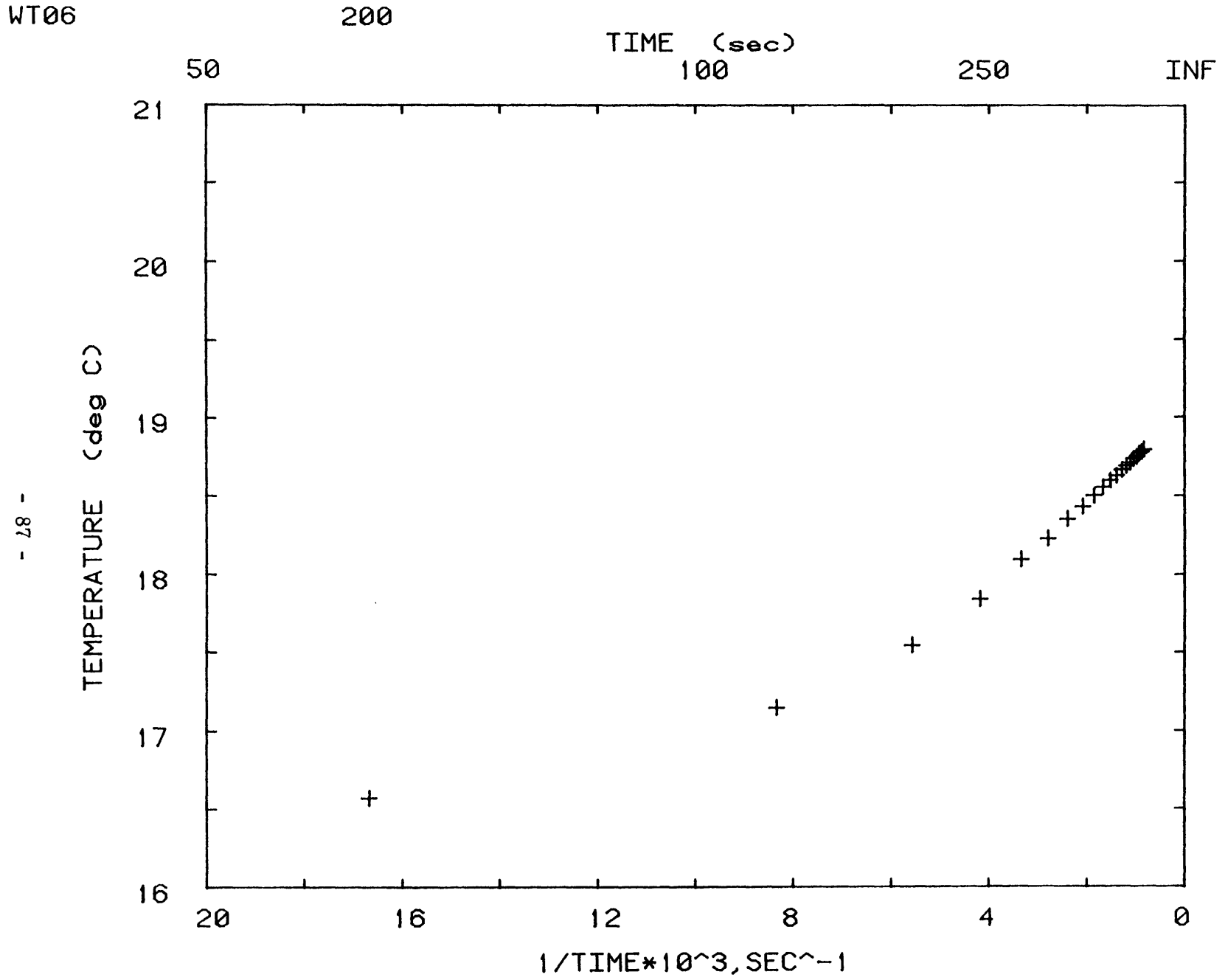

Figure 2-2. Temperature versus reciprocal time (from stopping of probe) for WT06, 200 feet, illustrating approach to equilibrium in a stable air column.

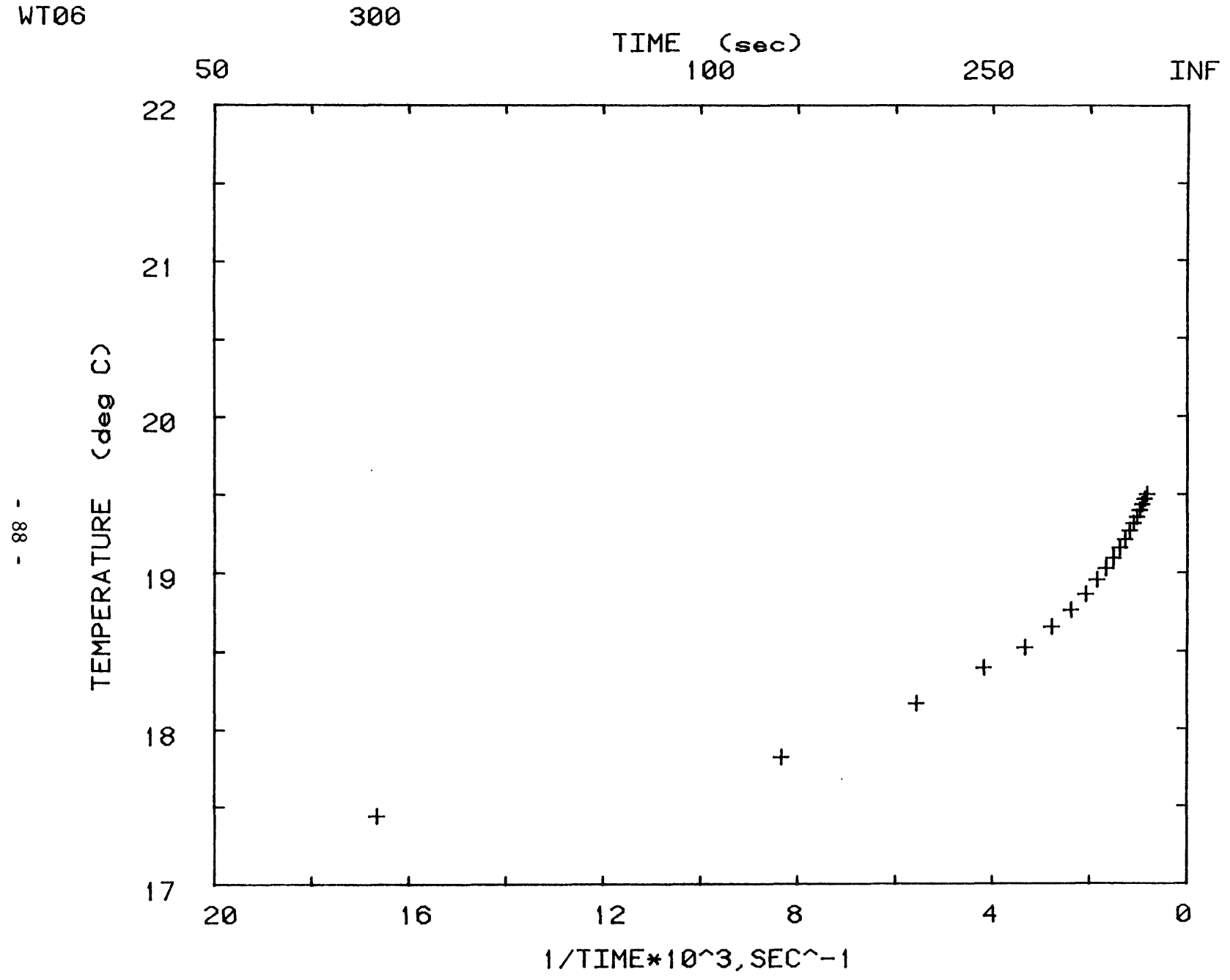

Figure 2-3. Temperature versus reciprocal time (from stopping of probe) for WT06, 300 feet, illustrating the effects of a long-period disturbance superimposed on a simple step change in temperature.

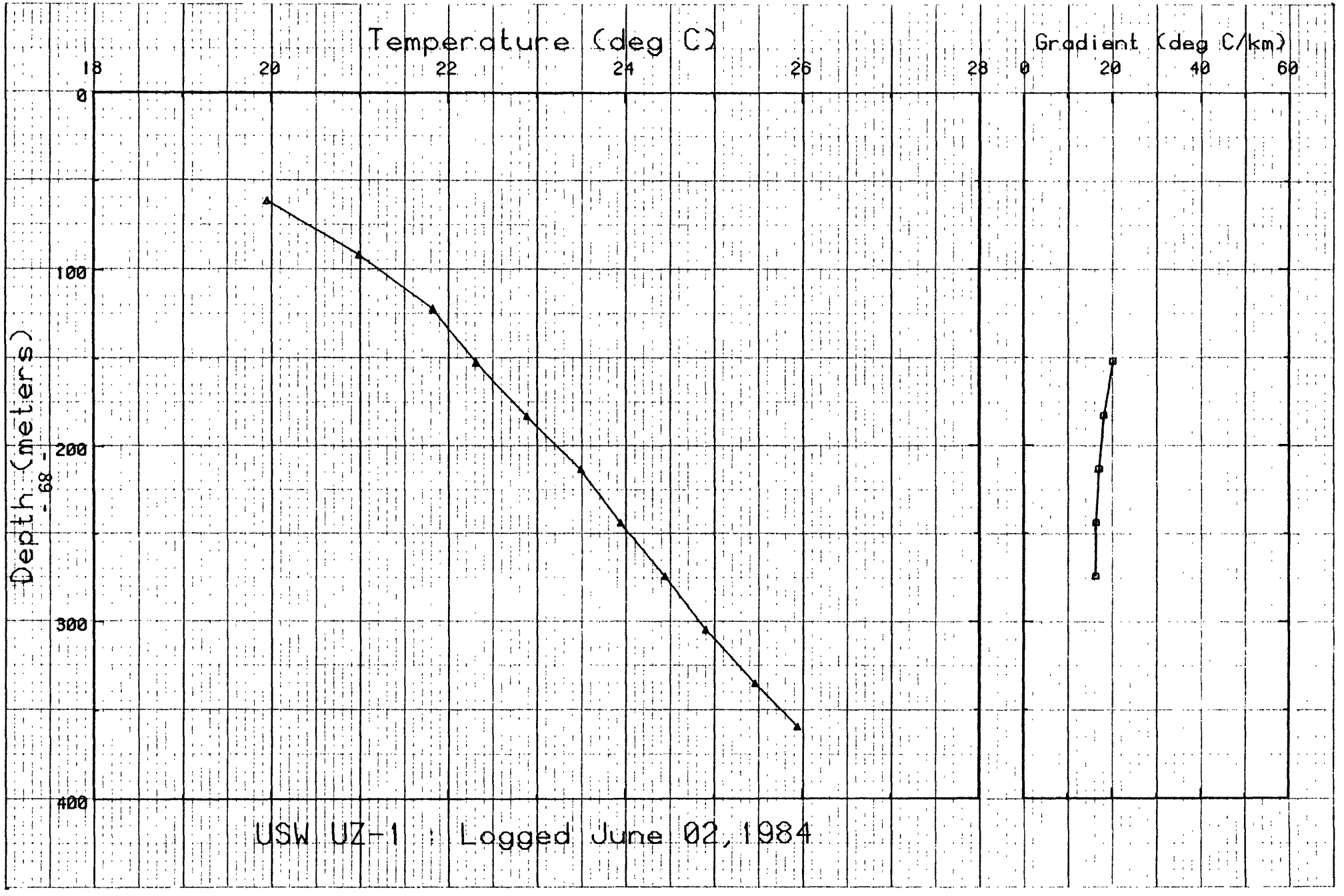
Temperature (deg C)
18
20
22
24
26
28
Gradient (deg C/km)
0
20
40
60
Depth (meters)
0
100
200
300
400
USW UZ-1 : Logged June 02, 1984
TEKTRONIX INFORMATION DISPLAY DIVISION 006-1695-00 10 x 15 in. LINEAR

Figure 2-4.

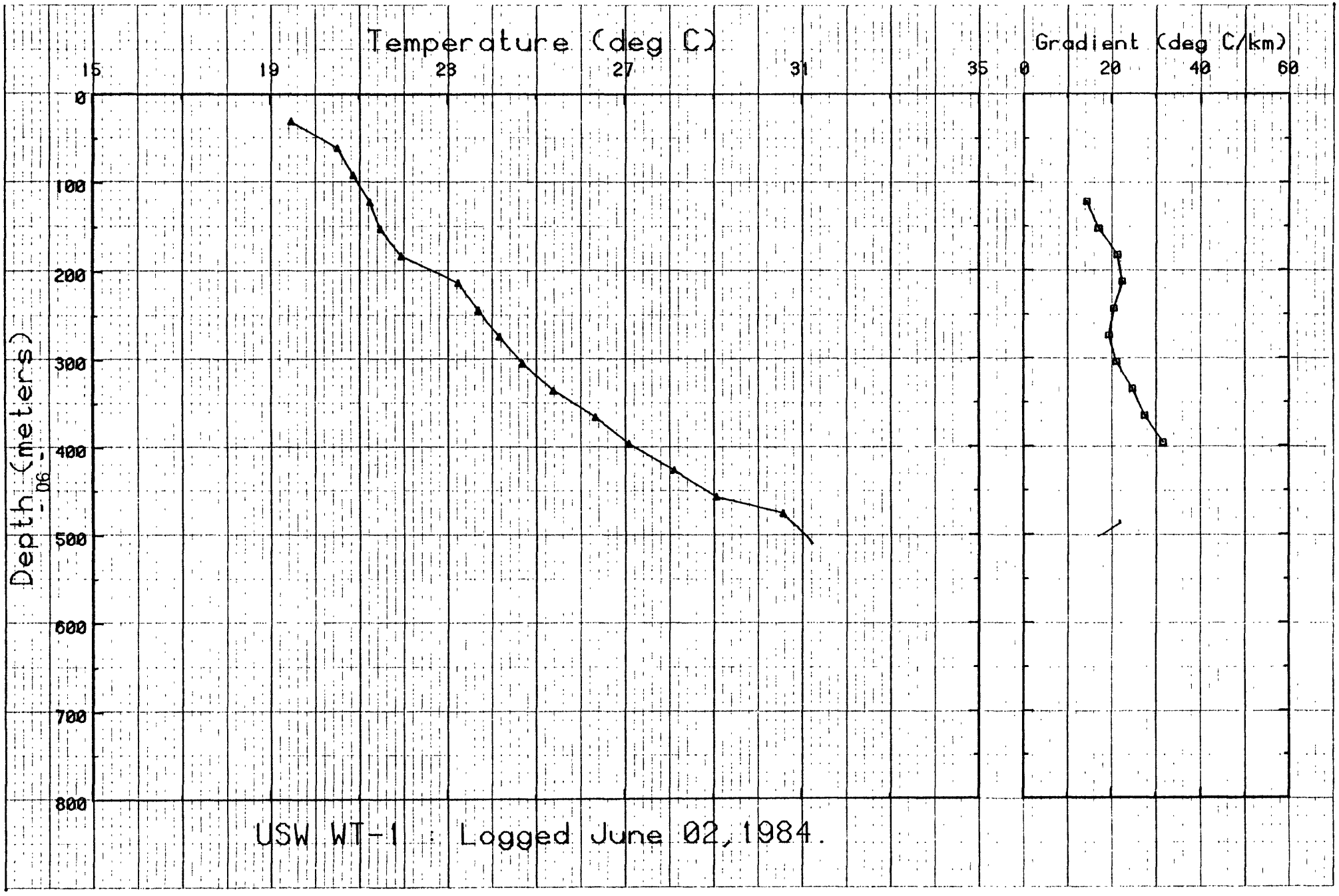
Temperature (deg C)
15
19
23
27
31
35
Gradient (deg C/km)
0
20
40
60
Depth (meters)
0
100
200
300
400
500
600
700
800
USW WT-1 : Logged June 02, 1984.
TEKTRONIX INFORMATION DISPLAY DIVISION 006-1688-00 10 x 15 in. LINEAR

Figure 2-5.

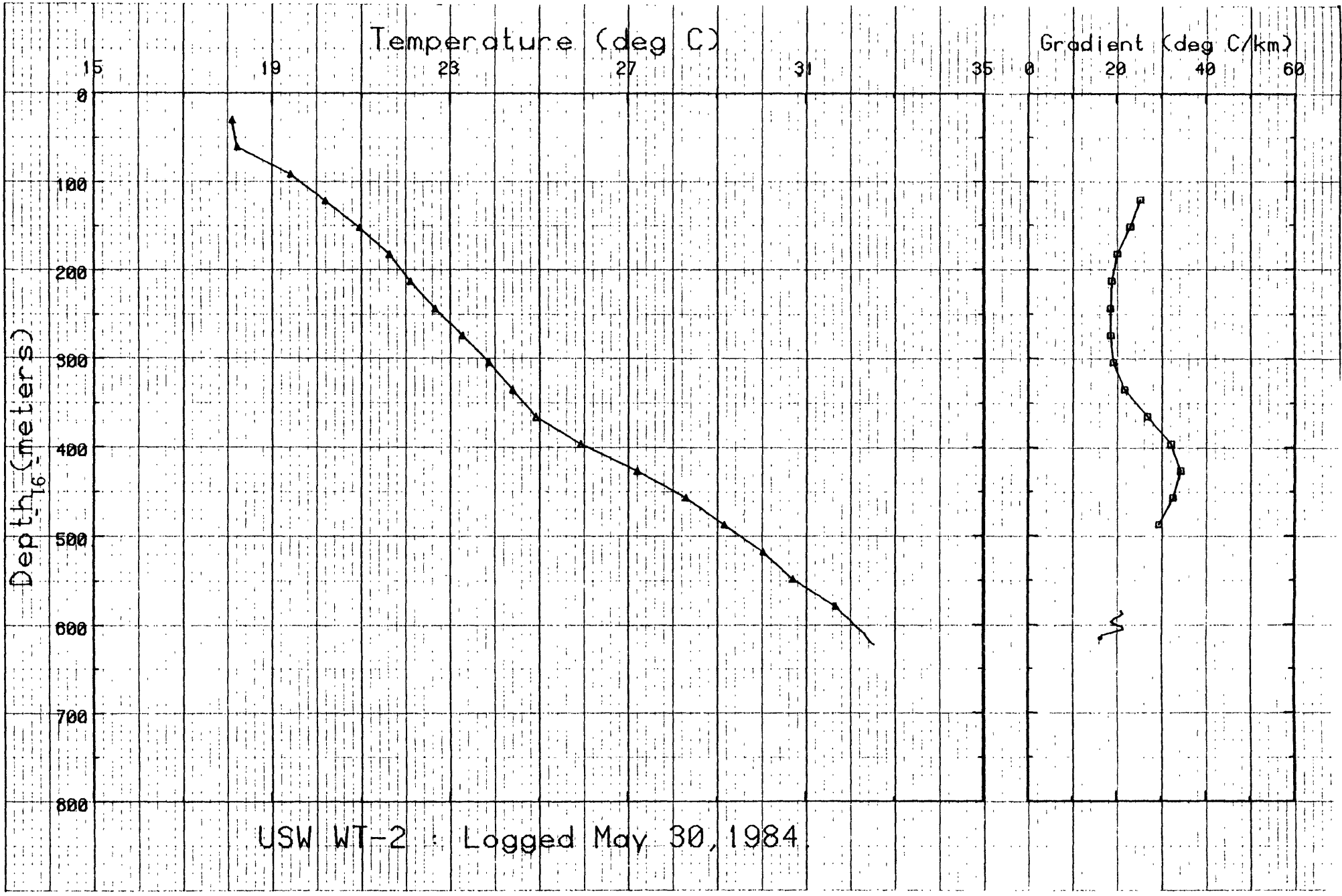
Temperature (deg C)
15
19
23
27
31
35
Gradient (deg C/km)
0
20
40
60
Depth (meters)
0
100
200
300
400
500
600
700
800
USW WT-2 : Logged May 30, 1984

Figure 2-6.

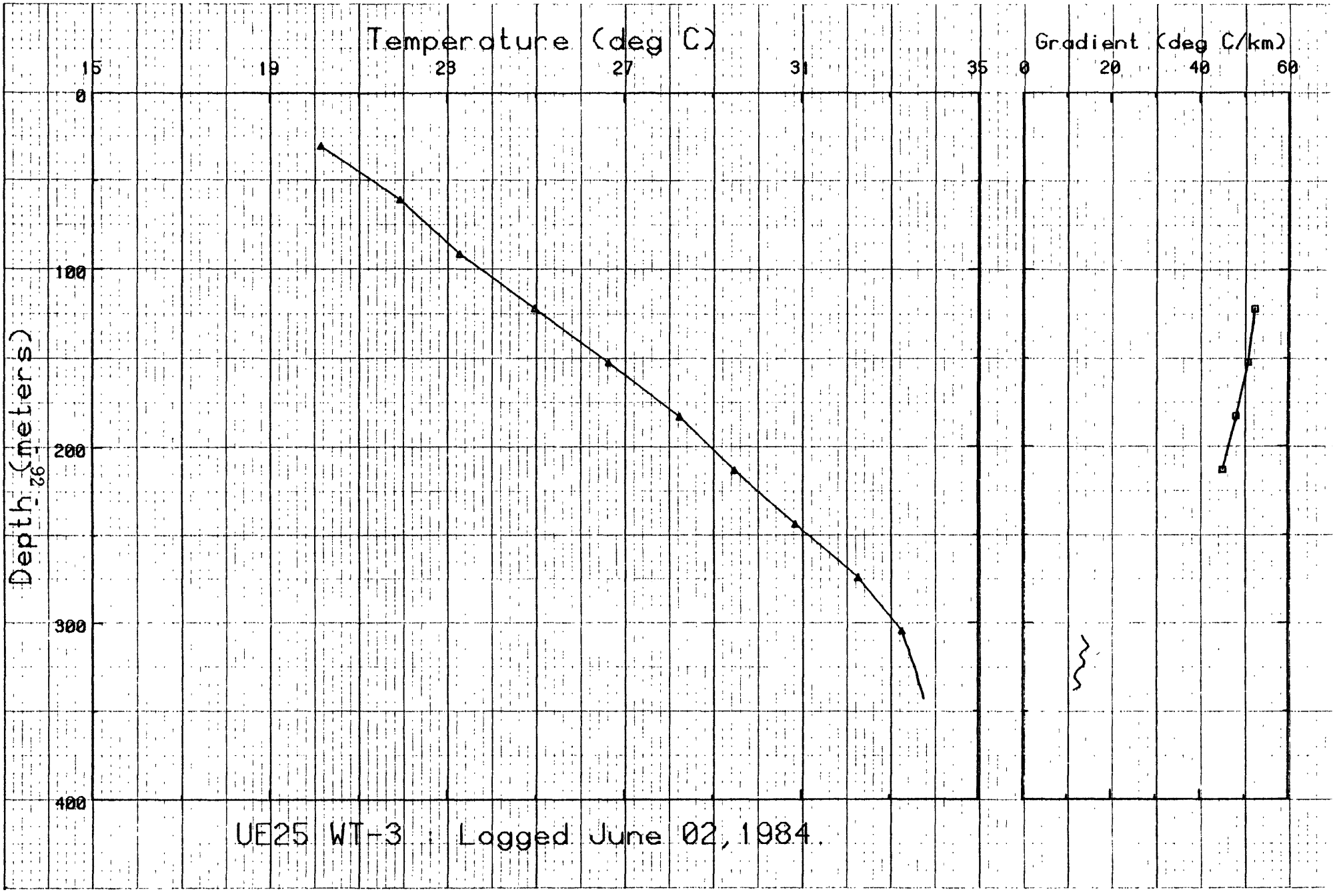
Temperature (deg C)
15
19
23
27
31
35
Gradient (deg C/km)
0
20
40
60
Depth (meters)
0
100
200
300
400
UE25 WT-3 : Logged June 02, 1984.
TEKTRONIX INFORMATION DISPLAY DIVISION
006-1698-00 10 x 15 in. LINEAR

Figure 2-7.

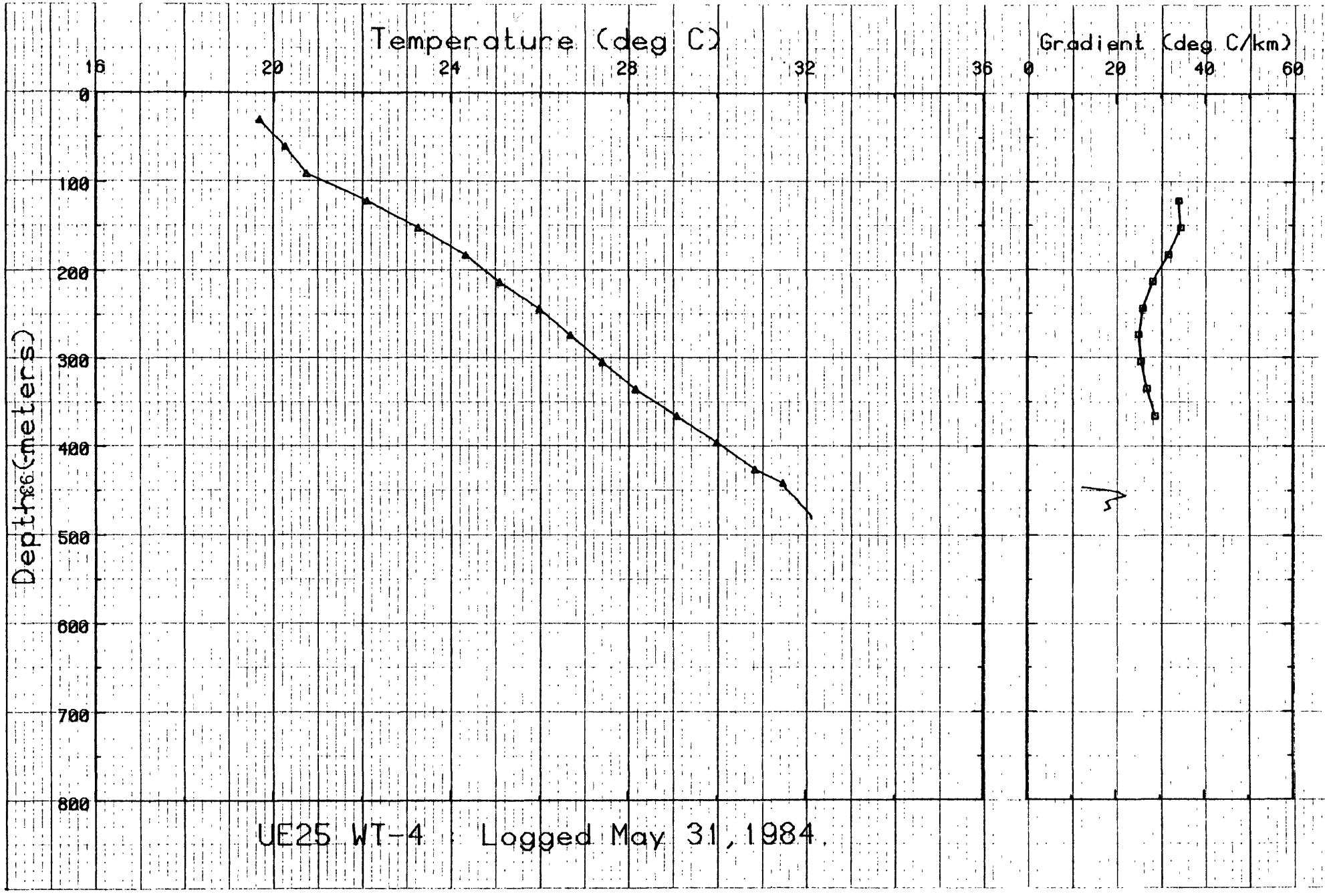
Temperature (deg C)
16
20
24
28
32
36
Gradient (deg C/km)
0
20
40
60
Depth (meters)
0
100
200
300
400
500
600
700
800
UE25 WT-4 : Logged May 31, 1984.
TEKTRONIX INFORMATION DISPLAY DIVISION 006-1695-00 10 x 15 in. LINEAR

Figure 2-8.

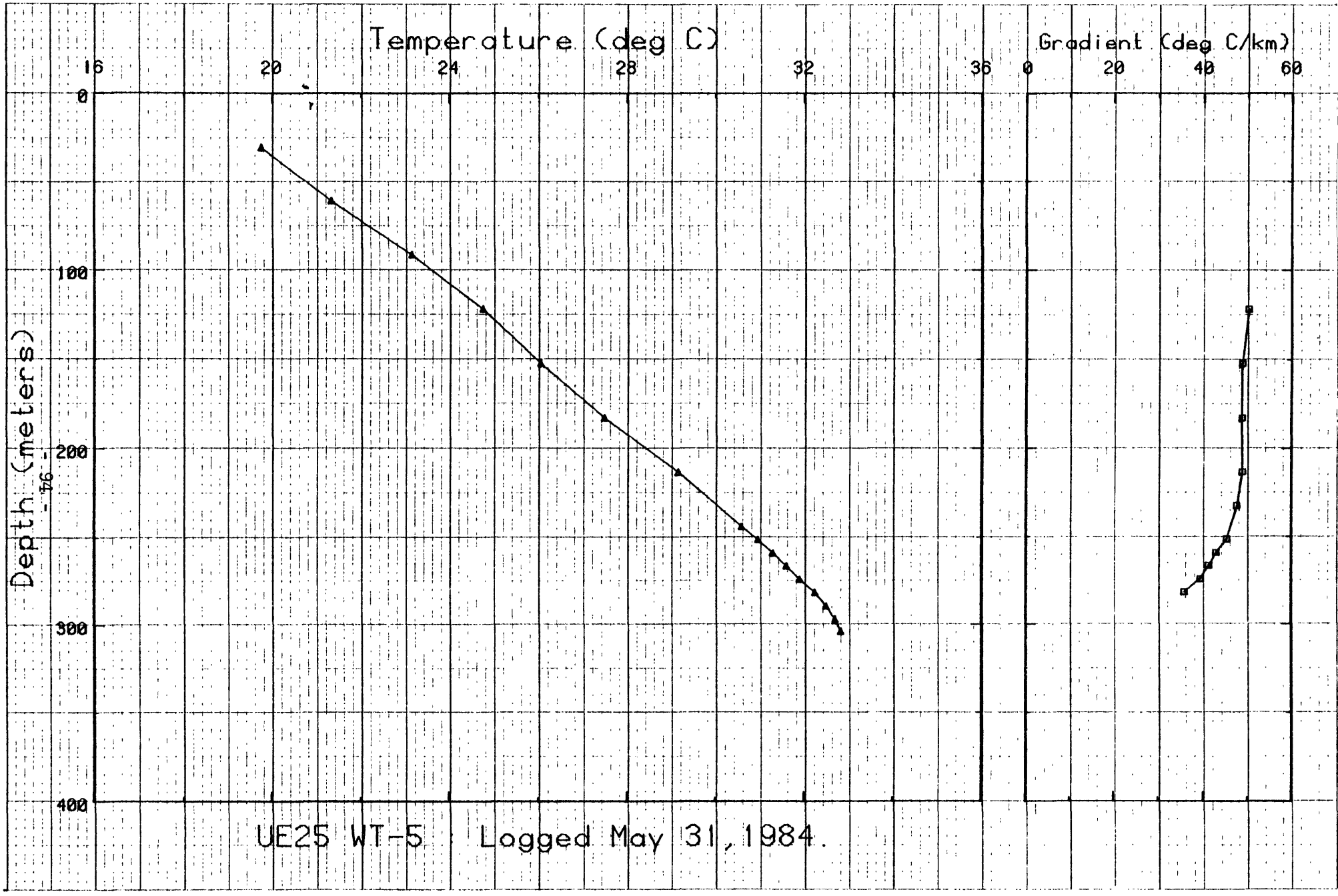
Temperature (deg C)
16
20
24
28
32
36
Gradient (deg C/km)
0
20
40
60
0
100
200
300
400
Depth (meters)
UE25 WT-5 : Logged May 31, 1984.

Figure 2-9.

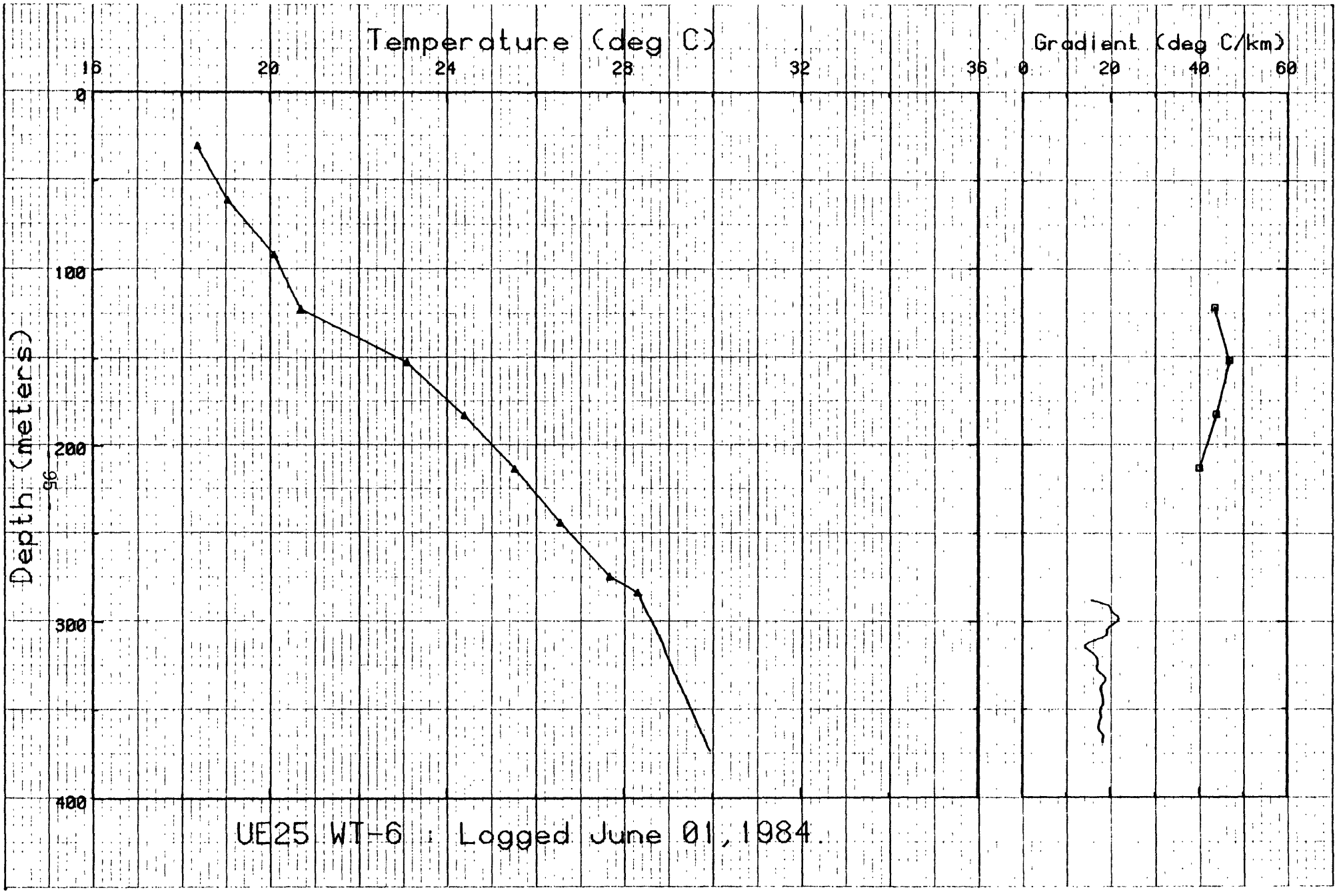
Temperature (deg C)
16
20
24
28
32
36
Gradient (deg C/km)
0
20
40
60
Depth (meters)
0
100
200
300
400
UE25 WT-6 : Logged June 01, 1984.

Figure 2-10.

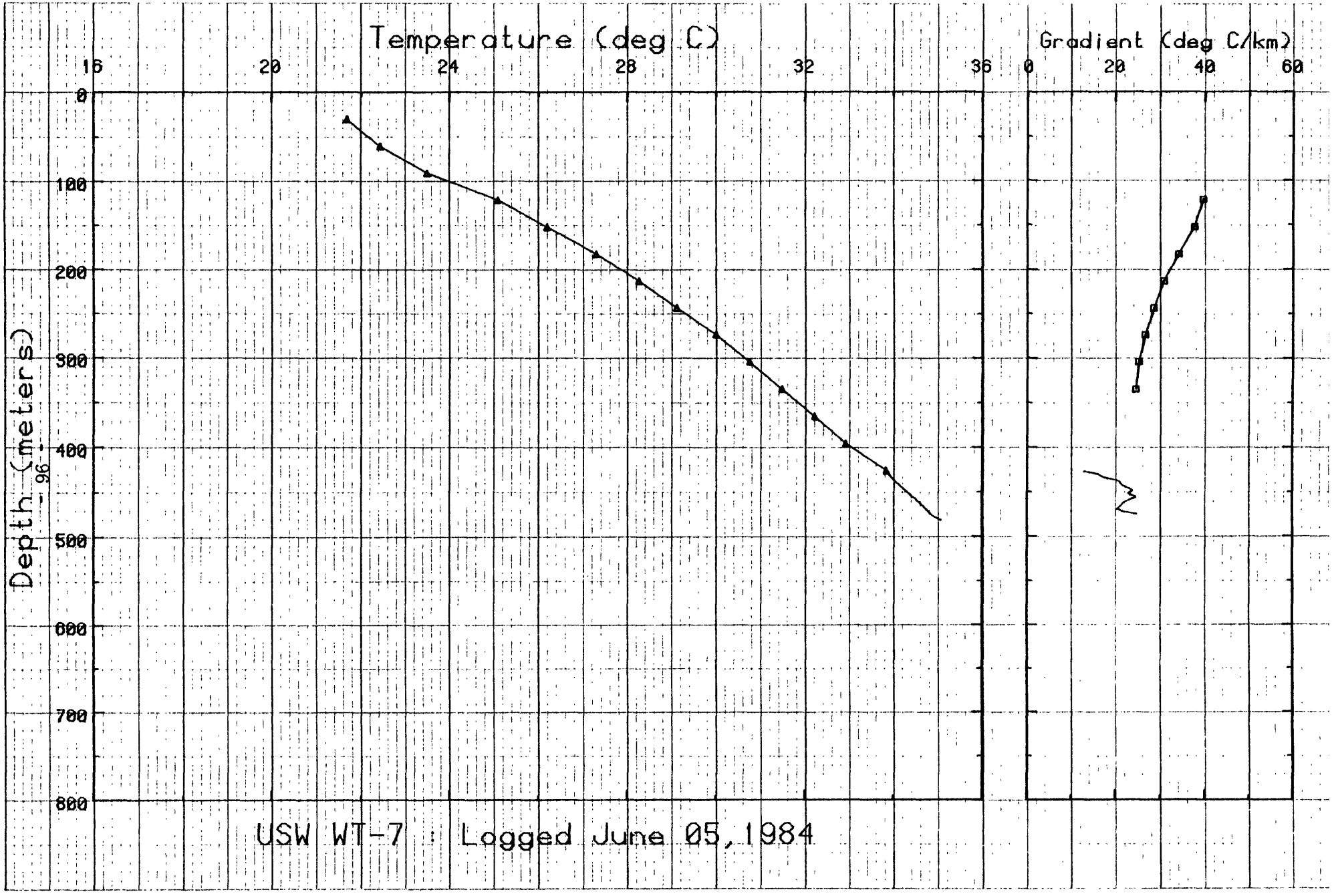
Temperature (deg C)
16
20
24
28
32
36
Gradient (deg C/km)
0
20
40
60
Depth (meters)
0
100
200
300
400
500
600
700
800
USW WT-7 : Logged June 05, 1984
TEKTRONIX INFORMATION DISPLAY DIVISION 006-1898-00 10 x 15 in. LINEAR

Figure 2-11.

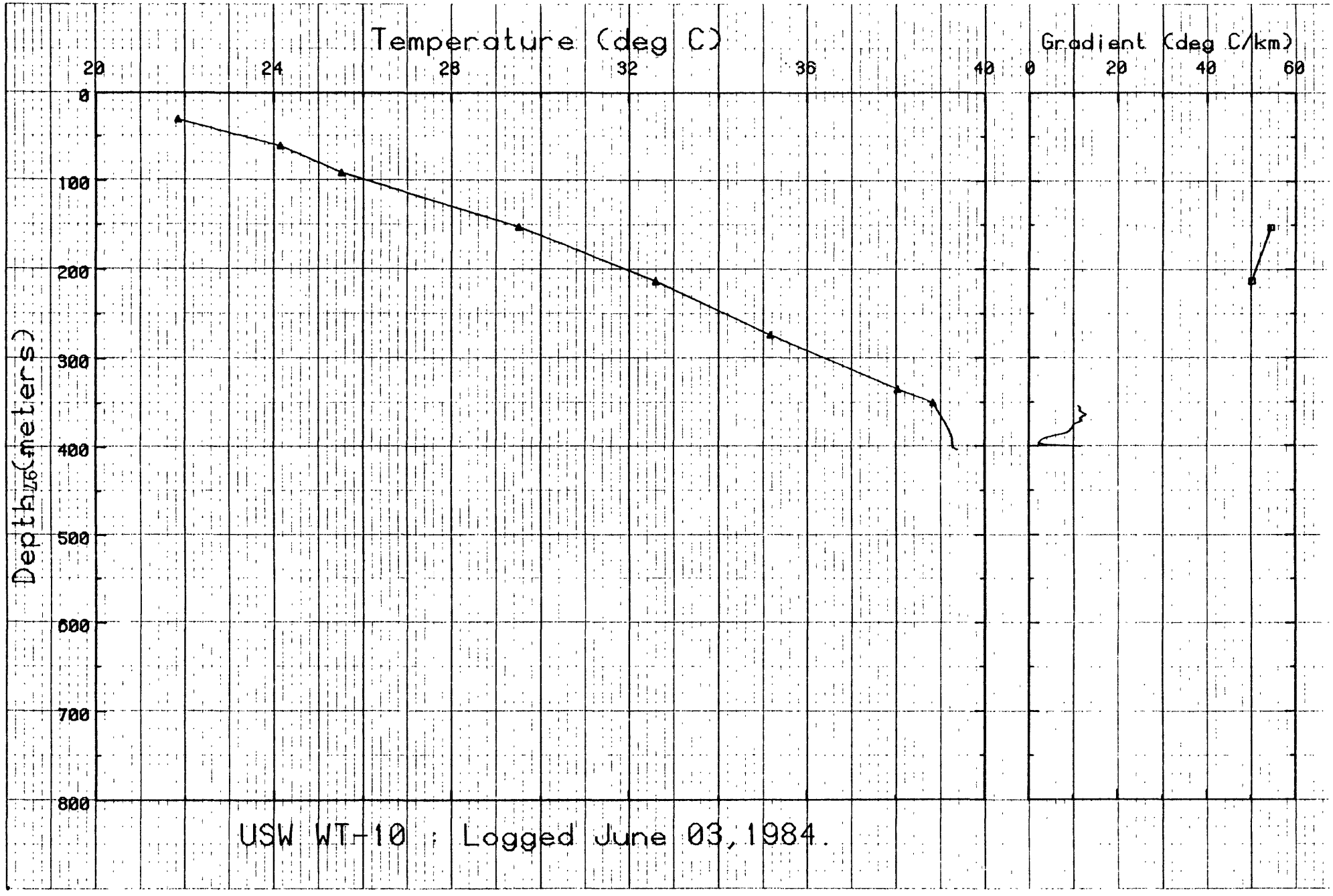
Temperature (deg C)
20
24
28
32
36
40
Gradient (deg C/km)
0
20
40
60
Depth (meters)
0
100
200
300
400
500
600
700
800
USW WT-10 ; Logged June 03, 1984.
TEKTRONIX INFORMATION DISPLAY DIVISION 006-1698.00 10 x 15 in. LINEAR

Figure 2-12.

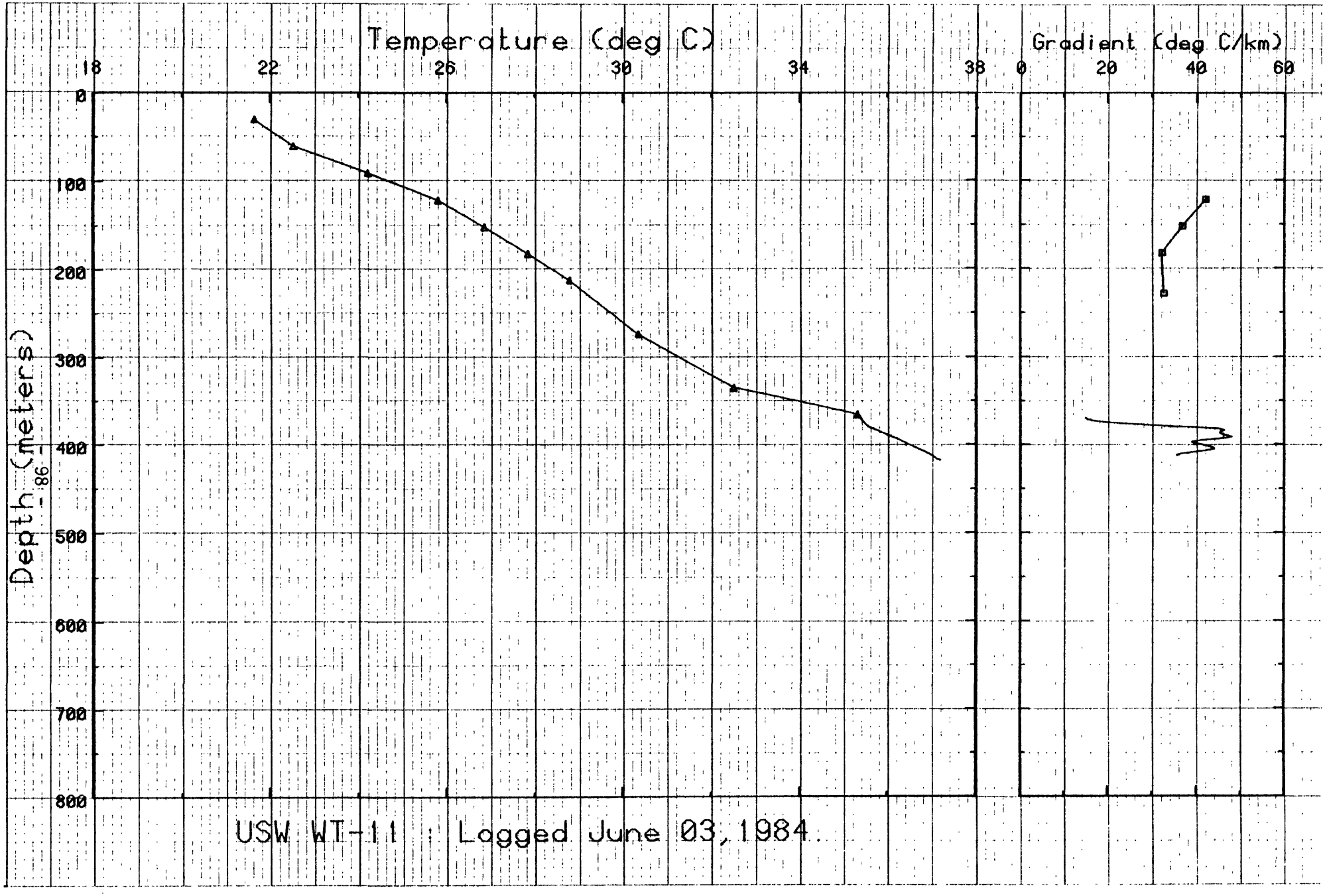
Temperature (deg C)
18
22
26
30
34
38
Gradient (deg C/km)
0
20
40
60
Depth (meters)
0
100
200
300
400
500
600
700
800
USW WT-11 : Logged June 03, 1984.
TEKTRONIX INFORMATION DISPLAY DIVISION 006 1698 00 10 x 15 in. LINEAR

Figure 2-13.

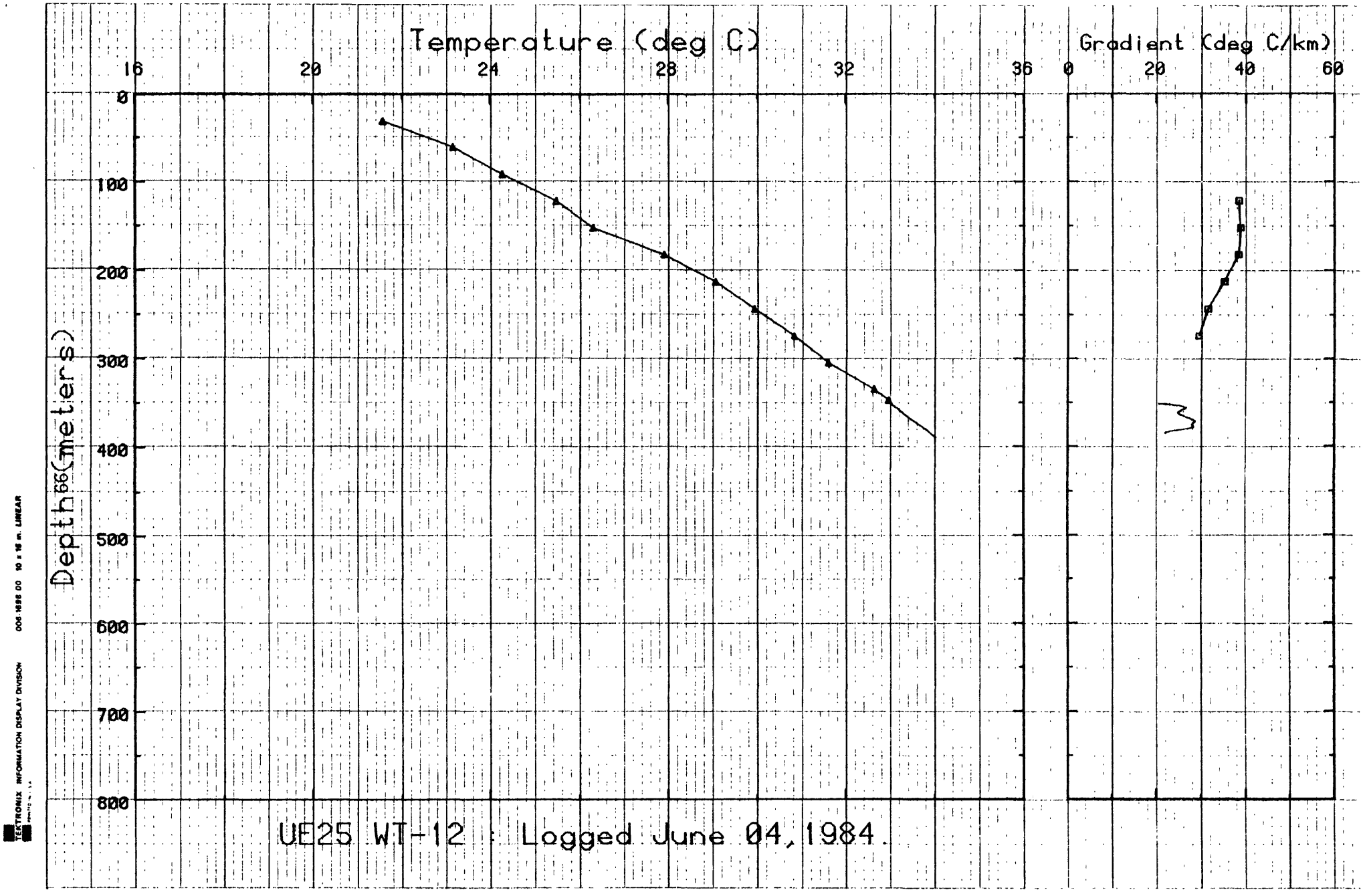
Temperature (deg C)
16
20
24
28
32
36
Gradient (deg C/km)
0
20
40
60
Depth(meters)
0
100
200
300
400
500
600
700
800
UE25 WT-12 : Logged June 04, 1984.
TEKTRONIX INFORMATION DISPLAY DIVISION 006-1695-00 10 x 15 in. LINEAR

Figure 2-14.

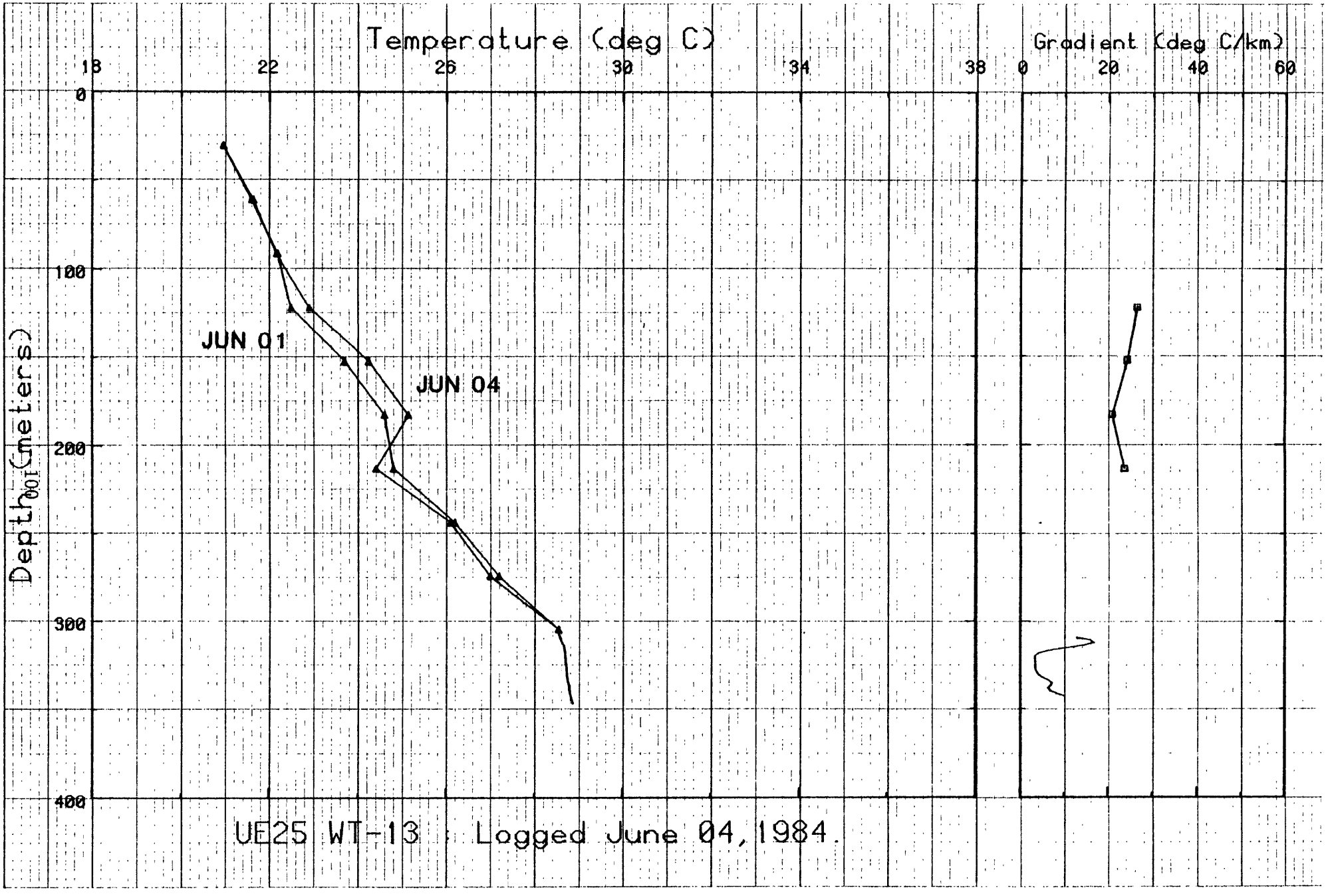
Temperature (deg C)
18
22
26
30
34
38
Gradient (deg C/km)
0
20
40
60
0
100
200
300
400
Depth (meters)
JUN 01
JUN 04
UE25 WT-13 : Logged June 04, 1984.

Figure 2-15.

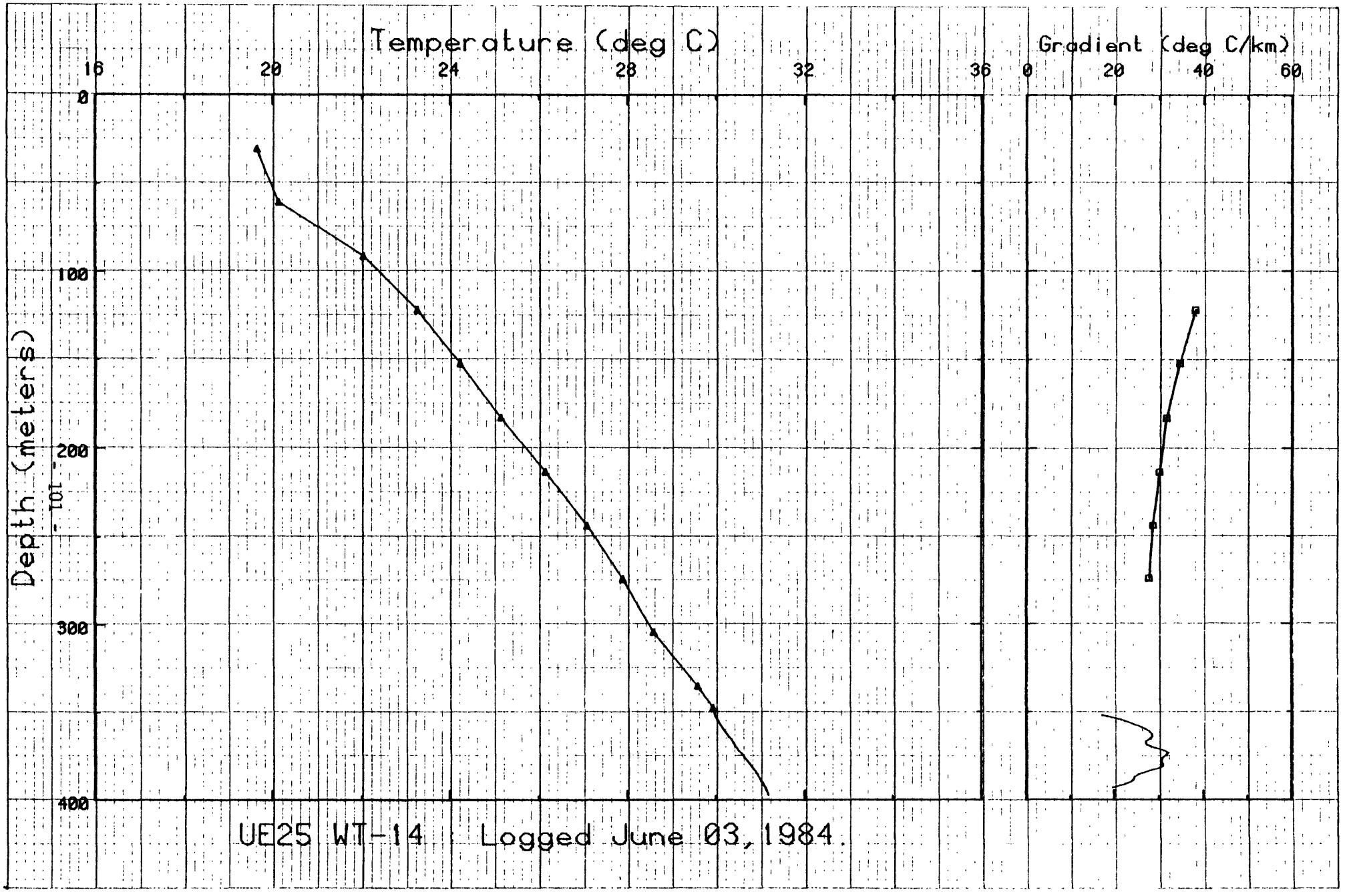
Temperature (deg C)
16
20
24
28
32
36
Gradient (deg C/km)
0
20
40
60
0
100
200
300
400
Depth (meters)
- 101 -
UE25 WT-14 : Logged June 03, 1984.

Figure 2-16.

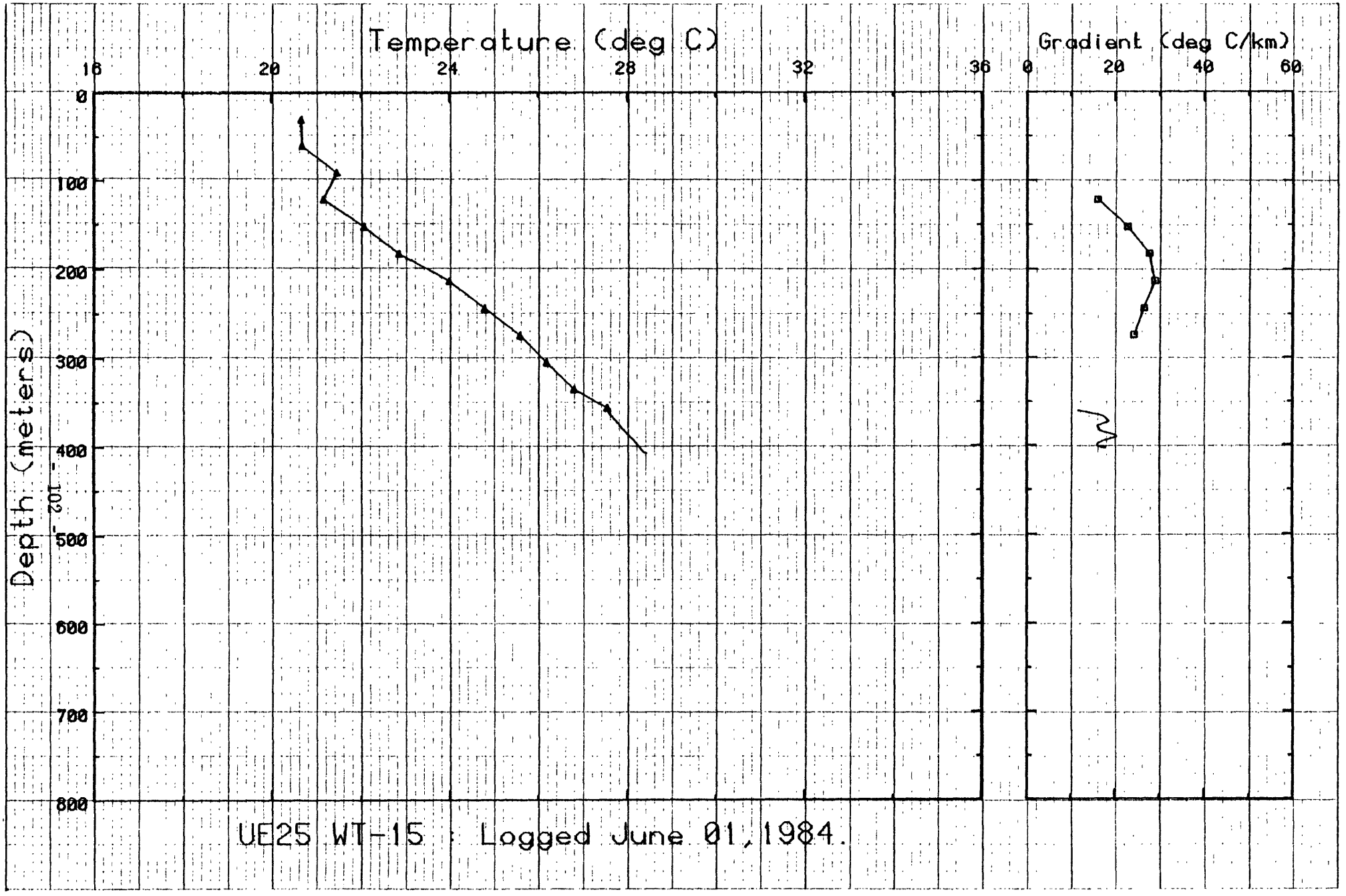
Temperature (deg C)
16
20
24
28
32
36
Gradient (deg C/km)
0
20
40
60
Depth (meters)
0
100
200
300
400
500
600
700
800
UE25 WT-15 : Logged June 01, 1984.

Figure 2-17.

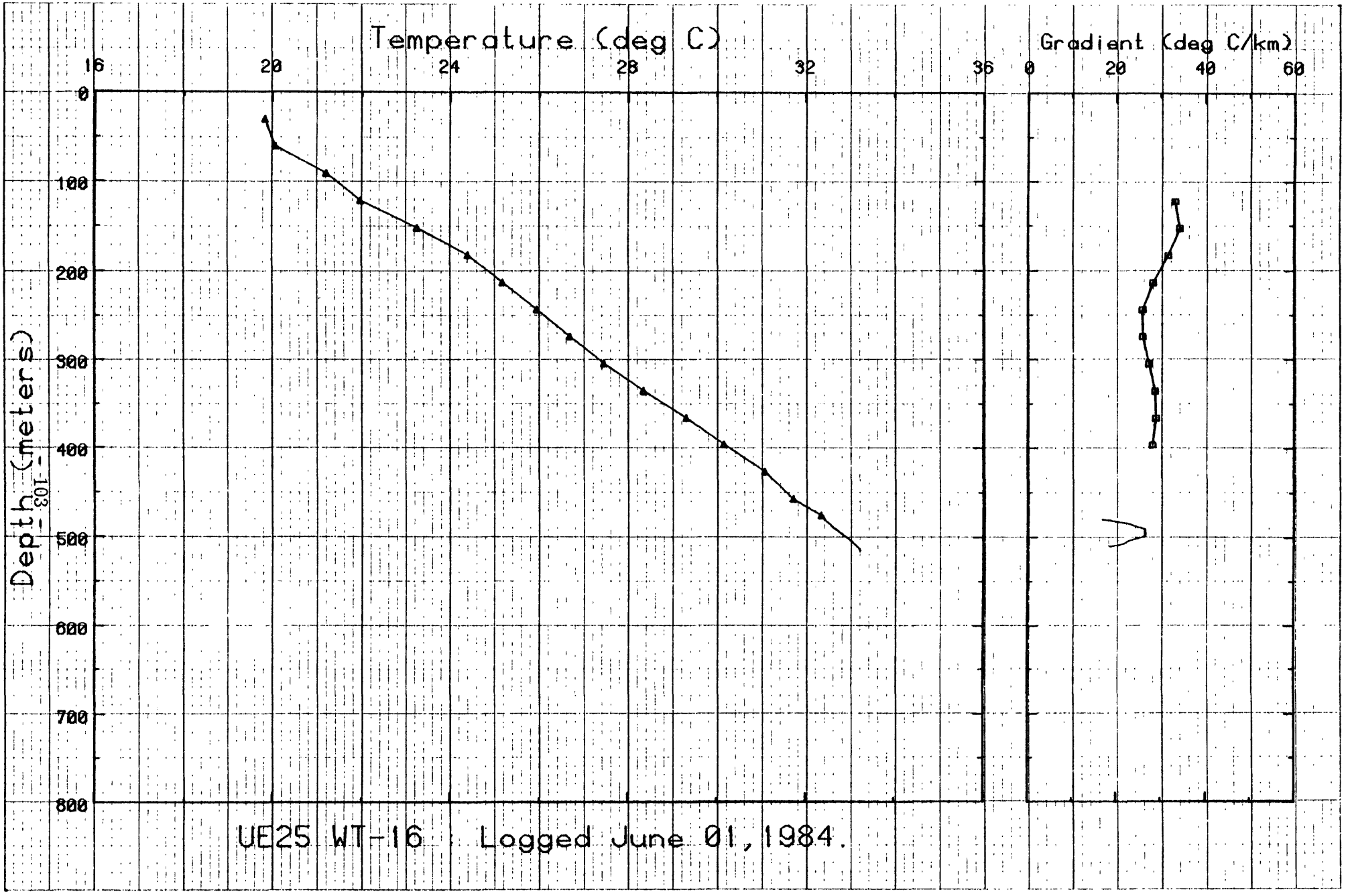
Temperature (deg C)
16
20
24
28
32
36
Gradient (deg C/km)
0
20
40
60
0
100
200
300
400
500
600
700
800
Depth (meters)
-103
UE25 WT-16 : Logged June 01, 1984.
TEKTRONIX INFORMATION DISPLAY DIVISION 006 1698.00 10 x 15 in. LINEAR

Figure 2-18.

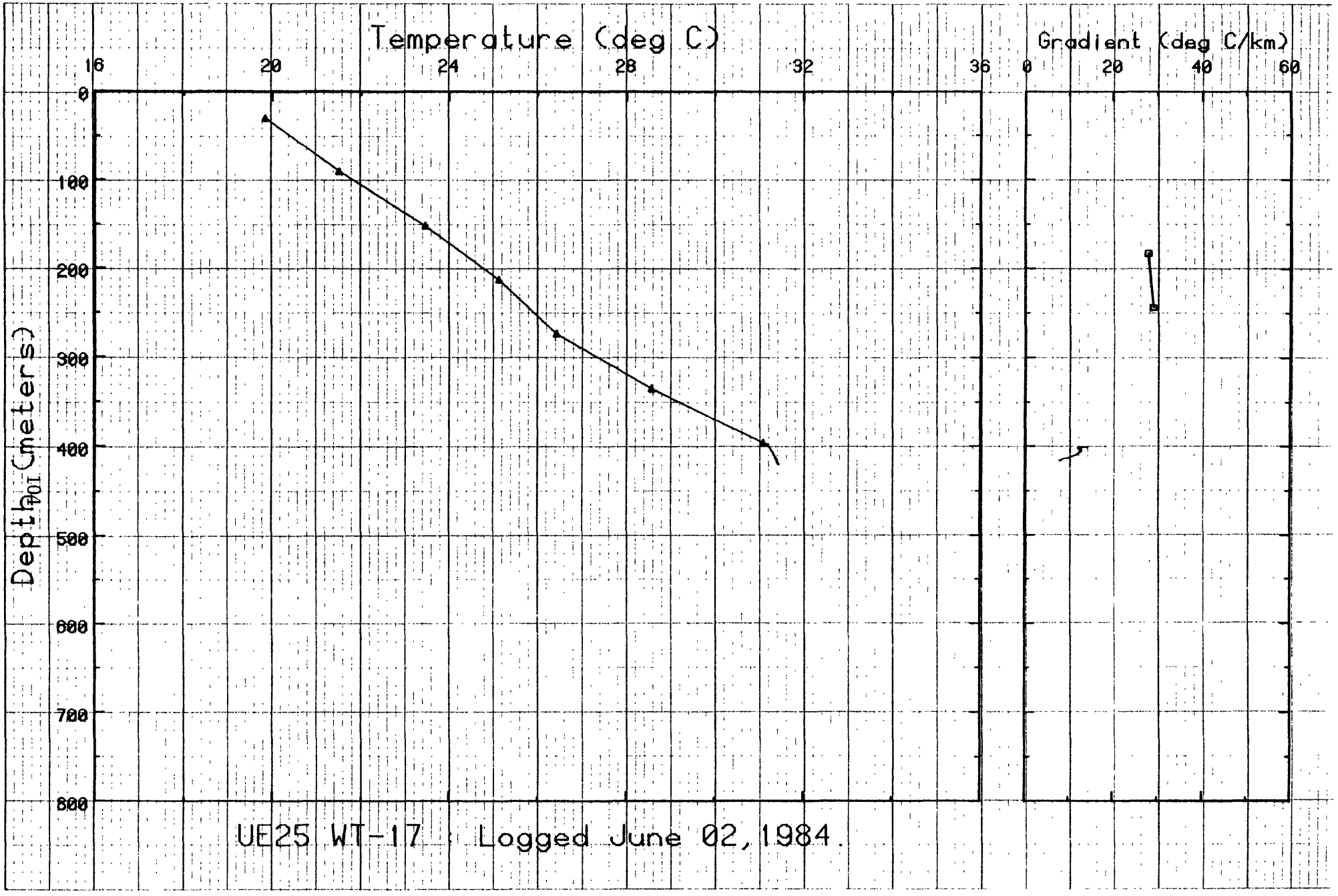
Temperature (deg C)
16
20
24
28
32
36
Gradient (deg C/km)
0
20
40
60
0
100
200
300
400
500
600
700
800
Depth (meters)
UE25 WT-17 : Logged June 02, 1984.

Figure 2-19.

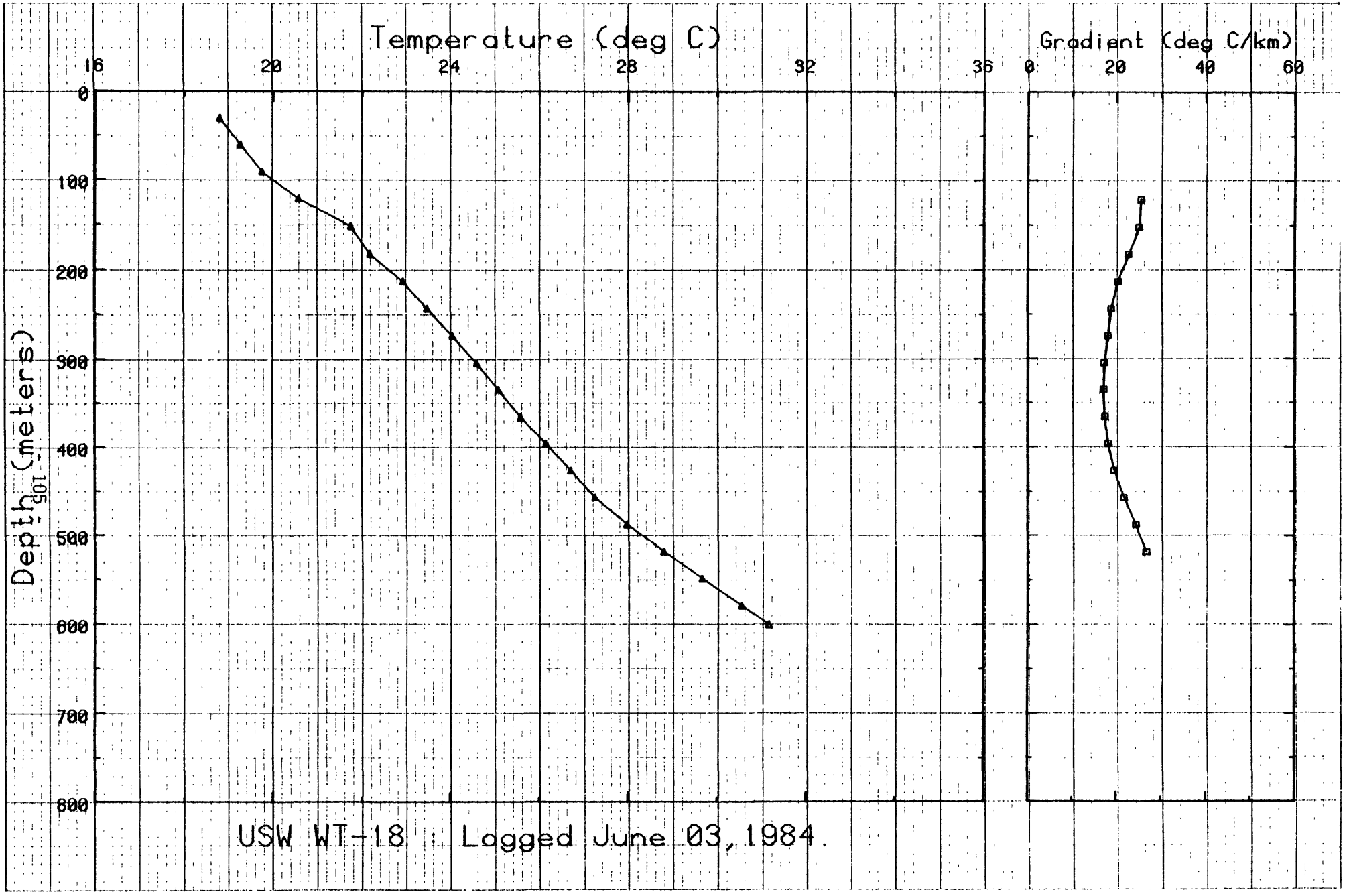
Temperature (deg C)
16
20
24
28
32
36
Gradient (deg C/km)
0
20
40
60
0
100
200
300
400
500
600
700
800
Depth (meters)
USW WT-18 : Logged June 03, 1984.
TEKTRONIX INFORMATION DISPLAY DIVISION 006-1698-00 10 x 15 in. LINEAR

Figure 2-20.

APPENDIX 3. Thermal conductivities

Thermal conductivity measurements were performed on core samples that had been wrapped in aluminum foil and dipped in hot wax to preserve in situ moisture conditions to the fullest extent possible. Thermal conductivity determinations were performed at an ambient temperature of about 25°C using the needle-probe method described by Sass and others (1971, 1984). Conductivity values are presented in Tables 3-1 through 3-5.

TABLE 3-1. Thermal conductivity of volcanic rocks from USW G-1

Depth, m	Formation (member)	Lithology	K $Wm^{-1} K^{-1}$	Saturation
242.3	Paintbrush Tuff (Topopah Spring Member)	Densely welded tuff	2.15	U
405.4		Densely welded tuff	1.18	U
458.1	Tuffaceous beds of Calico Hills	Non-welded tuff	1.30	U
520.0		Non-welded tuff	1.17	U
----------		SWL (static water level)	----------	
612.6	Crater Flat Tuff (Prow Pass Member)	Partially welded tuff	1.28	S
630.9		Partially welded tuff	1.33	S
693.1	(Bullfrog Member)	Non- to partially welded tuff	1.37	S
704.2		Non- to partially welded tuff	1.38	S
721.7		Partially welded tuff	1.88	S
753.6		Moderately to densely welded tuff	1.80	S
759.9		Moderately to densely welded tuff	1.88	S
773.0		Moderately to densely welded tuff	1.90	S
782.7		Moderately to densely welded tuff	1.36	S
823.3	Crater Flat Tuff (Tram Unit)	Partially to moderately welded tuff	1.39	S
857.7		Partially to moderately welded tuff	2.26	S
868.1*		Partially to moderately welded tuff	1.80	S
892.5		Partially to moderately welded tuff	2.07	S
892.8*		Partially to moderately welded tuff	1.94	S
892.9*		Partially to moderately welded tuff	1.87	S
895.7		Partially to moderately welded tuff	2.10	S
929.6		Partially to moderately welded tuff	1.95	S
930.2*		Partially to moderately welded tuff	1.42	S
940.4		Moderately welded tuff	1.54	S

TABLE 3-1. Thermal conductivity of volcanic rocks from USW G-1 (continued)

Depth, m	Formation (member)	Lithology	K $Wm^{-1} K^{-1}$	Saturation
967.3		Partially welded tuff	1.62	S
983.6		Non-welded tuff	1.67	S
1013.8		Vitrophyre	1.67	S
1044.5	Crater Flat Tuff (Tram Unit)	Vitrophyre	2.00	S
1065.6		Vitrophyre	1.80	S
1091.6	Flow breccia	Flow breccia	1.86	S
1123.4		Flow breccia	1.43	S
1157.9		Flow breccia	1.95	S
1187.9		Flow breccia	1.49	S
1219.4	Lithic Ridge Tuff	Partially welded tuff	1.65	S
1253.6		Partially welded tuff	1.80	S
1280.1		Partially welded tuff	1.88	S
1319.9		Partially welded tuff	1.72	S
1349.2		Partially welded tuff	1.77	S
1389.4		Partially welded tuff	1.86	S
1419.3		Partially welded tuff	1.75	S
1450.7	Lithic Ridge Tuff	Partially welded tuff	1.96	S
1477.5		Non-welded tuff	2.10	S
1511.6		Non-welded tuff	1.68	S
1540.0	Older ash flows to bedded tuffs. Units A, B, and C	Densely welded tuff	1.98	S
1573.0		Densely welded tuff	1.98	S
1600.0		Densely welded tuff	2.15	S
1632.6		Bedded tuffs	2.12	S
1675.7		Non-welded tuff	1.70	S

TABLE 3-1. Thermal conductivity of volcanic rocks from USW G-1 (continued)

Depth, m	Formation (member)	Lithology	K $Wm^{-1} K^{-1}$	Saturation
1716.9		Densely welded tuff	1.94	S
1747.7		Moderately welded tuff	1.91	S
1754.5		Moderately welded tuff	1.85	S
1783.3		Moderately welded tuff	1.97	S
1813.8		Moderately welded tuff	1.89	S
1814.0		Moderately welded tuff	1.86	S

TABLE 3-2. Thermal conductivity of volcanic rocks from USW G-2

Depth, m	Formation (member)	Lithology	K $Wm^{-1}K^{-1}$	Saturation
110.7	(Paintbrush Tuff)	Non-welded tuff	0.88	U
135.6		Non-welded tuff	0.69	U
166.8	(Pah Canyon Member)	Partially welded tuff	0.85	U
196.6		Moderately welded tuff	1.53	U
230.6		Bedded tuff	0.97	U
259.7	(Topopah Spring Member)	Welded tuff	1.67	U
279.4		Densely welded tuff	1.95	U
309.6		Densely welded tuff	2.01	U
337.2		Densely welded tuff	2.13	U
371.1		Densely welded tuff	2.15	U
394.2		Densely welded tuff	1.74	U
422.2		Densely welded tuff	1.71	U
451.6		Densely welded tuff	2.05	U
481.6		Densely welded tuff	2.09	U
495.5		Densely welded tuff	2.11	U
---------- SWL (static water level) ----------				
525.8		Bedded tuff	1.16	S
555.4	(Tuffaceous beds of Calico Hills)	Bedded tuff	1.10	S
579.3		Non-welded tuff	1.14	S
586.6		Non-welded tuff	1.06	S
617.4		Non-welded tuff	1.16	S
644.9		Non-welded tuff	1.16	S
675.7		Non-welded tuff	1.31	S

TABLE 3-2. Thermal conductivity of volcanic rocks from USW G-2 (continued)

Depth, m	Formation (member)	Lithology	K $Wm^{-1} K^{-1}$	Saturation
700.6		Non-welded tuff	1.28	S
731.6		Non-welded tuff	1.19	S
761.8		Non-welded tuff	1.24	S
793.0		Partially welded tuff	1.37	S
822.4		Moderately welded tuff	1.37	S
852.6	Crater Flat tuff (Prow Pass Member)	Moderately welded tuff	1.89	S
885		Partially welded tuff	1.65	S
916.9		Partially welded tuff	1.51	S
951.5		Partially welded tuff	1.43	S
982.1		Non-welded tuff	1.56	S
1010.8	(Bullfrog Member)	Moderately welded tuff	1.83	S
1013.0		Moderately welded tuff	1.78	S
1028.5		Moderately welded tuff	1.89	S
1041.2		Non-welded tuff	1.81	S
1071.6		Bedded tuff	1.60	S
1101.6	(Tram Unit)	Lithic-rich tuff	1.90	S
1137.2		Partially welded tuff	1.60	S
1166.9		Partially welded tuff	1.92	S
1202.7		Bedded tuff	1.97	S
1234.1		Bedded tuff	1.76	S
1294.5	(Tuff of Lithic Ridge)	Partially welded tuff	1.98	S
1324.4		Partially welded tuff	2.07	S
1355.0		Partially welded tuff	1.98	S

TABLE 3-2. Thermal conductivity of volcanic rocks from USW G-2 (continued)

Depth, m	Formation (member)	Lithology	K $Wm^{-1} K^{-1}$	Saturation
1385.1		Partially welded tuff	1.84	S
1416.0		Partially welded tuff	2.04	S
1444.8		Partially welded tuff	2.07	S
1461.9		Partially welded tuff	2.31	S
1498.1	(Rhyolitic lava and flow breccia)	Flow breccia	2.46	S
1535.6		Lava	2.16	S
1560.2		Lava	2.13	S
1588.9	(Quartz latitic lava and flow breccia)	Lava	2.40	S
1622.6		Lava	2.14	S
1650.5		Lava	1.77	S
1681.9		Flow breccia	1.92	S
1711.2		Flow breccia	2.11	S
1734.4	(Dacitic lava and flow breccia)	Lava	2.49	S
1765.8		Lava	2.04	S
1796.4		Bedded tuff	2.42	S
1827.0	(older tuffs of USW G-2)	Moderately welded tuff	2.21	S

TABLE 3-3. Thermal conductivity of volcanic rocks from USW G-3 and USW GU-3

Depth, m	Formation (member)	Lithology	K $Wm^{-1} K^{-1}$	Saturation
35.7	Paintbrush tuff (Tiva Canyon Member)	Welded tuff	2.03	U
61.0		Welded tuff	2.20	U
96.0		Welded tuff	1.89	U
133.2		Bedded tuff (non-welded)	1.28	U
152.4	(Topopah Spring Member)	Moderately welded tuff	1.54	U
183.3		Moderately welded tuff	1.95	U
214.0		Welded tuff	2.26	U
253.3		Welded tuff	2.22	U
276.5		Welded tuff	2.23	U
311.6		Welded tuff	2.17	U
335.7		Welded tuff	2.01	U
367.3		Densely welded tuff	1.34	U
396.5		Partially welded tuff	1.08	U
453.0	(Tuffaceous beds of Calico Hills?)	Non-welded tuff	0.84	U
457.3		Non-welded tuff	0.91	U
489.4	Crater Flat Tuff (Prow Pass Member)	Non-welded tuff	2.50	U
519.1		Partially welded tuff	1.61	U
549.9		Partially welded tuff	1.02	U
580.6		Partially welded tuff	1.07	U
608.5		Bedded tuff	1.15	U
640.3	Crater Flat Tuff (Bullfrog Member)	Partially welded tuff	1.90	U
669.4		Welded tuff	1.86	U

TABLE 3-3. Thermal conductivity of volcanic rocks from USW G-3 and USW GU-3 (continued)

Depth, m	Formation (member)	Lithology	K $Wm^{-1} K^{-1}$	Saturation
704.1		Welded tuff	1.98	U
734.7		Welded tuff	2.01	U
----------		SWL (static water level)	----------	
767.1		Moderately welded	1.91	S
791.2		Partially welded	1.31	S
- End GU-3 -				
795.4		Partially welded	1.20	S
829.7	Crater Flat Tuff (Tram Member)	Non- to partially welded tuff	1.73	S
859.9		Bedded tuff	1.69	S
920.6		Moderately welded	1.77	S
949.2		Partially to moderately welded tuff	1.77	S
986.4		Moderately to partially welded tuff	1.97	S
1011.9		Partially to moderately welded tuff	1.39	S
1042.9		Partially to moderately welded tuff	1.39	S
1074.1		Moderately welded tuff	1.66	S
1103.5		Moderately welded tuff	1.41	S
1134.1		Moderately to partially welded tuff	1.50	S
1162.1		Partially to moderately welded tuff	1.37	S
1194.8	Lithic Ridge Tuff	Moderately welded tuff	1.71	S
1224.7		Partially welded tuff	1.53	S
1255.9		Non- to partially welded tuff	1.60	S
1286.7		Partially to moderately welded tuff	1.64	S
1316.6		Partially welded tuff	1.74	
1347.6		Moderately welded tuff	1.71	

TABLE 3-3. Thermal conductivity of volcanic rocks from USW G-3 and USW GU-3 (continued)

Depth, m	Formation (member)	Lithology	K $Wm^{-1} K^{-1}$	Saturation
1347.6		Moderately welded tuff	1.71	
1377.6		Partially to moderately welded tuff	1.74	
1407.6		Partially to moderately welded tuff	1.75	
1438.9		Moderately to partially welded tuff	1.85	
1469.6		Moderately to partially welded tuff	1.86	
1499.8	Older tuffs (Unit A?)	Welded tuff	1.92	
1529.5		Welded tuff	1.80	

TABLE 3-4. Thermal conductivity of volcanic rocks from USW G-4

Depth, m	Formation (member)	Lithology	K $Wm^{-1} K^{-1}$	Saturation
27.6	Paintbrush Tuff (Tiva Canyon Member)	Densely welded tuff	1.88	U
77.2	(Tonopah Spring Member)	Densely welded tuff	1.33	U
116.1		Moderate to densely welded tuff	1.72	U
151.3		Densely welded tuff	2.03	U
183.8		Densely welded tuff	2.04	U
214.8		Densely welded tuff	2.17	U
253.0		Densely welded tuff	2.11	U
286.5		Densely welded tuff	2.21	U
324.8		Densely welded tuff	1.69	U
376.1		Densely welded tuff	1.87	U
418.5		Non-welded tuff	0.95	U
448.2	Rhyolite lavas and tuffs of Calico Hills (Tuffaceous beds of Calico Hills)	Non-welded tuff	1.11	U
479.6		Non-welded tuff	1.11	U
511.6		Non-welded tuff	1.14	U
---------- SWL (static water level) ----------				
544.3	Crater Flat Tuff (Prow Pass Member)	Non-welded tuff	1.23	S
570.8		Partially welded tuff	1.52	S
603.2		Non- to partially welded tuff	1.23	S
627.5		Partially welded tuff	1.21	S
660.5		Partially welded tuff	1.19	S
694.9	Crater Flat Tuff (Bullfrog Member)	Partially welded tuff	1.71	S
721.5		Partially welded tuff	1.25	S

TABLE 3-4. Thermal conductivity of volcanic rocks from USW G-4 (continued)

Depth, m	Formation (member)	Lithology	K $Wm^{-1} K^{-1}$	Saturation
752.5		Partially welded tuff	1.36	S
786.1		Partially welded tuff	1.91	S
820.2		Partially welded tuff	1.39	S
849.9	(Tram Member)	Non- to partially welded tuff	1.28	S
873.4		Tuff	1.99	S
905.7		Tuff	1.25	S

TABLE 3-5. Thermal conductivity of rocks from UE25p1

Depth, m	Formation (member)	K $Wm^{-1} K^{-1}$
1310.4	Lone Mtn. Dolomite	5.36
1330.5	Lone Mtn. Dolomite	5.08
1339.9	Lone Mtn. Dolomite	4.67
1351.6	Lone Mtn. Dolomite	4.91
1367.4	Lone Mtn. Dolomite	5.17
1387.0	Lone Mtn. Dolomite	4.71
1399.1	Lone Mtn. Dolomite	4.93
1414.5	Lone Mtn. Dolomite	4.76
1429.0	Lone Mtn. Dolomite	4.45
1454.1	Lone Mtn. Dolomite	5.09
1479.1	Lone Mtn. Dolomite	4.79
1490.5	Lone Mtn. Dolomite	4.94
1801.6	Roberts Mountains Formation	5.47